Study of Electromagnetic Reactions on Light Nuclei with the Lorentz Integral Transform Method

Thesis submitted for the degree of

Dottore di Ricerca in Fisica

Doktor der Naturwissenschaften

by

Sonia Bacca

to

Facoltà di Scienze MM.FF.NN
Università degli Studi di Trento, Italia

Fachbereich Physik der
Johannes Gutenberg-Universität in Mainz, Deutschland

February 2005

This work was carried out under the supervision of Professor X. xxx and Professor Y. yyy in a "Co-tutelle de Thèse" between the University of Trento (UNITN) and the Johannes Gutenberg-University in Mainz (UNIMZ)

Agreement of September 19, 2002.

Abstract

In this thesis, which is conducted in the field of few-body nuclear physics, we apply the recently developed method of the Lorentz Integral Transform (LIT) to the study of inelastic electromagnetic reactions on light nuclei. The two basic electromagnetic reactions, i.e. nuclear photoabsorption and electron scattering off nuclei, are treated. The LIT enables one to perform exact calculations, avoiding the complication of the explicit evaluation of the continuum final states and reducing the problem to the solution of a bound state like equation. With this method the final state interaction is fully taken into account. The bound state like calculations are performed with an hyperspherical harmonics expansion, whose convergence is accelerated by building an effective interaction in the hyperspherical formalism (EIHH).

In this work we present the first microscopic calculation of the total photoabsorption cross sections below pion production of ^{6}Li, ^{6}He and ^{7}Li. The calculations are performed with simple central semirealistic NN-interactions, which simulate partially the tensor force, since they reproduce binding energies of two and three-body nuclei. The obtained photoabsorption cross section of ^{6}Li shows a single broad giant dipole resonance, while the one of ^{6}He presents two well separated peaks corresponding to the break up of the neutron halo and the α core, respectively. The comparison with experimental data shows that the addition of a P-wave interaction improves substantially the agreement with data. For ^{7}Li a single broad giant dipole resonance is found and a good agreement with the available experimental data is achieved.

As concerns the electron scattering reaction, we present a calculation of the longitudinal and transverse response functions for ^{4}He in the quasi-elastic region at medium momentum transfers. A non-relativistic model for the electromagnetic charge and current excitation operators is used. The calculation is performed with a semirealistic interaction and a gauge invariant model is build by construction of a meson exchange current. The effect of the two-body current on the transverse response is investigated and preliminary results are discussed. The comparison of the first results with the available experimental data is also shown.

Sommario

In questa tesi, che si inserisce nell'ambito della fisica nucleare a pochi corpi, viene applicato il recente metodo della trasformata integrale di Lorentz (LIT) allo studio delle reazioni elettromagnetiche su nuclei leggeri. Vengono trattate le reazioni elettromagnetiche di fotoassobrimento e diffusione di elettroni da parte di nuclei. Il metodo della LIT permette di effettuare calcoli esatti, evitando la complicazione del calcolo esplicito degli stati finali nel continuo e riducendo il problema alla soluzione di un'equazione di stato legato. Con questo metodo l'interazione di stato finale viene trattata in maniera esatta. I calcoli di stato legato vengono effettuati tramite uno sviluppo in armoniche ipersferiche, la cui convergenza è accelerata introducendo un'interazione efficace nell'ambito del formalismo ipersferico (EIHH).

In questo lavoro si presenta il primo calcolo microscopico della sezione d'urto totale di fotoassorbimento sotto la soglia di produzione del pione per i nuclei di ^{6}Li, ^{6}He e ^{7}Li. I calcoli sono effettuati utilizzando interazioni NN di tipo centrale semirealistico, che simulano parzialmente la presenza di una forza tensoriale, in quanto riproducono le energie di legame di nuclei sia a due che a tre corpi. La sezione d'urto di fotoassorbimento ottenuta per il ^{6}Li presenta una singola risonanza gigante di dipolo, mentre quella del ^{6}He mostra due picchi ben separati che corrispondono rispettivamente alla disintegrazione della parte *halo* del nucleo e dell' α-*core* interno. Dal confronto coi dati sperimentali a disposizione si evince che l'addizione di un'interazione in onda P migliora sostanzialmente l'accordo con l'esperimento. Nel caso del ^{7}Li si trova un'unica risonanza gigante di dipolo, in buon accordo con i dati sperimentali.

Per quanto riguarda la reazione di elettrodiffusione si presenta un calcolo delle funzioni di risposta longitudinale e trasversale per il nucleo di ^{4}He nella regione del picco quasi-elastico per valori intermedi del momento trasferito. Per gli operatori di carica e di corrente è stato utilizzato un modello non relativistico. Il calcolo è stato effettuato con un'interazione semirealistica ed un modello invariante di gauge è stato costruito introducendo una corrente di scambio. Vengono discussi i risultati preliminari riguardo l'effetto della corrente a due corpi sulla funzione di risposta trasversa ed infine si confrontano i risultati ottenuti con i dati sperimentali disponibili.

Zusammenfassung

In dieser Arbeit aus dem Bereich der Wenig-Nukleonen-Physik wird die neu entwickelte Methode der Lorentz Integral Transformation (LIT) auf die Untersuchung von Kernphotoabsorption und Elektronenstreuung an leichten Kernen angewendet. Die LIT-Methode ermöglicht exakte Rechnungen durchzuführen, ohne explizite Bestimmung der Endzustände im Kontinuum. Das Problem wird auf die Lösung einer bindungzustandsähnlichen Gleichung reduziert, bei der die Endzustandswechselwirkung vollständig berücksichtigt wird. Die Lösung der LIT-Gleichung wird mit Hilfe einer Entwicklung nach hypersphärischen harmonischen Funktionen durchgeführt, deren Konvergenz durch Anwendung einer effektiven Wechselwirkung im Rahmem des hypersphärischen Formalismus (EIHH) beschleunigt wird. In dieser Arbeit wird die erste mikroskopische Berechnung des totalen Wirkungsquerschnittes für Photoabsorption unterhalb der Pionproduktionsschwelle an ^{6}Li, ^{6}He und ^{7}Li vorgestellt. Die Rechnungen werden mit zentralen semirealistischen NN-Wechselwirkungen durchgeführt, die die Tensor Kraft teilweise simulieren, da die Bindungsenergien von Deuteron und von Drei-Teilchen-Kernen richtig reproduziert werden. Der Wirkungsquerschnitt für Photoabsorption an ^{6}Li zeigt nur eine Dipol-Riesenresonanz, während ^{6}He zwei unterschiedliche Piks aufweist, die dem Aufbruch vom Halo und vom α-Core entsprechen. Der Vergleich mit experimentellen Daten zeigt, dass die Addition einer P-Wellen-Wechselwirkung die Übereinstimmung wesentlich verbessert. Bei ^{7}Li wird nur eine Dipol-Riesenresonanz gefunden, die gut mit den verfügbaren experimentellen Daten übereinstimmt. Bezüglich der Elektronenstreuung wird die Berechnung der longitudinalen und transversalen Antwortfunktionen von ^{4}He im quasi-elastischen Bereich für mittlere Werte des Impulsübertrages dargestellt. Für die Ladungs- und Stromoperatoren wird ein nichtrelativistisches Modell verwendet. Die Rechnungen sind mit semirealistischen Wechselwirkungen durchgefürt und ein eichinvarianter Strom wird durch die Einführung eines Mesonaustauschstroms gewonnen. Die Wirkung des Zweiteilchenstroms auf die transversalen Antwortfunktionen wird untersucht. Vorläufige Ergebnisse werden gezeigt und mit den verfügbaren experimentellen Daten verglichen.

Contents

Outline

This work has been undertaken during three years of PhD studies. The first part of this period has been spent in Italy at the University of Trento, in the Department of Physics, and the second half in Germany, at the "Institut für Kernphysik" of the Johannes Gutenberg-University in Mainz.

Some of the results of this thesis are summarized in these papers [Bac02, Bac04, Bac04b, Bac05]. The aim of writing this thesis is to give a thorough presentation of the results obtained in these years, explaining the details of the calculations and showing also the first developments of very recent investigations which are still under work.

The presentation follows this structure:

- **Chapter 1**
  We give an introduction to the subject of few-body nuclear problems concentrating on electromagnetic interactions. Particular attention is paid to the motivation of this work.

- **Chapter 2**
  The method of the Lorentz Integral Transform (LIT) is discussed in detail. The attention is focused on the application of this method to inclusive reactions, which are the main subject of the present work.

- **Chapter 3**
  A brief introduction to the electromagnetic interactions is presented. Particular attention is given to the multipole decomposition of the electromagnetic charge and current operators. At the end, an overview of the basic electromagnetic reactions, i.e. photoabsorption and electron scattering, is given.

- **Chapter 4**
  The evaluation of a matrix element in the internal coordinates of an A-body system is discussed. The hyperspherical formalism is used and the calculation

of the matrix elements for one-body and two-body operators is presented. At the end a brief discussion on the effective interaction with the hyperspherical harmonics (EIHH) is also given.

- **Chapter 5**
  An application of the LIT method in conjunction with the EIHH technique on nuclear photodisintegration reactions is shown. The first microscopic calculation of the total photoabsorption cross sections of six- and seven-body nuclei is presented. A general description of the calculation is given and the obtained results are discussed.

- **Chapter 6**
  We present an application of the LIT and EIHH methods to electron scattering showing the results obtained for the inclusive process on ^{4}He. Both the longitudinal and transverse response functions are investigated. The discussion is divided between the longitudinal and transverse response functions, and the corresponding charge and current operators are treated separately.

- **Chapter 7**
  We conclude with a summary of the obtained results, focusing the attention on the goals achieved and on the remaining open questions. We also present an overview on possible future developments.

Chapter 1

Introduction

This thesis is conducted in the field of few-body physics. The topic of the research is the microscopic study of the dynamics of light nuclear systems. The quantum mechanical few-body problem is an important still partially unsolved problem in physics. It refers to the difficulties of explaining how a collection of particles responds to the fundamental forces acting between them.

In order to study the dynamics of a nucleus, that is ruled by the nuclear force, we investigate its response to electromagnetic probes, like photons or electrons. Probing nuclei with electromagnetic interactions, which are weak ($e^2/\hbar c \ll 1$), enables a clear separation of the scattering process itself from the effects due to the nuclear structure. These probes can therefore be seen as a very useful tool to investigate the nuclear dynamics.

It is now accepted that QCD is the theory which underlines all of nuclear structure. However, how nuclear physics depends on the fundamental degrees of freedom is still an open question. In fact, in the low energy regime of nuclear physics, QCD is non perturbative and as of today the problem has not been solved exactly. Nowadays there are two main methods which try to solve this longstanding problem, i.e. lattice QCD and effective field theory (EFT). On the other hand, nuclear structure is very well described in terms of the nucleonic and mesonic degrees of freedom. The basic nuclear interaction is very well described by semi-phenomenological high precisions NN potentials, based on meson exchanges, which reproduce an enormous amount of scattering data. However, in the three-body problem it has been found that two-body forces alone are not enough to correctly describe the binding energies, but additional three-body interactions have to be considered. For havier nuclei the study of their structure using such semi-phenomenological two- and three-body interactions is a very interesting and actual topic.

Light nuclei composed by few nucleons are weakly bound systems and as such they present very few, if any, bound excited states. Experiments designed to investigate the dynamics of light nuclei normally deal with continuum excitations, studying the transition from the ground state to resonances embedded in the continuum. Inelastic continuum reactions, where the final state is different from the initial one and in which one or more nucleons are knocked out from the initial nucleus, are thus the main source of interest. Clearly, in such a scenario, the fragments in the final state interact with each other, giving rise to the so called final state interaction (FSI).

From a theoretical point of view, for the description of an inelastic reaction one needs to know the initial and final nuclear wave functions, i.e. one has to solve the Schrödinger equation to find the spectrum of the nuclear hamiltonian. However, it turns out that the study of the continuum states is much more difficult than the study of bound states.

In case of few-body systems, one can try to tackle the problem with a microscopic approach, solving exactly the Schrödinger equation to investigate the fine details of the dynamics. The explicit calculation of a final state wave function (FSWF) can be done for the lightest nucleus, the deuteron, but already for the $A = 3$ nuclei, at energies with various open channels, it is rather complicated from the numerical point of view. Modern calculations use either variational methods or solve the Faddeev equations [Glo83]. Such an approach is applicable up to the four-body problem (Faddeev-Yakubowski) only below the three-body disintegration threshold, but it is presently out of reach for systems with $A > 4$. For the "classical" few-body systems ($2 \leq A \leq 4$), where the explicit evaluation of the final states can be performed with the above mentioned restriction, detailed calculations with realistic potentials are available. However, for "bigger" light nuclei the situation is different. Traditionally, due to shortcomings of microscopic calculations, one often used to describe such systems within a cluster model, in which the excited nucleus is treated as a two or three-body system according to its fragmentation, reducing the calculation to a solvable two or three-body problem. The cluster approach has revealed to be very useful, although it has obvious limitations, in the sense that the genuine microscopic approach is then lost.

Nowadays, thanks to the enormous progresses made in the theory and thanks to new computational facilities, it is possible to perform ab initio calculations of continuum excitations in nuclei with $A \geq 4$ also above the three-body disintegration threshold. In fact, it has been shown that using an integral transform approach the extremely complicated calculation of the continuum wave functions is not anymore

necessary. With the help of the Lorentz Integral Transform [Efr94], the evaluation of a response function is reduced to a bound state like calculation and the full final state interaction is taken automatically into account. Though the FSWF is not explicitly calculated, FSI effects on the response are exactly considered. There are quite a few examples for the application of this approach to few-body nuclei up to A=4 (see e.g. Refs. [Efr97a, Efr97b, Efr00, Bar01b, Efr01, Rei03, Qua04]) and agreement of this new approach with standard methods has been shown, where possible.

In this thesis we apply this technique to the study of nuclear photoabsorption and electron scattering. In particular the inclusive photoabsorption of $A > 4$ nuclei is firstly tackled and then the first approach to the calculation of the inclusive longitudinal and transverse response functions for the electron scattering off the α particle is shown.

1.1 Nuclear Photoabsorption

It is important to note that measurements of nuclear photoabsorption reactions, $\gamma + A \rightarrow X$, have been performed some 20-30 years ago for a wide number of nuclei with different mass number A. The dominant feature in the measured cross sections was a giant resonance, peaked between 10 and 30 MeV, observed in almost all nuclei. Since it is mainly due to the absorption of the dipole component of the incoming photon and almost exhausted the Thomas-Reiche-Kuhn sum rule [Eis70], it was called giant dipole resonance (GDR). Unfortunately, after the '70s the experimental activity on this subject was not carried on further, also because of missing theoretical guidance. Namely, at that time the theoretical explanation of the giant dipole resonance was given in terms of collective motions of protons and neutrons and the big difficulties of performing a microscopic calculation had damped the interest. Only in the last years there is a renewed interest, however, merely for the halo nuclei (see e.g. [Aum98]).

Nowadays, thanks to the enormous progress in few-body theory new precise microscopic calculations can be carried out and some more light can be shed on this previously unsolved problem. One has also to note that in the last decade there has been a tremendous progress in microscopic bound state calculations of systems with A>4, which is only partly due to an increase of the numerical power of modern computers, but also to various new microscopical approaches (Green Function Monte Carlo (GFMC) [Wir01], Stochastic Variational Method (SVM) [Suz01], No Core Shell Model (NCSM) [Nav99, Nav00], Effective Interaction with the Hyper-

spherical Harmonics (EIHH) [Bar01, Bar01a]). In particular, the combination of the LIT method with the EIHH has enabled us to start a new project on microscopic calculations of inelastic reactions involving A>4 nuclei with full final state interaction. These pioneering calculations are performed with simple semirealistic potentials. In case of the three-body problem it has been shown that semirealistic potentials lead already to quite a realistic description of the total photoabsorption cross section [Efr00]. Of course this is not a guarantee that this will be the same in case of bigger systems. Nevertheless, since no other microscopic calculations of reactions on $A > 4$ nuclei exist, we would like to push forward the subject by starting with a simple interaction, expecting it to reproduce at least the gross properties of the reaction.

In this work we present the first microscopic calculation of the total photoabsorption cross sections of the six-body nuclei ^{6}Li and ^{6}He and of the seven-body nucleus ^{7}Li. Here we would like to mention that traditionally systems with a number of particles between 4 and about 15 were considered neither few-body nor many-body systems and thus they are seen as an interesting playground to test the validity of many-body approximations and to establish a transition region where few- and many-body physics merge. The final aim of the work is to go towards a microscopic view of collective aspects in nuclear physics and to test the effect of the different parts of the NN interactions on the reaction mechanism. Another motivation for this study is also represented by possible applications to astrophysics, where such inclusive photoabsorption reactions are relevant to explain the nucleosyntesis process.

1.2 Electron Scattering

In lowest order of electron scattering, a virtual photon is exchanged between the probing electron and the target. Energy and momentum transfer can vary independently, in contrast to the case of real photoabsorption. For this reason it constitutes a much richer field to study the dynamics of a nuclear system. In case of inclusive unpolarized electron scattering, i.e. in the reaction $A(e, e')$, where no fragment of the target is detected in coincidence with the scattered unpolarized electron, the cross section can be written in terms of the longitudinal and transverse response functions, which can be disentangled via a Rosenbluth separation.

The quasi-elastic region of the response has attracted particular attention in the past as a good playground to study the effect of the nuclear tensor correlations and

of the two-body electromagnetic currents. However, providing a good description of the initial bound and of the final continuum states has always constituted the main theoretical difficulty.

In the literature several calculations of the longitudinal and transverse response functions for different nuclei have been shown, mainly in the plane wave impulse approximation (PWIA), where no FSI is considered, see e.g. [Cio91, Lag91]. Such calculations tend to drastically overestimate the experimental data in case of the longitudinal response and to slightly underestimate the transverse response in the quasi-elastic region. In case of heavy nuclei it is difficult to understand the reason of that, especially because in that case higher order contributions like Coulomb corrections become relevant and difficult to treat. Nevertheless, for massive nuclei it is almost impossible to give a description of the FSI, if not in terms of phenomenological optical potentials.

On the contrary, in case of few-body nuclei, where the one photon exchange approximation can be used and where also the final state interaction can be considered, it has been shown that the excess of strength in the longitudinal response is mainly due to the effect of the FSI, see e.g. [Are99, Glo04, Efr04]. The interaction in the final state is stronger in case of the monopole and therefore is not present in the transverse response, where the PWIA fails only by about 10%.

On the other hand, the lack of transverse strength found by the theory for various nuclei was usually attributed to the contribution of the two-body current to the response function, which was missing or not completely treated. Theoretical calculations of two-body contributions in the region of the quasi-elastic peak have been performed by many groups, but the effect found varies between 10 and 40%, such that the picture is not yet clear. Usually, calculations based on a independent-particle initial state lead to a small contribution of the two-body current, while calculations including short range correlation show appreciable effects, see e.g. [Fab97, Lei90, Car94, Car02]. For few-body systems detailed calculations of the transverse response which include a complete treatment of the FSI and of the two-body currents exist up to the three-body problem, with fully realistic forces. However, in case of ^{4}He the only "exact" calculations of the transverse response function which takes into account the FSI are performed via a Laplace transform with a Green Function Monte Carlo technique and results are shown in the euclidian space [Car94, Car02]. Although a significant effect of the consistent two-body current is found and fully realistic interactions have been used, it is difficult to understand how the effect of the nuclear hamiltonian and of the current operator is

reflected in going from the euclidian space to the response function.

This difficulty is not found in case of the LIT transform, as will be pointed out. With the help of the LIT and EIHH methods we would like to gain insight on this scenario in the few-body regime, performing calculations where the FSI is exactly taken into account and the current is constructed imposing gauge invariance.

In this thesis the first important steps in this direction are presented. As a test case ^{4}He has been chosen and a semirealistic interaction model is used. Clearly, with this model we will not be able to clarify the role of the pionic degrees of freedom, such as tensor force and pion in flight or contact term of the two-body current, in the reaction. This is certainly the final aim of this project, towards which we start with a simpler example.

Chapter 2

The Lorentz Integral Transform Method

In this chapter the method of the Lorentz Integral Transform (LIT) will be discussed in detail. Although the method is very general and can be applied also to exclusive processes [Lap00, Qua04], we will focus the attention on the application to inclusive reactions, since only these are studied in the present work.

2.1 Introduction

The study of inclusive and exclusive reactions is of great importance for the understanding of the dynamics of nuclear systems. From the theoretical point of view, one of the major obstacles in such a study is the need of an explicit calculation of the wave functions that describe the final states in the continuum, which is in practice much more complicated than a calculation of a bound state. Nowadays it is possible to calculate explicitly final states in the continuum for nuclei with mass number $A \leq 4$, but it is presently out of reach for nuclei with $A > 4$. For this reason, alternative methods have been proposed, like the integral transform method, that do not require the explicit calculation of continuum wave functions, thus leading to a big simplification of the problem. One example is the Lorentz Integral Transform (LIT) method, that recently has been applied to the study of electromagnetic reactions on few-body nuclei, see e.g. [Efr97b, Efr97c, Efr00, Lap00, Efr01, Bar01b, Rei03, Qua04].

2.2 Integral Transform Method for Inclusive Processes

In an inclusive electromagnetic reaction the response function of the system to an external electromagnetic probe, described by an operator $O(\mathbf{q})$, is defined as

$$R(\omega, \mathbf{q}) = \sum\!\!\!\!\!\!\int_f |\langle \Psi_0 | O(\mathbf{q}) | \Psi_f \rangle|^2 \, \delta(E_f - E_0 - \omega), \tag{2.1}$$

where $\left|\Psi_{0/f}\right\rangle$ and $E_{0/f}$ denote initial and final state wave functions and energies, respectively, and ω the energy of the probe. The δ-function ensures energy conservation. One readily notes that the definition of the response function includes a sum over all possible final states, also in the continuum, which are induced by the electromagnetic probe (the notation $\sum\!\!\!\!\!\!\int_f$ in (2.1) means an integration over the continuum states plus a summation over the bound states). As mentioned above, this quantity cannot be calculated exactly using standard techniques for an arbitrary A-body system, since the explicit calculation of the final state wave functions constitutes the main bottleneck. Using an integral transform approach these difficulties can be circumvented, and the problem is reduced to the solution of a bound state like equation.

The starting point of such an approach is the application of an integral transform to the response function as follows

$$\phi(\sigma, \mathbf{q}) = \int_{0^-}^{\infty} d\omega R(\omega, \mathbf{q}) K(\omega, \sigma), \tag{2.2}$$

where $K(\omega, \sigma)$ is the kernel of the transform, which depends on a continuous parameter σ. The integration over the energy extends from 0^- to take into account the possible elastic contributions in the response function. In case that no elastic channel exists, but only inelastic bound state excitations are present, the integration extends from ω^{*-}, where ω^* is the energy of the first excited state. Finally, in case that only reactions in the continuum are induced by the operator O the integration has to start from the disintegration threshold ω_{th}, below which the response function is identically zero. The only requirement to be fulfilled is the convergence of the integral in (2.2), which will depend on the particular choice of the functional form of the kernel and on the behavior of the response function itself, which one assumes to go to zero at high energies. In case that the transform $\phi(\sigma, \mathbf{q})$ exists, it can be calculated solving a bound state problem, as will be shown in the next section. The

response $R(\omega, \mathbf{q})$ is then obtained by inverting (2.2) and it automatically includes the complete final state interaction.

2.3 Choice of the Kernel

In the literature several transforms with different kernels have been proposed, like, for example, the Laplace transform with

$$K(\omega, \sigma) = e^{-\sigma\omega}$$

or the Stieltjes transform with

$$K(\omega, \sigma) = \frac{1}{\omega + \sigma}.$$

A criterion for the choice of the kernel is of course the possibility to calculate numerically the transform. Furthermore, one can discuss the choice of the kernel from the point of view of a stable reconstruction of the response from the integral equation (2.2). For a given numerical accuracy the inversion of the transform ϕ is more stable if the kernel is chosen as narrow as possible. If the kernel is broad with respect to structures in the response, then such structures having an energy range smaller than the range of the kernel itself will be smeared out. This can make the reconstruction of the response difficult in view of the presence of unavoidable numerical inaccuracies of ϕ.

Keeping in mind that the best kernel has to be very narrow, one could firstly think of the δ-function

$$K(\omega, \sigma) = \delta(\omega - \sigma)$$

as the best choice. In this case, however, ϕ would be identical to the response, thus leading back to the problem of the calculation of continuum states. The idea is then to use a kernel

$$K(\omega, \sigma) = f(\omega - \sigma, \varepsilon),$$

which is an approximation of the δ-function [Wea75], such that

$$\lim_{\varepsilon \to 0} f(\omega - \sigma, \varepsilon) = \delta(\omega - \sigma).$$

The gaussian and the lorentzian curves are two possible examples in this sense

$$\begin{aligned} f(\omega-\sigma,\varepsilon) &= \frac{1}{\varepsilon\sqrt{\pi}} e^{-(\omega-\sigma)^2/\varepsilon^2}, \\ f(\omega-\sigma,\varepsilon) &= \frac{\varepsilon}{\pi\left((\omega-\sigma)^2+\varepsilon^2\right)}. \end{aligned}$$

The choice of the best kernel is obviously governed by the properties of the equation for the determination of the transform. In case of the gaussian-shaped kernel one would have to deal with an operator like e^{-H^2}, where H is the hamiltonian of the system[1]. Of course this would make the numerical calculations much more difficult. This problem does not arise in case one deals with the lorentzian kernel, which leads to a simple equation as will be shown in the following section.

2.4 The Lorentz Integral Transform

For the Lorentz Integral Transform (LIT) one chooses a kernel with lorentzian shape

$$K(\omega,\sigma) = \frac{1}{(\omega-\sigma_R)^2+\sigma_I^2},$$

where $\sigma = -\sigma_R + i\sigma_I$ is a complex parameter. The LIT is then defined by

$$\mathcal{L}(\sigma,\mathbf{q}) = \int_{0^-}^{\infty} d\omega \frac{R(\omega,\mathbf{q})}{(\omega-\sigma_R)^2+\sigma_I^2}, \tag{2.3}$$

that may be viewed as a generalized sum rule depending on a continuous parameter σ. The main advantage of the LIT method is that the evaluation of $\mathcal{L}(\sigma,\mathbf{q})$ does not require the explicit knowledge of the response function, and therefore of the final states $|\Psi_f\rangle$. As soon as $\mathcal{L}(\sigma,\mathbf{q})$ is given, the response $R(\omega,\mathbf{q})$ is obtained from an inversion of the transform.

For the calculation of the $\mathcal{L}(\sigma,\mathbf{q})$ one notes first that it can be expressed as

$$\mathcal{L}(\sigma,\mathbf{q}) = \int_{0^-}^{\infty} d\omega R(\omega,\mathbf{q}) \frac{1}{(\omega+\sigma^*)} \frac{1}{(\omega+\sigma)}. \tag{2.4}$$

[1]This can be understood performing a calculation analogous to that shown in Section 2.4 for the lorentzian kernel.

Then, using the definition of the response function in (2.1) one gets

$$\mathcal{L}(\sigma,\mathbf{q}) = \int_{0^-}^{\infty} d\omega \sum\!\!\!\!\!\!\int_f \langle\Psi_0|\, O^\dagger(\mathbf{q}) \frac{1}{(\omega+\sigma^*)} \,|\Psi_f\rangle\langle\Psi_f|\, \frac{1}{(\omega+\sigma)} O(\mathbf{q})\,|\Psi_0\rangle\, \delta(E_f - E_0 - \omega),$$

which yields

$$\mathcal{L}(\sigma,\mathbf{q}) = \sum\!\!\!\!\!\!\int_f \langle\Psi_0|\, O^\dagger(\mathbf{q}) \frac{1}{(E_f - E_0 + \sigma^*)} \,|\Psi_f\rangle\langle\Psi_f|\, \frac{1}{(E_f - E_0 + \sigma)} O(\mathbf{q})\,|\Psi_0\rangle\,,$$

after integrating out the δ-function. Using then the fact that the states $|\Psi_f\rangle$ are eigenstates of the hamiltonian H of the system, namely

$$H\,|\Psi_f\rangle = E_f\,|\Psi_f\rangle\,,$$

one gets for the LIT the following expression

$$\mathcal{L}(\sigma,\mathbf{q}) = \sum\!\!\!\!\!\!\int_f \langle\Psi_0|\, O^\dagger(\mathbf{q}) \frac{1}{(H - E_0 + \sigma^*)} \,|\Psi_f\rangle\langle\Psi_f|\, \frac{1}{(H - E_0 + \sigma)} O(\mathbf{q})\,|\Psi_0\rangle\,.$$

As last step one uses the closure relation

$$\sum\!\!\!\!\!\!\int_f |\Psi_f\rangle\,\langle\Psi_f| = 1,$$

yielding for the LIT

$$\mathcal{L}(\sigma,\mathbf{q}) = \langle\Psi_0|\, O^\dagger(\mathbf{q}) \frac{1}{(H - E_0 + \sigma^*)} \frac{1}{(H - E_0 + \sigma)} O(\mathbf{q})\,|\Psi_0\rangle\,. \tag{2.5}$$

This expression obviously has the simple form of a squared norm

$$\mathcal{L}(\sigma,\mathbf{q}) = \left\langle \widetilde{\Psi} \;\middle|\; \widetilde{\Psi} \right\rangle, \tag{2.6}$$

with

$$\left|\widetilde{\Psi}\right\rangle = \frac{1}{(H - E_0 + \sigma)} O(\mathbf{q})\,|\Psi_0\rangle\,.$$

Therefore, the evaluation of the Lorentz transform requires the solution of the following differential equation

$$(H - E_0 + \sigma)\left|\widetilde{\Psi}\right\rangle = O(\mathbf{q})\,|\Psi_0\rangle\,. \tag{2.7}$$

This equation has an unique solution and is Schrödinger-like, since it has the same formal structure as the Schrödinger equation, except for an inhomogeneous source term on the right-hand-side. Furthermore, since the norm of the right-hand-side is finite because of the presence of the ground state $|\Psi_0\rangle$, also the left-hand-side of the equation has to fulfil the same boundary condition. This means that the state $\left|\widetilde{\Psi}\right\rangle$ has a finite norm, i.e. it goes to zero at large distances similarly to a bound state.

In the light of the last considerations it is clear that in the Lorentz Integral Transform method the difficulty of the continuum wave functions is avoided and the problem is reduced to the solution of a bound state like equation, thus leading to a big simplification of the task.

2.5 Method of the Inversion

Once one has evaluated an integral transform $\phi(\sigma, \mathbf{q})$ of the response, one has to invert it in order to obtain the desired response function $R(\omega, \mathbf{q})$, which is the observable one would like to compare with experimental measurements.

From a mathematical point of view the integral transform in (2.2) can be written as

$$\mathcal{I}\{R(\omega, \mathbf{q})\} = \phi(\sigma),$$

where $\mathcal{I}$ denotes the integral transform as a functional of $R(\omega, \mathbf{q})$, and "inverting" the transform means finding the inverse kernel of the inverse functional $\mathcal{I}^{-1}$ such that

$$\mathcal{I}^{-1}\{\phi(\sigma)\} = R(\omega, \mathbf{q}).$$

Unfortunately, $\mathcal{I}^{-1}$ is not always analytically given, and in this case the transform cannot be analytically inverted. The numerical inversion belongs to a class of problems denoted in the literature as "ill posed problems". The LIT case is an example of transform, whose inverse kernel is not analytically defined.

In principle, one could also compare the calculated transform of a response function with the corresponding transform of the response function determined by experimental data [Car94, Car02]. This is possible only when measurements extend on a wide energy spectrum which enable an integration up to infinity or a clear data extrapolation of the high energy behavior. Furthermore, although this procedure does not require the inversion of the transform and therefore the solution of an "ill posed problem", it can be misleading because the underlying physics may be obscured by the fact that dynamical aspects of different nature of the response are

combined in the transform (low energy and high energy properties). Therefore it is preferable to go through the inversion.

In order to perform the inversion of the LIT one has to solve the integral equation in (2.2), which is recalled here

$$\mathcal{L}(\sigma, \mathbf{q}) = \int_{0^-}^{\infty} d\omega R(\omega, \mathbf{q}) \frac{1}{(\omega - \sigma_R)^2 + \sigma_I^2},$$

numerically. One method for finding a numerical solution is based on an expansion

$$R(\omega, \mathbf{q}) = \sum_{n=1}^{N} c_n \chi_n(\omega, \mathbf{q}, \alpha), \tag{2.8}$$

where $\{\chi_n(\omega, \mathbf{q}, \alpha)\}$ is a set of known functions that depend on a parameter α. For each α they form a complete set. These functions are chosen such that their integral transform is well known

$$\mathcal{L}_n(\sigma, \mathbf{q}, \alpha) = \mathcal{I}\{\chi_n(\omega, \mathbf{q}, \alpha)\}.$$

This means that the integral transform of the response will be

$$\mathcal{L}(\sigma, \mathbf{q}) = \sum_{n=1}^{N} c_n \mathcal{L}_n(\sigma, \mathbf{q}, \alpha), \tag{2.9}$$

via the same coefficients c_n of (2.8), since the integral transform is a linear operation. The coefficients of the expansion are obtained from a best fit requiring

$$\sum_{k=1}^{K} \left| \mathcal{L}(\sigma_R^k, \sigma_I, \mathbf{q}) - \sum_{n=1}^{N} c_n \mathcal{L}_n(\sigma_R^k, \sigma_I, \mathbf{q}, \alpha) \right|^2 = \min, \tag{2.10}$$

for fixed α and σ_I, and for a sufficiently large set of $\{\sigma_R^k, k = 1, ..., K\}$ values. This problem then reduces to the solution of a system of linear equations, which still can become "ill posed" if N is of the order of K. Namely, it is well known that a solution to Eq. (2.2) is unstable with respect to high frequency oscillations. This means that one has to apply a regularization procedure [Efr99b, Efr99a] in order to find a regularized solution that suppresses the high frequency oscillations. In this case one chooses the number N of basis function of the expansion (2.8) much smaller than the number K of values for the parameter σ_R. Therefore N plays then the role of a regularization parameter and solutions for the response are found in a

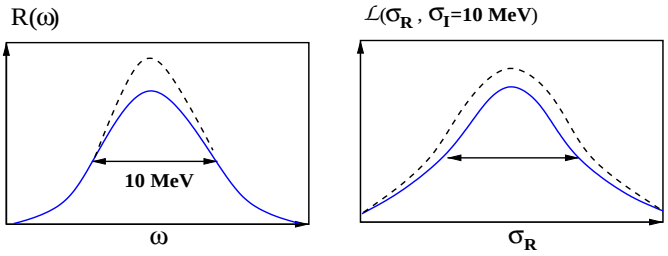

Figure 2.1: Two responses that differ from each other in an energy range of the order of σ_I correspond to two different curves in the transformed space.

region of stability of N, which can be checked using different sets of functions for the expansion of the response in (2.8). Two possible sets, that have been used, are presented below

$$\begin{aligned} \chi_n(\omega,\alpha) &= \omega^{n+\frac{1}{2}} e^{-\frac{\omega}{\alpha}}, \\ \chi_n(\omega,\alpha) &= \omega^{n_0} e^{-\frac{\omega}{n\alpha}}, \text{with } n_0 \text{ const.} \end{aligned}$$

It turns also out that the inclusion of the known threshold behavior of $R(\omega,\mathbf{q})$ into the basis functions increases the accuracy of the inversion. For similar reasons every known information of the response function should be taken into account in the choice of the basis functions for the inversion. Finally, the quality of the inversion can be checked by calculating known sum rules via the integration of the response.

A big advantage of the Lorentz transform is the presence of a complex parameter σ, which means that in practice one has an additional degree of freedom, the imaginary part σ_I, with respect to a transform with only a purely real parameter. Since it determines the size of the "range" of the transform, it plays the role of an energy resolution. It therefore has to be chosen sufficiently small, since any two responses different form each other in an energy interval comparable with σ_I lead to different transforms, as shown in Fig. 2.1, and thus can be discriminated also in the presence of numerical errors in the calculation of $\mathcal{L}$. Clearly, the smaller σ_I is, the more difficult it is to reach high precision in the calculation of the Lorentz transform. Therefore the most convenient value for σ_I is of the order of the width of the response function. Different values of σ_I can then be chosen for performing a test on the inversion procedure, since the resultant $R(\omega,\mathbf{q})$ has not to depend on this parameter. This constitutes a very strong check on the method, and it is an additional reason to consider the lorentzian kernel as the preferable choice.

Chapter 3

Electromagnetic Interaction

The electromagnetic interaction is the best understood force in physics and it also constitutes a very important tool for the study of nuclear structure. The excitation of nuclei with electromagnetic probes enables one to obtain information on the nuclear dynamics, which, on the other hand, is governed by the strong interaction.

Since the interaction is relatively weak, of the order of the fine structure constant $\alpha = 1/137$, a perturbative approach can be used and in most of the cases the lowest order of perturbation theory is sufficient. This allows a simple interpretation of the observables. In other words

"*With the electromagnetic probe, we can immediately relate the cross section to the transition matrix element of the current operator and thus directly to the structure of the target itself*"
[De Forest-Walecka, Ann. Phys. 1966].
This is not the case for the reactions on nuclei with strongly interacting projectiles, e.g. with pions or protons. The big advantage of studying electromagnetic reactions on nuclei is that the observables are related to the current matrix element

$$J^{\mu}_{f0} = \langle \Psi_f | \, J^{\mu} \, | \Psi_0 \rangle \, , \tag{3.1}$$

where $|\Psi_0\rangle$ and $|\Psi_f\rangle$ describe the initial ground state and final state of the studied nucleus, respectively, and J^{μ} is the electromagnetic current operator.

From a theoretical point of view one has to construct an electromagnetic current consistent with the dynamical framework and then the main effort has to be addressed to a good description of the wave functions of the system. This part will be discussed in the next chapter. In the following a brief review of the electromagnetic current and of its multipole decomposition is presented.

3.1 The Electromagnetic Current

Since the electromagnetic interaction is weak, it is reasonable to assume that it admits a Taylor expansion with respect to the electromagnetic potential $A_\mu(x)$ [Are99], which means that the interaction hamiltonian is

$$H_{int}(A) = \int d^3x j_\mu(x) A^\mu(x)|_{x_0=t} + ...$$

at first order. For a given hamiltonian $H_{int}(A)$, the current is obtained by taking the first functional derivative with respect to $A(x)$ at $A \equiv 0$

$$j_\mu(x) = \left.\frac{\delta H_{int}(A)}{\delta A^\mu(x)}\right|_{A\equiv 0}. \tag{3.2}$$

An important property is the gauge invariance which leads to the conservation of the electromagnetic current according to the Noether theorem, that reads

$$\partial^\mu j_\mu(x) = 0, \tag{3.3}$$

written in a covariant way. The above continuity equation can also be written in this way

$$\boldsymbol{\nabla} \cdot \mathbf{j}(\mathbf{x}) = -i[H, \rho(\mathbf{x})], \tag{3.4}$$

if the charge operator $\rho(\mathbf{x})$ does not depend explicitly on time. In the last equation H is the nuclear hamiltonian. Clearly, the gauge invariance condition implies the conservation of the electromagnetic charge

$$\frac{d}{dt}Q = 0,$$

where

$$Q = \int d^3x \rho(x).$$

The continuity equation has important consequences since it enables a simple expression for the current in the low energy regime, i. e. in the limit of zero momentum of the photon. This property, known as Siegert theorem [Sie37], will be shown later on, after the discussion of the multipole decomposition of the current.

3.2 Multipole Decomposition

The information on the internal dynamics of the nuclear system is contained in the current matrix elements (3.1). Since the intrinsic states of the nucleus can be classified according to the total angular momentum, it is very useful to perform a multipole decomposition of the charge and of the current operators, where each multipole transfers a definite angular momentum. The advantage of this approach is that one can use angular momentum selection rules and Wigner-Eckart theorem, separating the geometrical aspects form the dynamical properties of the system, which remain in the reduced matrix element.

First of all one considers the Fourier transform of the four-vector current operator

$$\tilde{\rho}(\mathbf{q}) = \int d^3x e^{i\mathbf{q}\cdot\mathbf{x}}\rho(\mathbf{x}), \tag{3.5}$$

$$\mathbf{J}(\mathbf{q}) = \int d^3x e^{i\mathbf{q}\cdot\mathbf{x}}\mathbf{j}(\mathbf{x}), \tag{3.6}$$

where one writes separately the charge and the current operators. In the following the multipole decomposition is performed separately for these two operators.

3.2.1 Charge Operator

The starting point of a multipole decomposition is the expansion of the plane wave in spherical harmonics [Edm74]

$$e^{i\mathbf{q}\cdot\mathbf{x}} = 4\pi \sum_{J\mu} i^J j_J(qx) Y^J_\mu(\hat{x}) Y^{J*}_\mu(\hat{q}), \tag{3.7}$$

where $\hat{x}$ denotes the angular coordinates of the vector $\mathbf{x}$ expressed in spherical coordinates (x, θ_x, φ_x), and $\hat{q}$ is the same for the vector $\mathbf{q}$. The symbols $j_J(qr)$ are the Bessel functions. Using this expression in the (3.5) one has

$$\tilde{\rho}(\mathbf{q}) = 4\pi \sum_{J\mu} i^J Y^{J*}_\mu(\hat{q}) \int d^3x \rho(\mathbf{x}) j_J(qx) Y^J_\mu(\hat{x}), \tag{3.8}$$

where one defines the Coulomb multipole to be

$$C_{J\mu}(q) = \frac{i^{-J}}{4\pi} \int d\hat{q}' \tilde{\rho}(\mathbf{q}') Y^J_\mu(\hat{q}') = \int d^3x \rho(\mathbf{x}) j_J(qx) Y^J_\mu(\hat{x}), \tag{3.9}$$

which is a spherical tensor of rank J, and therefore the corresponding matrix element can be calculated using the Wigner-Eckart theorem. The expression of the current operator in terms of the Coulomb multipoles is then

$$\tilde{\rho}(\mathbf{q}) = 4\pi \sum_{J\mu} i^J Y_\mu^{J*}(\hat{q}) C_{J\mu}(q). \tag{3.10}$$

3.2.2 Current Operator

Since the current operator is a vector, the expansion is done in terms of the vector spherical harmonics [Edm74]

$$\mathbf{Y}^\mu_{Jl1}(\hat{q}) = \sum_{m\xi} \langle l1J|m\xi\mu\rangle \, Y^l_m(\hat{q}) \mathbf{e}_\xi, \tag{3.11}$$

where $\mathbf{e}_\xi$, with $\xi = 0, \pm 1$, is a set of vectors defined with respect to a spherical basis

$$\begin{aligned} \mathbf{e}_1 &= -\frac{1}{\sqrt{2}}(\mathbf{e}_x + i\mathbf{e}_y) \\ \mathbf{e}_0 &= \mathbf{e}_z \\ \mathbf{e}_{-1} &= \frac{1}{\sqrt{2}}(\mathbf{e}_x - i\mathbf{e}_y). \end{aligned}$$

Here $(\mathbf{e}_x, \mathbf{e}_y, \mathbf{e}_z)$ are the three vectors defining the reference system. The vector spherical harmonics form a complete set on the unit sphere with

$$\int d\hat{q}' \; \mathbf{Y}^{\mu'*}_{J'l'1}(\hat{q}') \cdot \mathbf{Y}^\mu_{Jl1}(\hat{q}') = \delta_{JJ'}\delta_{ll'}\delta_{\mu,\mu'}. \tag{3.12}$$

The expansion of the electromagnetic current in momentum space reads [Gol00]

$$\mathbf{J}\,(\mathbf{q}) = 4\pi \sum_{lJ\mu} J^\mu_{Jl}(q) \mathbf{Y}^{\mu*}_{Jl1}(\hat{q}), \tag{3.13}$$

where the coefficients of the expansion are given by

$$J^\mu_{Jl}(q) = \frac{1}{4\pi} \int d\hat{q}' \mathbf{J}\,(\mathbf{q}') \cdot \mathbf{Y}^\mu_{Jl1}(\hat{q}'). \tag{3.14}$$

With the notation q the modulus $|\mathbf{q}|$ is meant, while $\hat{q}$ clearly denotes the angular coordinates (θ_q, φ_q). The vectors $\mathbf{q}$ and $\mathbf{q}'$ differ only for the orientation and not for the modulus.

According to angular momentum rules it is clear that l can assume only the

values $|J-1|$, J, and $J+1$, and therefore in (3.13) one can explicitly write the sum on l as

$$\mathbf{J}(\mathbf{q}) = 4\pi \sum_{J\mu} \left(J^{\mu}_{JJ-1}(q)\mathbf{Y}^{\mu *}_{JJ-11}(\hat{q}) + J^{\mu}_{JJ}(q)\mathbf{Y}^{\mu *}_{JJ1}(\hat{q}) + J^{\mu}_{JJ+1}(q)\mathbf{Y}^{\mu *}_{JJ+11}(\hat{q}) \right). \quad (3.15)$$

Defining then the following quantities with good parity

$$\mathbf{J}^{el}_{J\mu}(\mathbf{q}) = 4\pi \big(J^{\mu}_{JJ-1}(q)\mathbf{Y}^{\mu *}_{JJ-11}(\hat{q}) + J^{\mu}_{JJ+1}(q)\mathbf{Y}^{\mu *}_{JJ+11}(\hat{q}) \big), \quad (3.16)$$

$$\mathbf{J}^{mag}_{J\mu}(\mathbf{q}) = 4\pi J^{\mu}_{JJ}(q)\mathbf{Y}^{\mu *}_{JJ1}(\hat{q}) \quad (3.17)$$

with the meaning of electric and magnetic multipoles, respectively, the total current operator becomes

$$\mathbf{J}(\mathbf{q}) = \sum_{J\mu} \left(\mathbf{J}^{el}_{J\mu}(\mathbf{q}) + \mathbf{J}^{mag}_{J\mu}(\mathbf{q}) \right). \quad (3.18)$$

In this way one can collect the vector spherical harmonics with different parity $(-1)^J$ and $(-1)^{J+1}$, in the electric and magnetic part of the operator, respectively.

Concentrating firstly on the electric multipoles, one can show (see also [Bac01]) that the following expression holds

$$\begin{aligned} \mathbf{J}^{el}_{J\mu}(\mathbf{q}) &= \hat{\mathbf{q}} Y^{J*}_{\mu}(\hat{q}) \int d\hat{q}' \left(\hat{\mathbf{q}}' \cdot \mathbf{J}(\mathbf{q}') \right) Y^{J}_{\mu}(\hat{q}') \\ &+ \left(\hat{\mathbf{q}} \times \mathbf{Y}^{\mu *}_{JJ1}(\hat{q}) \right) \int d\hat{q}' \left(\hat{\mathbf{q}}' \times \mathbf{Y}^{\mu}_{JJ1}(\hat{q}') \right) \mathbf{J}(\mathbf{q}'), \end{aligned}$$

which means a separation into longitudinal and transverse components with respect to $\mathbf{q}$. Note that $\hat{\mathbf{q}}$ denotes the unitary vector $\frac{\mathbf{q}}{|\mathbf{q}|}$. Then one can define accordingly the longitudinal and the transverse electric multipoles as

$$L^{el}_{J\mu}(q) = \frac{1}{4\pi} \int d\hat{q}' \left(\hat{\mathbf{q}}' \cdot \mathbf{J}(\mathbf{q}') \right) Y^{J}_{\mu}(\hat{q}'), \quad (3.19)$$

$$T^{el}_{J\mu}(q) = \frac{i}{4\pi} \int d\hat{q}' \left(\hat{\mathbf{q}}' \times \mathbf{Y}^{\mu}_{JJ1}(\hat{q}') \right) \cdot \mathbf{J}(\mathbf{q}'). \quad (3.20)$$

The longitudinal and the transverse electric multipole are related to the multipoles in (3.14) as

$$L^{el}_{J\mu}(q) = \frac{\sqrt{J}}{\hat{J}} J^{\mu}_{JJ-1}(q) - \frac{\sqrt{J+1}}{\hat{J}} J^{\mu}_{JJ+1}(q), \quad (3.21)$$

$$T^{el}_{J\mu}(q) = -\frac{\sqrt{J+1}}{\hat{J}} J^{\mu}_{JJ-1}(q) - \frac{\sqrt{J}}{\hat{J}} J^{\mu}_{JJ+1}(q). \quad (3.22)$$

For the magnetic current, in an analogous way, one obtains

$$\mathbf{J}^{mag}_{J\mu}(\mathbf{q}) = \mathbf{Y}^{\mu *}_{JJ1}(\hat{q}) \int d\hat{q}' \mathbf{J}\left(\mathbf{q}'\right) \cdot \mathbf{Y}^{\mu}_{JJ1}(\hat{q}'), \tag{3.23}$$

from where one can get the definition of the magnetic multipoles

$$T^{mag}_{J\mu}(q) = \frac{1}{4\pi} \int d\hat{q}' \mathbf{J}\left(\mathbf{q}'\right) \cdot \mathbf{Y}^{\mu}_{JJ1}(\hat{q}') = J^{\mu}_{JJ}(q), \tag{3.24}$$

according to the (3.14), which is purely transverse, since

$$\hat{\mathbf{q}} \cdot \mathbf{Y}^{\mu}_{JJ1}(\hat{q}) = 0.$$

If one now chooses the direction of the photon momentum to be along the z-axis

$$\mathbf{q} = q\mathbf{e}_z = q\mathbf{e}_0,$$

then

$$\mathbf{Y}^{\mu}_{Jl1} = \langle l1J|0\mu\mu\rangle \frac{\hat{l}}{\sqrt{4\pi}}\mathbf{e}_{\mu}.$$

The multipole expansion of the current is therefore

$$\begin{aligned} \mathbf{J}\left(\mathbf{q}\right) &= \sum_{J\mu} \sqrt{4\pi}\hat{J}\left[L^{el}_{J\mu}(q)\mathbf{e}_0 + \mu\left\langle J1J|0\mu\mu\right\rangle T^{el}_{J\mu}(q)\mathbf{e}^*_{\mu}\right] \\ &+ \sum_{J\mu} \sqrt{4\pi}\hat{J}\left\langle J1J|0\mu\mu\right\rangle T^{mag}_{J\mu}(q)\mathbf{e}^*_{\mu}. \end{aligned} \tag{3.25}$$

Since the current is a vector, it has three components

$$J_{\lambda}\left(q\right) = \mathbf{e}_{\lambda} \cdot \mathbf{J}\left(\mathbf{q}\right)$$

with $\lambda = 0, \pm 1$ with respect to the spherical basis (3.12), where

$$J_{\lambda}\left(q\right) = (-)^{\lambda}\sqrt{2\pi(1+\delta_{\lambda 0})}\sum_{J} \hat{J}\left[L^{el}_{J\lambda}(q)\delta_{\lambda 0} + \left(T^{el}_{J\lambda}(q) + \lambda T^{mag}_{J\lambda}(q)\right)\delta_{|\lambda|1}\right]. \tag{3.26}$$

3.2.3 Siegert Theorem

The Siegert theorem states that in the low energy limit the transverse electric multipoles can be related to the Coulomb multipoles. This is a very important theorem, since it enables one to calculate electric transition matrix element knowing only the

charge density and therefore without an explicit expression of the current operator. Making use of

$$\hat{\mathbf{q}} \times \mathbf{Y}^{\mu}_{JJ1}(\hat{q}) = i\sqrt{\frac{J+1}{J}}\hat{\mathbf{q}}Y^{J}_{\mu}(\hat{q}) + i\frac{\hat{J}}{\sqrt{J}}\mathbf{Y}^{\mu}_{JJ+11}(\hat{q}),$$

the transverse electric multipole in (3.20) can be written as

$$T^{el}_{J\mu}(q) = -\frac{1}{4\pi}\int d\hat{q}' \left[\sqrt{\frac{J+1}{J}}\hat{\mathbf{q}}' \cdot \mathbf{J}(\mathbf{q}')\ Y^{J}_{\mu}(\hat{q}') + \frac{\hat{J}}{\sqrt{J}}\mathbf{Y}^{\mu}_{JJ+11}(\hat{q}') \cdot \mathbf{J}(\mathbf{q}')\right], \tag{3.27}$$

where the part proportional to $\mathbf{q}' \cdot \mathbf{J}(\mathbf{q}')$ can be written in terms of the Coulomb multipoles making use of the continuity equation. In momentum space current conservation reads

$$\mathbf{q} \cdot \mathbf{J}(\mathbf{q}) = \omega\tilde{\rho}(\mathbf{q}), \tag{3.28}$$

which means that the transverse multipole is given by

$$\begin{aligned} T^{el}_{J\mu}(q) &= -\frac{1}{4\pi}\int d\hat{q}' \left[\sqrt{\frac{J+1}{J}}\frac{\omega}{q}\tilde{\rho}(\mathbf{q}')Y^{J}_{\mu}(\hat{q}') + \frac{\hat{J}}{\sqrt{J}}\mathbf{Y}^{\mu}_{JJ+11}(\hat{q}') \cdot \mathbf{J}(\mathbf{q}')\right] \\ &= S^{el}_{J\mu}(q) + K^{el}_{J\mu}(q), \end{aligned} \tag{3.29}$$

introducing the Siegert operator

$$S^{el}_{J\mu}(q) = -\frac{1}{4\pi}\sqrt{\frac{J+1}{J}}\frac{\omega}{q}\int d\hat{q}'\tilde{\rho}(\mathbf{q}')Y^{J}_{\mu}(\hat{q}') \tag{3.30}$$

and the correction to the Siegert operator

$$K^{el}_{J\mu}(q) = -\frac{1}{4\pi}\frac{\hat{J}}{\sqrt{J}}\int d\hat{q}'\mathbf{Y}^{\mu}_{JJ+11}(\hat{q}') \cdot \mathbf{J}(\mathbf{q}'). \tag{3.31}$$

In the limit that the photon momentum goes to zero the dominant part of the electric transverse multipole is given by the Siegert operator, since the correction $K^{el}_{J\mu}(q)$ is two powers higher in q (this is easily shown in coordinate space, see also [Bac01]). Obviously, the Siegert operator is given by the Coulomb operator of (3.9) as

$$S^{el}_{J\mu}(q) = -\sqrt{\frac{J+1}{J}}\frac{\omega}{q}i^{J}C_{J\mu}(q). \tag{3.32}$$

The approximation of the electric transverse multipole by the Siegert operator is quite reliable at low photon momentum, i.e. $qR \ll 1$, where R characterizes the spatial extension of the system. However, with increasing $\mathbf{q}$, it is necessary to calculate also the contribution of $K^{el}_{J_\mu}(q)$, where one has to know the explicit form of the current operator.

3.3 Models for the Electromagnetic Operators

The construction of the electromagnetic current is straightforward for point particles. For a given hamiltonian one can use the method of minimal substitution and then the current is found using (3.2), applying the derivative with respect to the electromagnetic potential [Are82, Are90].

If one considers a free particle with mass m and charge e, described by a non-relativistic hamiltonian $H_0 = \frac{\mathbf{p}^2}{2m}$, using the method of minimal substitution

$$\begin{aligned} H_0 &\to H_0 - eA_0(\mathbf{r}), \\ \mathbf{p} &\to \mathbf{p} - e\mathbf{A}(\mathbf{r}), \end{aligned}$$

one obtains

$$H(A) = H_0 - \frac{e}{2m}(\mathbf{p}\cdot\mathbf{A}(\mathbf{r}) + \mathbf{A}(\mathbf{r})\cdot\mathbf{p}) + eA_0(\mathbf{r}) + \mathcal{O}(\mathbf{A}^2).$$

Performing then the derivative (3.2) one recovers the expression for the point charge density and for the pure convection current

$$\begin{aligned} \rho(\mathbf{x}) &= e\ \delta(\mathbf{x}-\mathbf{r}), \\ \mathbf{j}^c(\mathbf{x}) &= \frac{e}{2m}\{\mathbf{p}, \delta(\mathbf{x}-\mathbf{r})\}. \end{aligned}$$

No spin current term is generated in this way, since it is a relativistic property. However, adding formally to the hamiltonian a vanishing term term like

$$H_0 = H_0 + i\frac{\mu}{2m}\boldsymbol{\sigma}\cdot(\mathbf{p}\times\mathbf{p}).$$

where μ is the magnetic moment of the particle, then minimal substitution generates the spin current

$$\mathbf{j}^s(\mathbf{x}) = i\frac{e\mu}{2m}\boldsymbol{\sigma}\times[\mathbf{p}, \delta(\mathbf{x}-\mathbf{r})], \tag{3.33}$$

which is purely transverse and therefore $\boldsymbol{\nabla}\cdot\mathbf{j}^{\mathbf{s}} = 0$. From this last example it is

clear that within this minimal substitution method there is an arbitrariness, since one can always add purely transverse terms to the electromagnetic current without violating its conservation.

Up to now, using the minimal coupling scheme, we have derived the non-relativistic expression for the one-body charge, convection and spin current operators. Therefore, in an A-body nuclear system the charge operator has the form

$$\rho_{(1)}(\mathbf{x}) = e\sum_k \frac{1+\tau_k^3}{2}\,\delta(\mathbf{x}-\mathbf{r}_k), \tag{3.34}$$

where the charge e_k of the k-th nucleon is described within the isospin formalism, introducing the third component τ_k^3 of its isospin. The convection and spin current operators for an A-body system will look like

$$\begin{aligned}
\mathbf{j}^c_{(1)}(\mathbf{x}) &= \frac{e}{2m}\sum_k \frac{1+\tau_k^3}{2}\{\mathbf{p}_k, \delta(\mathbf{x}-\mathbf{r}_k)\},\\
\mathbf{j}^s_{(1)}(\mathbf{x}) &= i\frac{e}{2m}\sum_k \mu_k \frac{1+\tau_k^3}{2}\boldsymbol{\sigma}_k \times [\mathbf{p}_k, \delta(\mathbf{x}-\mathbf{r}_k)],
\end{aligned} \tag{3.35}$$

where μ_k are the magnetic moments of proton and neutron $\mu_{p/n}$. The subscript (1) in the last formulas indicates that they are one-body operators. The charge operator of (3.34) and the currents in (3.35) satisfy the continuity equation

$$\boldsymbol{\nabla}\cdot\mathbf{j}_{(1)}(\mathbf{x}) = -i[T, \rho(\mathbf{x})], \tag{3.36}$$

with the total current $\mathbf{j}_{(1)} = \mathbf{j}^c_{(1)} + \mathbf{j}^s_{(1)}$, where T is the total kinetic energy of the A-body system

$$T = \sum_k \frac{\mathbf{p}_k^2}{2m}.$$

However, if one considers an interacting system with a hamiltoninan $H = H_0 + V$, the continuity equation will contain also the commutator $[V, \rho(\mathbf{x})]$, which is not always vanishing. This means, that, depending on the kind of interaction one uses to describe the system, additional terms will be required for the electromagnetic current in order to satisfy the continuity equation.

Already in the early days of nuclear physics it was clear that, since the nuclear force has an exchange character, an additional electromagnetic current had to exist. Namely, if one considers a simple exchange potential $V = V_0(\mathbf{r}_{\rm pn})P_{\rm pn}$, with $\mathbf{r}_{\rm pn}$ being the distance between a proton and a neutron and $P_{\rm pn}$ the exchange operator, then

the commutator $[V, \rho(\mathbf{x})] \neq 0$ and an additional current density is needed to fulfil gauge invariance. This will be a two-body operator, since the commutator $[V, \rho(\mathbf{x})]$ has a two-body character for a given two-body potential and one-body charge.

In practice, in case one has a potential with isospin dependence or a momentum dependence, such that $[V, \rho(\mathbf{x})] \neq 0$, an electromagnetic current operator has to be introduced to satisfy

$$\boldsymbol{\nabla} \cdot \mathbf{j}_{(2)}(\mathbf{x}) = -i[V, \rho(\mathbf{x})]. \tag{3.37}$$

Again, for a given potential, the form of the two-body current can be recovered using the minimal coupling procedure. Clearly, the problem of the arbitrariness introduced by such an approach remains and the consequence is the non-uniqueness of the current that satisfies the symmetry principle. For this reason it is desirable to have an underlying physical model for the NN interaction with well defined degrees of freedom, such that the construction of the consistent current is uniquely defined. If one interprets the NN interaction as due to the exchange of mesons (pion, rho, etc.), the corresponding two-body current will be called meson exchange current (MEC), since it is the electromagnetic current generated by the interaction of photons with exchanged mesons.

In Appendix A the derivation of the two-body current in case of the one pion exchange potential is shown in detail. In Chapter 6 this subject will be discussed further, where we will define a meson exchange current consistent with the potential model used.

3.4 Basic Electromagnetic Processes

If one considers the first order of perturbation theory, the processes in which only one photon is involved are real photoabsorption (see e.g. [Eis70]) and virtual one-photon exchange in electron scattering (see e.g. [Cio80, Fru84, Ahk94, Don03]). In the following we will discuss these two processes for a general nuclear systems with A nucleons. The described formalism will then be needed in the chapters where the obtained results are discussed.

3.4.1 Photoabsorption

In photoabsorption a real photon γ with momentum $\mathbf{q}$ and energy $\omega = |\mathbf{q}|$ is absorbed by an A-body system that makes a transition from the ground state $|\Psi_0\rangle$ to a final state $|\Psi_f\rangle$ with energies and momenta $(E_0, \mathbf{P}_0)$ and $(E_f, \mathbf{P}_f)$, respectively.

In case of inclusive photoabsorption no final state is measured.

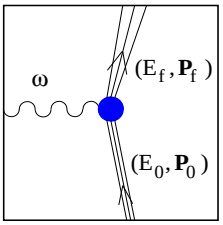

Figure 3.1: Diagram for photoabsorption; a real photon γ is absorbed by the system that undergoes a transition from the initial state $|\Psi_0\rangle$ to a final state $|\Psi_f\rangle$.

The total cross section of the process [Bac01] is related to the response function $R(\omega)$ in this way

$$\sigma(\omega) = \frac{4\pi^2\alpha}{2J_0+1}\omega R(\omega)\,, \tag{3.38}$$

where α is the fine structure constant, J_0 is the initial total angular momentum of the nucleus and $R(\omega)$ is defined as

$$R(\omega) = \frac{1}{2}\sum\!\!\!\!\!\!\int_{f,\lambda} |\langle\Psi_f|\, J_\lambda(\vec{\omega})\, |\Psi_0\rangle|^2\, \delta(E_f - E_0 - \omega)\,, \tag{3.39}$$

where J_λ is the transverse current. Since the photon is real it can only have transverse polarization $\lambda = \pm 1$. This is the reason why only transverse electromagnetic currents are relevant in such a reaction. It is well known that in most of the cases, in the energy region above particle emission threshold and below pion photoproduction, $\omega \leq 140$ MeV, only the lowest multipole of the transverse electromagnetic current is needed, namely the electric dipole $E1$. Furthermore, as shown in the previous section, it can be expressed in terms of the Coulomb multipole C_1, via the Siegert theorem (see e.g. [Sie37, Efr99b]), where the effects of meson exchange currents are already included.

3.4.2 Electron Scattering

In case of electron scattering, a virtual photon γ^* is exchanged between the probing electron and the nuclear system of the target. An electron with four-momentum $k^\mu = (\epsilon, \mathbf{k})$ is scattered through an angle θ_e to a four-momentum state $k'^\mu = (\epsilon', \mathbf{k}')$. The virtual photon carries four-momentum transfer $q^\mu = (\omega, \mathbf{q})$ and, in interacting with the nucleus, causes it to make a transition from the ground state $|\Psi_0\rangle$ with four-momentum $P_0^\mu = (E_0, \mathbf{P}_0)$ to a final state $|\Psi_f\rangle$ with four-momentum $P_f^\mu =$

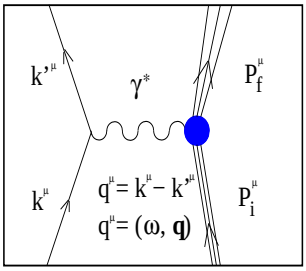

Figure 3.2: Diagram for the electron scattering in the one photon exchange approximation. A virtual photon γ^* is exchanged between an electron of initial and final four-momenta k^μ and k'^μ, respectively, and a given system described by the ground and final state four-momenta P_0^μ and P_f^μ, respectively.

$(E_f, \mathbf{P}_f)$. For the conservation of the four-momentum one has $q^\mu = k^\mu - k'^\mu = P_f^\mu - P_0^\mu$. Furthermore one has that $q_\mu^2 = \omega^2 - \mathbf{q}^2 < 0$[1] for electron scattering corresponding to the exchange of space-like virtual photons. This means that energy and momentum transfer $(\omega, \mathbf{q})$ can vary independently, in contrast to the case of real photoabsorption, with the restriction mentioned before. For this reason, one can say that electron scattering is a more rich reaction to study the dynamics of a system, since it already contains in the limit $|\mathbf{q}| \to \omega$ the information obtained in real photoabsorption.

The polarization of the exchanged virtual photon can also vary between transverse and longitudinal direction, depending on the scattering angle θ_e. Therefore in electron scattering all terms of the current, also the longitudinal parts, play a role. Namely, in case of inclusive unpolarized electron scattering, i.e. in the reaction $A(e, e')$, where no fragment of the target is detected in coincidence with the scattered unpolarized electron, the cross section in the laboratory system takes the form

$$\frac{d^2\sigma}{d\Omega_e d\omega} = \sigma_M \left[\frac{Q^4}{q^4} R_L(\omega, \mathbf{q}) + \left(\frac{Q^2}{2q^2} + \tan^2 \frac{\theta_e}{2} \right) R_T(\omega, \mathbf{q}) \right] \tag{3.40}$$

with $q = |\mathbf{q}|$ and $Q^2 = -q_\mu^2$, where the longitudinal and transverse response functions are defined as

$$R_L(\omega, \mathbf{q}) = \sum\!\!\!\!\!\!\int_f |\langle \Psi_f | \, \tilde{\rho}(\mathbf{q}) \, | \Psi_0 \rangle|^2 \, \delta(E_f - E_0 - \omega) \tag{3.41}$$

$$R_T(\omega, \mathbf{q}) = \sum\!\!\!\!\!\!\int_f \sum_{\lambda=\pm 1} |\langle \Psi_f | \, J_\lambda(\mathbf{q}) \, | \Psi_0 \rangle|^2 \, \delta(E_f - E_0 - \omega), \tag{3.42}$$

[1] Clearly, the four-vector squared $q_\mu q^\mu$ is here denoted with q_μ^2.

in which one recognizes the charge and the transverse current operators. Furthermore, the Mott cross section σ_M is given by

$$\sigma_M = \left\{ \frac{\alpha \cos\theta_e/2}{2\epsilon \sin^2 \theta_e/2} \right\}^2 .$$

The expression in (3.40) is valid in plane wave Born approximation for the electron, i.e. where Coulomb distortions are negligible (which is the case for light nuclei). Furthermore, the extreme relativistic limit has been used, which means that the electron mass has been neglected with respect to its energy. This is clearly true when $\epsilon \gg 0.5$ MeV, which is the case of all laboratories where nuclear reactions are studied.

Using a Rosenbluth separation it is possible to disentangle the longitudinal response function $R_L(\omega, \mathbf{q})$ from the transverse one $R_T(\omega, \mathbf{q})$. Here one can note that, contrary to photoabsorption, there is a longitudinal response. The longitudinal part of the current is related to the charge operator by the continuity equation (3.28).

Since ω and $\mathbf{q}$ can vary independently, one can study the response functions as functions of the energy ω, keeping the momentum $q = |\mathbf{q}|$ fixed or vice versa, one can vary the momentum, keeping ω unchanged. In any case, depending on the values of energy and momentum transfer in the reaction a varying number of multipoles has to be considered in the expansion of the charge and current operators.

These aspects will be discussed further in Chapter 6 where results on electron scattering off ^{4}He are presented.

Chapter 4

Evaluation of the Matrix Elements

In this chapter the evaluation of a matrix element in the internal coordinates of an A-body system is discussed. The hyperspherical formalism is used, and two separated sections for the matrix elements of one-body and two-body operators are presented. At the end a brief discussion on the effective interaction in the hyperspherical harmonics expansion (EIHH) is also given.

4.1 Basic Concepts

For the calculation of electromagnetic reactions on A-body nuclei it is necessary to evaluate matrix elements of a given operator that acts on an A-body wave function. This is required first of all for the solution of the Schrödinger equation, where matrix elements of the kinetic energy and of the potential have to be calculated. Furthermore, within the LIT method, additional matrix elements for the source term in the right-hand-side of equation (2.7) are needed. These matrix elements are of the kind of those shown in Eq. (3.1), where the form of the operator depends on the reaction under study.

Our approach consists in the calculation of matrix elements with respect to internal wave functions, where the center of mass motion has already been separated from the internal dynamics. This is very useful since in the Schrödinger equation and in the current matrix elements only the internal degrees of freedom are relevant. The A-body internal coordinates are

$$\mathbf{r}'_i = \mathbf{r}_i - \mathbf{R}_{cm}, \tag{4.1}$$

where

$$\mathbf{R}_{cm} = \frac{1}{A}\sum_{i=1}^{A}\mathbf{r}_i,$$

denotes the center of mass coordinate. We work in the center of mass frame, with

$$\sum_i \mathbf{r}'_i = 0.$$

The matrix elements we are interested in are of this kind

$$\langle\Psi|\, O(\mathbf{r}'_1, ..., \mathbf{r}'_A)\, |\Psi'\rangle\,,$$

where O is a generic operator as function of the relative coordinates, while $|\Psi\rangle$ and $|\Psi'\rangle$ are internal states of the system. We will use the hyperspherical formalism to calculate this matrix element. In order to do that, the internal wave function of the A-body system is described in terms of a set of $A-1$ independent 3-dimensional Jacobi coordinates, $\{\boldsymbol{\eta}_k, k = 1, ..., A-1\}$ defined as

$$\boldsymbol{\eta}_{k-1} = \sqrt{\frac{k-1}{k}}\left(\mathbf{r}_k - \frac{1}{k-1}\sum_{i=1}^{k-1}\mathbf{r}_i\right);\quad k = 2, ..., A, \tag{4.2}$$

instead of using the $\mathbf{r}'_i$ coordinates, which are not linearly independent. Then, starting from the Jacobi coordinates one can apply the recursive transformation to hyperspherical coordinates in Eq. (B.4). The aim is to expand the A-body internal states $|\Psi\rangle$ and $|\Psi'\rangle$ in terms of the hyperspherical harmonics (HH), introduced in Appendix B, and then to write the operator in terms of the hyperspherical coordinates. The crucial point is that, since we are working with identical fermions it is necessary that the basis states are fully antisymmetrized. The hyperspherical harmonics for an A-body system shown in Appendix B are linear combinations of products of Jacobi polynomials times ordinary spherical harmonics. They do not possess any peculiar property under permutation of particles. However, in our case we need a set of hyperspherical harmonics that are irreducible representations of the permutation group $\mathcal{S}_A$ of A particles.

There are different algorithms available that enable one to construct hyperspherical harmonics with well defined symmetry properties under permutation of particles, such as the NKG (Novoselsky-Katriel-Gilmore) [Nov88] and the FE (Fomin-Efros) [Fom81] algorithms.

In this work we use for the construction of antisymmetrized hyperspherical states

a Fortran90 code, developed by Z. zzz, where an extension of the NKG algorithm is implemented [Bar97a]. In the NKG method the hyperspherical functions belonging to a well defined irreducible representation (irrep) of the symmetric group $\mathcal{S}_A$ are constructed recursively by building all the coefficients of fractional parentage (cfps), see e.g. [Sit72]. In the algorithm proposed by Z. zzz the hyperspherical harmonics are also constructed in a recursive way, but one first builds the irreps of the kinematic rotational group $\mathcal{O}(A-1)$, and then one performs the reduction $\mathcal{O}(A-1) \downarrow \mathcal{S}_A$. In this way one obtains the symmetrization with respect to permutation of particles $\mathcal{S}_A$ of functions that were already irreps of the group $\mathcal{O}(A-1)$. Note that the word "symmetrization" is used in the sense of constructing any irreducible representation of the permutation group. The power of this algorithm lies in the big reduction one obtains in the total number of cfps needed, which results in a much faster code where less memory is needed. Therefore, with this method one can construct the antisymmetrized states for the A-body problem also for $A \geq 4$.

The advantage of using antisymmetrized states is that for a generic one-body operator $O_{(1)} = \sum_{i=1}^{A} O_i$, the evaluation of the matrix element is reduced to the calculation of the matrix element of an operator that acts only on the last coordinate, as

$$\langle \Psi | \, O_{(1)} \, | \Psi' \rangle = A \, \langle \Psi | \, O_A \, | \Psi' \rangle \, . \tag{4.3}$$

In an analogous way, in case of a two-body operator $O_{(2)} = \sum_{i<j=1}^{A} O_{ij}$, the evaluation of the matrix element is reduced to the calculation of the matrix element of an operator acting only on the two last coordinates, as

$$\langle \Psi | \, O_{(2)} \, | \Psi' \rangle = \frac{A(A-1)}{2} \, \langle \Psi | \, O_{A,A-1} \, | \Psi' \rangle \, . \tag{4.4}$$

Note that in the matrix elements (4.3) and (4.4), while the operators depend only on one and two coordinates, respectively, the wave functions still depend on all A particles.

Furthermore, if one expands the wave functions $|\Psi\rangle$ and $|\Psi'\rangle$ in terms of the A-body antisymmetrized hyperspherical harmonics, which are irreducible representations of the group $\mathcal{S}_A$ according to the chain of symmetry groups $\mathcal{S}_A \supset \mathcal{S}_{A-1} \supset \cdot\cdot \supset \mathcal{S}_2 \supset \mathcal{S}_1$, one can reduce the dimension of the above matrix elements to a linear combination of single particle matrix elements in case of (4.3) and of two particle matrix elements for (4.4), making use of the coefficients of fractional parentage, as will be discussed briefly later.

4.2 The Hyperspherical Basis

In the hyperspherical formalism (for details see Appendix B), one always has to deal with $3(A-1)$ internal coordinates of the system, among them one is the hyper-radial coordinate $\rho_{A-1} = \rho$ and all the others constitute a set of $(3A-4)$ angles, which are collected under one single symbol Ω.

The internal wave function of an A-body system, that depends on the $A-1$ vector Jacobi coordinates and on the A spins and isospins of the constituent particles, is written in the hyperspherical formalism in the following way [Bar97a, Bar99]

$$\Psi(\boldsymbol{\eta}_1, ..., \boldsymbol{\eta}_{A-1}, s_1, ..., s_A, t_1, ..., t_A) = \sum_{K\nu} R_{K\nu}(\rho) H_{K\nu}(\Omega, s_1, ..., s_A, t_1, ..., t_A), \quad (4.5)$$

where $R_{K\nu}$ are hyper-radial functions depending only on the hyper-radius and $H_{K,\nu}$ are the totally antisymmetrized hyperspherical harmonics coupled with spin-isospin basis functions, depending on Ω and on the A spin-isospins of the particles. Note that the hyper-radius is symmetric under permutation of particles. The functions $H_{K\nu}$ are defined as

$$H_{K\nu}(\Omega, s_1, ..., s_A, t_1, ..., t_A) = \sum_{Y_{A-1}} \frac{\Lambda_{\Gamma_A, Y_{A-1}}}{\sqrt{|\Gamma_A|}} \times$$
$$\times \left[\mathcal{Y}_{K_{A-1} L_{A-1} \Gamma_A Y_{A-1} \alpha^K_{A-1}}(\Omega) \otimes \chi_{ST\tilde{\Gamma}_A \tilde{Y}_{A-1} \alpha^{ST}_A}(s_1, ..., s_A, t_1, ..., t_A) \right]^J_{J^z}. \quad (4.6)$$

The symmetrized hyperspherical harmonics $\mathcal{Y}_{K_{A-1} L_{A-1} M_{A-1} \Gamma_{A-1} Y_{A-1} \alpha^K_{A-1}}$ possess grandangular momentum K_{A-1} (see Appendix B), good angular momentum $L \equiv L_{A-1}$, with projection $M \equiv M_{A-1}$, and belong to well defined irreducible representations $\Gamma_1 \in \Gamma_2 \in ... \in \Gamma_A$ of the permutation group-subgroup chain $\mathcal{S}_1 \subset \mathcal{S}_2 \subset ... \subset \mathcal{S}_A$, denoted by the Yamanouchi symbol $[\Gamma_A, Y_{A-1}] \equiv [\Gamma_A, \Gamma_{A-1}, ..., \Gamma_1]$. The dimension of the irreducible representation Γ_i is denoted by $|\Gamma_i|$ and $\Lambda_{\Gamma_A, Y_{A-1}}$ is a phase factor. Analogously, the functions $\chi_{SS_zTT_z\tilde{\Gamma}_{A-1}, \tilde{Y}_{A-1}\alpha^{ST}_A}$ are properly symmetrized spin-isospin states with total spin S, with projection S_z, and total isospin T, with projection T_z as good quantum numbers. The label α^K_{A-1} (α^{ST}_A) is needed to remove the degeneracy of the hyperspherical (spin-isospin) states with a given symmetry. In the expression of the functions $H_{K,\nu}$ in (4.6) ν represents all indices but $K = K_{A-1}$. We have furthermore coupled the spin and space parts of the wave function to a total angular momentum J with projection J^z.

The construction of the spin-isospin wave function as well as hyperspherical harmonics is done recursively. Each A-body spin-isospin function is written as linear

combination of coupled products of $(A-1)$-particles wave functions and the $A-$th particle states. The coefficients of the expansion are a sort of coefficients of fractional parentage. The spin $(A-1)$-particles wave functions are constructed recursively, coupling s_1 with s_2 to S_2, S_2 with s_3 to S_3, and so on up to S_{A-1}. In an analogous way one builds also the isospin part of the wave function. Finally, for the spin-isospin functions we write

$$\begin{aligned}&\chi_{ST\tilde{\Gamma}_A,\tilde{Y}_{A-1}\alpha_A^{ST}}(s_1,...,s_A,t_1,...,t_A) = \\ &\sum_{S_{A-1}T_{A-1}\alpha_{A-1}^{ST}} \left[(S_{A-1};s)S(T_{A-1};t)T\tilde{\Gamma}_{A-1}\alpha_{A-1}^{ST}|\}ST\tilde{\Gamma}_A\alpha_A^{ST}\right] \times \\ &\left[\chi_{S_{A-1}T_{A-1}\tilde{\Gamma}_{A-1},\tilde{Y}_{A-2}\alpha_{A-1}^{ST}} \otimes s\ t\right]^{S,T}.\end{aligned} \tag{4.7}$$

Here the spin and isospin of the last particle are indicated with $s \equiv s_A$ and $t \equiv t_A$, respectively, while S_{A-1} and T_{A-1} denote isospin and spin of the residual $(A-1)$-body system, respectively.

Similarly one can use a recursive procedure to construct the A-particle symmetrized HH, where the expansion coefficients are made of two types of coefficients of fractional parentage

$$\begin{aligned}&\mathcal{Y}_{K_{A-1}L_{A-1}\boldsymbol{\lambda}_{A-1}\Gamma_A Y_{A-1}\alpha_{A-1}^K}(\Omega) = \\ &\sum_{\lambda_{A-2}\beta_{A-1}^\lambda} \left[(\boldsymbol{\lambda}_{A-2}\Gamma_{A-1}\beta_{A-1}^\lambda)\boldsymbol{\lambda}_{A-1}|\}\lambda_{A-1}\Gamma_A\beta_A^\lambda\right] \times \\ &\sum_{K_{A-2}L_{A-2}\beta_{A-2}^K\ell} \left[(K_{A-2}L_{A-2}\boldsymbol{\lambda}_{A-2}\beta_{A-2}^K;\ell)K_{A-1}L_{A-1}|\}K_{A-1}L_{A-1}\boldsymbol{\lambda}_{A-1}\beta_{A-1}^K\right] \times \\ &\mathcal{Y}_{(K_{A-2}L_{A-2}\boldsymbol{\lambda}_{A-2}\beta_{A-2}^K\Gamma_{A-1}Y_{A-2}\beta_{A-1}^\lambda;\ell)K_{A-1}L_{A-1}}(\Omega).\end{aligned} \tag{4.8}$$

The two types of coefficients of fractional parentage are the orthogonal-hyperspherical cfps for the construction of the HH as irreducible representation of the group $\mathcal{O}_{A-1}$ and the orthogonal cfps for the reduction $\mathcal{O}(A-1) \downarrow \mathcal{S}_A$ [Bar99, Bar01, Bar01a]. The indices $\boldsymbol{\lambda}_{A-2}$ and $\boldsymbol{\lambda}_{A-1}$ label the states according to the canonical chain of subgroups $O_{A-1} \supset O_{A-2} \supset ... \supset O_2$ used in the construction (for details see [Bar97a]). The degeneracy removing indices β_{A-1}^K and β_A^λ are condensed in $(\beta_{A-1}^K, \beta_A^\lambda) \equiv \alpha_{A-1}^K$ in the starting expression of the HH in Eq. (4.8).

Instead of coupling a total spin state S, given by the recursive coupling of $1, 2, ..A$-spin particles, with an angular momentum L of $A-1$ Jacobi coordinate, constructed again recursively, to a total angular momentum J (LS scheme), one can use another

coupling scheme. Namely, one can couple the the spin and angular momenta of the last particle s and ℓ to j, and then j with the total angular momentum J_{A-1} of the $(A-1)$ particle system, given by the coupling of $(S_{A-1}L_{A-2})$ (JJ scheme). In this way one can work more comfortably with all degrees of freedom of the last particle ℓ, s and j. It is obtained by using standard recoupling methods introducing the nine-j symbols. Thus, the hyperspherical spin-isospin internal basis function $H_{K\nu}$, that we now call simply $|[K]\rangle$, with $[K] \equiv K\nu$, looks like

$$
\begin{aligned}
|[K]\rangle = & \sum_{Y_{A-1}} \frac{\Lambda_{\Gamma_A, Y_{A-1}}}{\sqrt{|\Gamma_A|}} \sum_{\lambda_{A-2}\beta^{\lambda}_{A-1}} \left[(\boldsymbol{\lambda}_{A-2}\Gamma_{A-1}\beta^{\lambda}_{A-1})\boldsymbol{\lambda}_{A-1}|\}\lambda_{A-1}\Gamma_A\beta^{\lambda}_A\right] \times \\
& \sum_{K_{A-2}L_{A-2}\beta^K_{A-2}\ell} \left[(K_{A-2}L_{A-2}\boldsymbol{\lambda}_{A-2}\beta^K_{A-2};\ell)K_{A-1}L_{A-1}|\}K_{A-1}L_{A-1}\boldsymbol{\lambda}_{A-1}\beta^K_{A-1}\right] \times \\
& \sum_{S_{A-1}T_{A-1}\alpha^{ST}_{A-1}} \left[(S_{A-1};s)S(T_{A-1};t)T\tilde{\Gamma}_{A-1}\alpha^{ST}_{A-1}|\}ST\tilde{\Gamma}_A\alpha^{ST}_A\right] \times \\
& \sum_{j,J_{A-1}} \hat{J}_{A-1}\hat{S}\hat{L}\hat{j} \left\{ \begin{array}{ccc} L_{A-2} & S_{A-1} & J_{A-1} \\ \ell & s & j \\ L & S & J \end{array} \right\} |(T_{A-1}t)TT^z\rangle \\
& \left|\left((S_{A-1}K_{A-2}L_{A-2}\boldsymbol{\lambda}_{A-2}\alpha^K_{A-2}\Gamma_{A-1}Y_{A-2})J_{A-1};(s\ell)j\right)JJ^z\right\rangle . \qquad (4.9)
\end{aligned}
$$

Note that the indices of the quantum numbers for the $(A-1)$-body system refer to the number of Jacobi coordinates in case of the angular momentum L_{A-2}, and to the number of particles in case of spin S_{A-1} and total angular momentum J_{A-1}.

In the following we will show how one can calculate the matrix element of a one-body operator with the hyperspherical basis state. This formalism will be used later on in Chapter 5 and 6 where we will dela with the one-body charge and current operators.

4.3 One-body Operators

We will now consider a general one-body spherical tensor operator of the form

$$
O^{\mathcal{J}\mathcal{M}\mathcal{T}\mathcal{T}_z}_{(1)} = \sum_i O^{\mathcal{J}\mathcal{M}}(\mathbf{r}'_i, \sigma_i) O^{\mathcal{T}\mathcal{T}_z}(\tau_i), \qquad (4.10)
$$

that acts in the coordinate-spin space with $O^{\mathcal{J}\mathcal{M}}$, carrying angular momentum $\mathcal{J}$ with projection $\mathcal{M}$, and in the isospin space with $O^{\mathcal{T}\mathcal{T}_z}$, carrying isospin $\mathcal{T}$ with projection $\mathcal{T}_z$.

First of all one would like to use the antisymmetrization of the function like in Eq. (4.3). Before proceeding, it is useful to note the relation between the relative

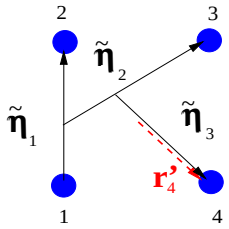

Figure 4.1: Example of the three Jacobi coordinates in a four-body system. Only the unnormalized ones, $\tilde{\boldsymbol{\eta}}_i$, are shown for simplicity. The last Jacobi coordinate, i.e. $\tilde{\boldsymbol{\eta}}_3$, is proportional to the coordinate of the last particle in the center of mass, i.e. $\mathbf{r}'_4$ in the specific case.

position of the A-th particle and the last Jacobi coordinate (see Eq. (4.2))

$$\boldsymbol{\eta}_{A-1} = \sqrt{\frac{A}{A-1}}\mathbf{r}'_A. \tag{4.11}$$

An example of this relation is shown in Fig. 4.1 for a four-particle system. Furthermore, within the hyperspherical formalism one uses the notation $\boldsymbol{\eta}_{A-1} \equiv (\eta_{A-1}, \hat{\eta}_{A-1})$ and then the modulus of the last Jacobi coordinate is adopted to build the hyperradius and the last hyperangle using the transformation in (B.4). In fact

$$\eta_{A-1} = \rho \sin\varphi,$$

where $\rho \equiv \rho_{A-1} = \sum_i \eta_i^2$ is the hyper-radius and $\varphi = \varphi_{A-1}$ is the last hyperspherical angle defined in Appendix B. This means that the coordinate of the last particle becomes, in the hyperspherical formalism,

$$\mathbf{r}'_A \equiv (r'_A, \hat{r}'_A) = \left(\sqrt{\frac{A-1}{A}}\rho\sin\varphi, \hat{\eta}_{A-1}\right), \tag{4.12}$$

where for the angular part it yields $\hat{r}'_A \equiv \hat{\eta}_{A-1}$.

At this point we can finally reduce the hyperspherical matrix element of the one-body operator on the antisymmetrized basis states of the (4.9) to

$$\langle [K]|\, O_{(1)}^{\mathcal{J}\mathcal{M}\mathcal{T}\mathcal{T}_z}\, |[K']\rangle = A\, \langle [K]|\, O^{\mathcal{J}\mathcal{M}}\left(r'_A, \hat{r}'_A, \sigma_A\right) O^{\mathcal{T}\mathcal{T}_z}(\tau_A)\, |[K']\rangle\,, \tag{4.13}$$

where the operator acts now only on the last particle degrees of freedom. Note that

we are not considering for the moment the hyper-radial part of the wave function $R_{K,\nu}(\rho)$, which will be discussed later. For this reason the matrix element in (4.13) depends still on the hyper-radius ρ. The spatial-spin operator is assumed to be also separable in a scalar radial part and an angular tensorial part as

$$O^{\mathcal{J}\mathcal{M}}\left(r'_A, \hat{r}'_A, \sigma_A\right) = \mathcal{R}^{\mathcal{J}}\left(r'_A\right) \widetilde{O}^{\mathcal{J}\mathcal{M}}\left(\hat{r}'_A, \sigma_A\right). \tag{4.14}$$

Any one-body operator can be written at most as a sum of terms like (4.14). Using then the coefficients of fractional parentage, the matrix element can be reduced to a linear combination of one-body matrix elements as

$$\begin{aligned}
&\langle [K]|\, O^{\mathcal{J}\mathcal{M}}(\mathbf{r}'_A, \sigma_A) O^{\mathcal{T}\mathcal{T}_z}(\tau_A)\, |[K']\rangle = \\
&\sum_{\Gamma_{A-1}} c(A, A-1) c(A', A-1) \frac{\Lambda_{\Gamma_A \Gamma_{A-1}} \Lambda_{\Gamma'_A \Gamma_{A-1}} |\Gamma_{A-1}|}{\sqrt{|\Gamma_A||\Gamma'_A|}} \\
&\sum_{J_{A-1}, j, j'} \hat{L}' \hat{S}' \hat{L} \hat{S} \hat{J}^2_{A-1} \hat{j} \hat{j}' \left\{ \begin{array}{ccc} L_{A-2} & S_{A-1} & J_{A-1} \\ \ell' & s' & j' \\ L' & S' & J' \end{array} \right\} \left\{ \begin{array}{ccc} L_{A-2} & S_{A-1} & J_{A-1} \\ \ell & s & j \\ L & S & J \end{array} \right\} \times \\
&\langle K_{A-2}\ell; K_{A-1}|\, \mathcal{R}^{\mathcal{J}} \left(\sqrt{\frac{A-1}{A}} \rho \sin\varphi \right) \left| K'_{A-2}\ell'; K_{A-1} \right\rangle \times \\
&(-)^{J-M} \begin{pmatrix} J & \mathcal{J} & J' \\ -M & \mathcal{M} & M' \end{pmatrix} (-)^{J_{A-1}+j'+J+\mathcal{J}}\, \hat{J}' \hat{J} \left\{ \begin{array}{ccc} j & J & J_{A-1} \\ J' & j' & \mathcal{J} \end{array} \right\} \times \\
&\langle (\ell\ s) j \|\, \tilde{O}^{\mathcal{J}}(\hat{r}'_A, \sigma_A) \,\|(\ell'\ s') j' \rangle \times \\
&(-)^{T-T^z} \begin{pmatrix} T & \mathcal{T} & T' \\ -T^z & \mathcal{T}^z & T'^z \end{pmatrix} (-)^{T_{A-1}+t'+T+\mathcal{T}} \hat{T} \hat{T}' \left\{ \begin{array}{ccc} t & T & T_{A-1} \\ T' & t' & \mathcal{T} \end{array} \right\} \\
&\langle t \|\, O^{\mathcal{T}}(\tau_A) \,\| t' \rangle
\end{aligned} \tag{4.15}$$

where $\Lambda_{\Gamma_A \Gamma_{A-1}}$ and $\Lambda_{\Gamma'_A \Gamma_{A-1}}$ are phase factors, Γ_{A-1}, Γ'_A and Γ_A are the dimension of the irreps, and finally the coefficients $c(A, A-1)$ and $c(A', A-1)$ are the cfps of (4.9), that are not written again in order to simplify the notation. The sum in (4.15) runs over all the possible irreps denoted with $\Gamma_{A-1} \in \Gamma_A$ and also $\Gamma_{A-1} \in \Gamma_{A'}$. In (4.15) we have made use of the Wigner-Eckart theorem both for the spatial-spin tensor part and for the isospin part of the operator, to separate the geometrical information of the three-j symbols from the reduced matrix elements. Then we have used the fact that the operator acts only on the last particle. Note that the

dynamical one-body reduced matrix elements in the angular-spin space

$$\langle(\ell\ s)j\|\,\widetilde{O}^{\mathcal{J}}(\hat{r}'_A,\sigma_A)\,\|(\ell'\ s')j'\rangle \tag{4.16}$$

and in the isospin space

$$\langle t\|\,O^{\mathcal{T}}(\tau_A)\,\|t'\rangle \tag{4.17}$$

can be calculated analytically with standard angular momentum methods. This is not the case of the radial matrix element that appears also in the (4.15). Namely, in the hyperspherical formalism it has the following form [Bar97a]

$$\begin{aligned}
&O^{\mathcal{J}}(\rho) = \langle K_{A-2}\ell; K_{A-1}|\,\mathcal{R}^{\mathcal{J}}\left(\sqrt{\frac{A-1}{A}}\rho\sin\varphi\right)\left|K'_{A-2}\ell'; K_{A-1}\right\rangle \\
&= \mathcal{N}(K_{A-1};\ell K_{A-2})\mathcal{N}'(K'_{A-2};\ell' K_{A-2})\int_0^{\frac{\pi}{2}} d\varphi(\sin\varphi)^2(\cos\varphi)^{3A-7}(\sin\varphi)^{\ell}(\cos\varphi)^{K_{A-2}} \\
&P_n^{(\alpha,\beta)}\cos(2\varphi)\mathcal{R}^{\mathcal{J}}\left(\sqrt{\frac{A-1}{A}}\rho\sin\varphi\right)(\sin\varphi)^{\ell'}(\cos\varphi)^{K_{A-2}}P_{n'}^{(\alpha',\beta)}\cos(2\varphi),
\end{aligned} \tag{4.18}$$

where the normalization constants are given in (B.20), $P_n^{(\alpha,\beta)}$ and $P_{n'}^{(\alpha',\beta')}$ are the Jacobi polynomials introduced in Appendix B with n and n' as in Eq. (B.19), with $\alpha = \ell + \frac{1}{2}$, $\alpha' = \ell' + \frac{1}{2}$ and finally $\beta = K_{A-2} + \frac{3A-8}{2}$. This one-dimensional hyperangular integral can be calculated numerically with a Gauss-Jacobi quadrature method [Pre92], where the grid points are defined on the variable $x = \cos(2\varphi)$. The result is clearly a matrix element that still depends on the hyper-radius, over which we have not yet integrated.

The hyper-radial part of the wave function in Eq. (4.6) is expanded [Bar99]

$$R_{K\nu}(\rho) = \sum_{n_\rho} C_{n_\rho}^{K\nu}\phi_{n_\rho}(\rho), \tag{4.19}$$

in terms of the functions ϕ_{n_ρ} that contain the generalized Laguerre polynomials and are defined by

$$\phi_{n_\rho}(\rho) = \sqrt{\frac{n_\rho!}{(n_\rho+a)!}}b^{\frac{-3(A-1)}{2}}\left(\frac{\rho}{b}\right)^{\frac{a-(3A-4)}{2}}L_{n_\rho}^{a}\left(\frac{\rho}{b}\right)e^{-\frac{\rho}{2b}}, \tag{4.20}$$

where a and n_ρ are parameters of the polynomials. The hyper-radial matrix element

becomes then

$$\langle R_{K\nu}(\rho)|\, O^{\mathcal{J}}(\rho)\, |R_{K'\nu'}(\rho)\rangle = \sum_{n_\rho n'_\rho} C^{K\nu}_{n_\rho} C^{K'\nu'}_{n'_\rho} \int_0^\infty d\rho \rho^{3A-4} \phi_{n_\rho}(\rho) O^{\mathcal{J}}(\rho) \phi_{n'_\rho}(\rho), \quad (4.21)$$

where we have used the proper measure in the integration on the hyperangle (see Eq. (B.6)). The one-dimensional hyper-radial integration in (4.21) is performed numerically with a Gauss-Laguerre quadrature method [Pre92], where the grid points are defined on the variable $z = \frac{\rho}{b}$, such that the quantity b plays the role of a scaling parameter for the range of integration.

Here, we would like to stress again that within the present approach, the complicated calculation of the many-body matrix elements (4.3) of a given one-body operator, which in general would be a $(3A-3)$-dimensional matrix element, is reduced to a linear combination of one-body matrix elements, that consists each in a two-dimensional numerical integration, while the rest is completely analytically calculable. In the following we will proceed with an analogous treatment for a two-body operator.

4.4 Two-Body Operators

We would like now to consider a two-body spherical tensor operator in the form

$$O^{\mathcal{J}\mathcal{M}\mathcal{T}\mathcal{T}_z}_{(2)} = \sum_{i<j} O^{\mathcal{J}\mathcal{M}}(\mathbf{r}'_i, \mathbf{r}'_j, \sigma_i, \sigma_j) O^{\mathcal{T}\mathcal{T}_z}(\tau_i, \tau_j), \quad (4.22)$$

that acts in the coordinate-spin space with $O^{\mathcal{J}\mathcal{M}}$, carrying angular momentum $\mathcal{J}$ with projection $\mathcal{M}$, and in the isospin space with $O^{\mathcal{T}\mathcal{T}_z}$, carrying isospin $\mathcal{T}$ with projection $\mathcal{T}_z$. We are interested in calculating the matrix element of such an operator between totally antisymmetrized states using the hyperspherical formalism, as introduced in the previous sections. They are needed for the calculation of any two-body current matrix element and of course in the solution of the Schrödinger equation, where matrix elements of the potential are required. We would like to firstly reduce such matrix elements to matrix elements of the operator acting only on the last two particles, A and $A-1$, as in Eq. (4.4). Then, following an approach like for the one-body operator, one would like to write them as linear combination of two-body matrix elements via the cfps. It is clear that, since any of these two-body matrix elements depends on the relative coordinates $\mathbf{r}'_A$ and $\mathbf{r}'_{A-1}$, and on the spin-isospins of the last two particles σ_{A-1}, τ_{A-1} and σ_A, τ_A, one would need to consider

a further generation of the cfps with respect to the (4.9), in order to disentangle the degrees of freedom of the last two particles and not only of the last one. This makes the calculation of a two-body matrix element more difficult.

However, this complication is not completely necessary in case of the potential matrix element, since it depends only on the relative distance between particle A and particle $A-1$, which can be related to one Jacobi coordinate only. In fact, the normal Jacobi coordinates are defined such that the first one is the relative distance between particle 1 and 2, and the last one is the distance between particle A and the center of mass of the residual $A-1$ system (see Figure 4.1). This means that for an operator that depends only on the distance between particle A and $A-1$, one needs to rotate the Jacobi coordinate such that the last coordinate represents the interparticle distance. Performing this kinematical rotation one can then consider only one generation of the cfps in case of the HH. Clearly, for the spin-isospin wave functions, one always has to take into account two generations of cfps.

The complication can be reduced further with some shrewdness. Namely, constructing the coordinates in the reverse order as,

$$\boldsymbol{\eta}_k = \sqrt{\frac{A-k}{A+1-k}} \left(\mathbf{r}_k - \frac{1}{A-k} \sum_{i=k+1}^{A} \mathbf{r}_i \right) ; \quad k = 1, ..., A-1. \tag{4.23}$$

one can simplify the calculation of two-body matrix elements, since no further rotation is required. Namely, the last Jacobi coordinate in this case is proportional to

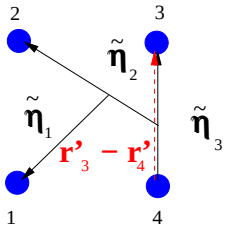

Figure 4.2: Example of the three reverse Jacobi coordinate in a four-body system. Only the unnormalized ones are shown for simplicity. The last Jacobi coordinate, i.e. $\tilde{\boldsymbol{\eta}}_3$, is proportional to the distance between last two particle, i.e. particle 3 and 4 in the specific case.

the distance between particle A and $A-1$

$$\boldsymbol{\eta}_{A-1} = \sqrt{\frac{1}{2}}(\mathbf{r}_{A-1} - \mathbf{r}_A),$$

as one can see also in the example presented in Figure 4.2.

This means that, in case of a two-body operator that depends only on the relative distance between particles, as

$$O_{(2)}^{\mathcal{J}\mathcal{M}\mathcal{T}\mathcal{T}_z} = \sum_{i<j} O^{\mathcal{J}\mathcal{M}}((\mathbf{r}'_i - \mathbf{r}'_j), \sigma_i, \sigma_j) O^{\mathcal{T}\mathcal{T}_z}(\tau_i, \tau_j), \tag{4.24}$$

using antisymmetrized states is easy to see that

$$\begin{aligned} &\langle [K]| \, O_{(2)}^{\mathcal{J}\mathcal{M}\mathcal{T}\mathcal{T}_z} \, |[K']\rangle = \\ &\frac{A(A-1)}{2} \langle [K]| \, \tilde{O}^{\mathcal{J}\mathcal{M}} \left(\sqrt{2}\rho \sin\varphi, \hat{\eta}_{A-1}, \sigma_A, \sigma_{A-1} \right) O^{\mathcal{T}\mathcal{T}_z}(\tau_A, \tau_{A-1}) \, |[K']\rangle \end{aligned} \tag{4.25}$$

in the hyperspherical formalism. The matrix element of such a two-body operator can be constructed in a very similar way as in (4.9), where only one generation of cfps is needed for the HH but two generations are needed for the spin-isospin wave functions. This means that in case of the spin-isospin cfps, as those in (4.7), one has to go back one step further in the irreps tree, considering also those irreps with $\Gamma_{A-2} \in \Gamma_{A-1} \in \Gamma_A$ (see for details [Bar01a]). Apart from that, the main structure of the matrix elements is the same as in (4.9), with a difference in the interpretation of the symbols in the spin-isospin part. In fact now one couples the states describing the last two particles with the residual $(A-2)$-body system. Therefore, in the spin-isospin wave function one should now substitute the index $A-1$ with $A-2$ in (4.9), and the quantum numbers s and t refer now to the last two-particle system, in the sense that they are obtained from the coupling of $(s_{A-1}s_A)s$ and $(t_{A-1}t_A)t$, respectively. Concerning the hyperspherical coordinates the wave function remains the same as in (4.9), since the operator acts finally only on the last Jacobi coordinate. For these reasons, within this approach, the calculation of the matrix element of a two-body operator that depends only on the relative distance of particles is the same as the calculation of the matrix element of a one-body operator. Therefore we will not write the formal expression as in the previous section.

Summarizing, within the HH formalism one can treat the two-body operators, which depend on the relative distance only, in two ways, namely, using the forward order of the Jacobi coordinate as in (4.2) and performing a kinematical rotation or, starting directly from the reverse Jacobi coordinate (4.23), where the rotation is saved. It turns out that in both procedures the calculation of the matrix element of such two-body operator is similar to the calculation of a one-body operator, since at the end only the integration over one Jacobi coordinate is performed.

As already mentioned, this procedure can be applied in case of any two-body

nuclear interaction, but not for every two-body current operator. In case of the matrix element for a general two-body operator a further generation of cfps also in case of the HH would be required and one would need to perform the integration on the two last Jacobi coordinates.

Nevertheless, in the present work, only matrix elements of two-body operators which depend on the relative distance only are calculated and in case of the meson-exchange current an approximation is made to treat the general two-body operator with this restriction. The validity of such an approximation will be discussed in Chapter 6, where the results obtained for electron scattering are presented.

In the following a brief discussion of the effective interaction in the hyperspherical harmonics is given, since it is used in the solution of the Schrödinger and Schrödinger-like equation.

4.5 Effective Interaction with the Hyperspherical Harmonics

Let us consider an A-body nuclear system, described by the following hamiltonian

$$H = \sum_{i=1}^{A} \frac{p_i^2}{2m} + \sum_{i<j}^{A} V_{ij}$$

with a two body interaction V_{ij}. Our goal is to solve the Schrödinger equation in an exact way working with internal degrees of freedom via the hyperspherical formalism. After the subtraction of the center of mass motion the hamiltonian in the hyperspherical coordinates is given by

$$H_{int} = -\frac{1}{2m}\left(\Delta_\rho - \frac{\hat{K}^2}{\rho^2}\right) + \sum_{i<j}^{A} V_{ij}$$

where one recognizes the Laplace operator $\Delta_\rho \equiv \Delta_{\rho_{A-1}}^{A-1}$ for $A-1$ Jacobi coordinates (see Eq. (B.9) and (B.10)) and the hyperspherical grandangular momentum operator $\hat{K} \equiv \hat{K}_{A-1}$. We would like to solve the internal Schrödinger equation

$$H_{int}\Psi(\boldsymbol{\eta}_1, ..., \boldsymbol{\eta}_{A-1}, s_1, ..., s_A, t_1, ..., t_A) = E\Psi(\boldsymbol{\eta}_1, ..., \boldsymbol{\eta}_{A-1}, s_1, ..., s_A, t_1, ..., t_A),$$

expanding the wave function $\Psi(\boldsymbol{\eta}_1, ..., \boldsymbol{\eta}_{A-1}, s_1, ..., s_A, t_1, ..., t_A)$ in terms of the antisymmetrized hyperspherical harmonics (see (4.5) and (4.6)). The hyperspherical

harmonics are, by definition, the eigenvectors of the operator $\hat{K}^2$ with eigenvalues $K(K+3A-5)$. They can be used to describe the angular part of the internal A-body wave function. Note that the kinetic energy $T = -\frac{1}{2m}\left(\Delta_\rho - \frac{\hat{K}^2}{\rho^2}\right)$ in the hyperspherical formalism is made of a purely hyper-radial part $T_\rho = -\frac{1}{2m}\Delta_\rho$, depending only on ρ, and of another part $T_K = \frac{1}{2m}\frac{\hat{K}^2}{\rho^2}$, called hyperspherical kinetic energy, which is clearly diagonal in the hyperspherical basis. Therefore, expanding the hyper-radial part of the wave functions in terms of the Laguerre polynomials, as in Eq. (4.19) and Eq. (4.20), one can show that the solution of the Schrödinger equation is reduced to the solution of an hyper-radial equation (see [Bar97a]).

Although the hyperspherical harmonics constitute a very good basis, it turns out that the convergence of the expansion is very slow especially in case of hard-core potentials, which is the situation in nuclear physics. In order to speed up the convergence of the expansion several methods have been proposed in the literature. One solution is to insert a two-body correlation factor into the basis wave functions (CHH), e.g. [Fen72, Ros92]. In the present work we have used another approach, where an effective interaction has been built within the hyperspherical formalism (EIHH) [Bar01, Bar01a].

The idea of the effective interaction is a very old one in physics. Since we perform an expansion on a set of basis states and clearly the expansion has to be truncated at some point, we always have to work in a model space, called P-space and characterized by a projection operator P. In our case this model space is constituted by all the hyperspherical harmonics that possess a grandangular momentum $K \leq K_{max}$. It turns out that it is not necessary to build also an effective interaction in the hyper-radial space, since full convergence is reached already with $30-50$ Laguerre polynomials. The complementary space is called Q-space and is characterized by a projection operator Q. This means that the union of these two spaces covers the entire Hilbert space, i.e. $P+Q = \mathbb{1}$. One can define an effective interaction that, acting only in the P-space, contains the influence of the Q-space and which leads for the corresponding effective hamiltonian to the same eigenvalues of the original hamiltonian. One method to build the effective interaction is to use the Lee-Suzuki procedure with the similarity transformation X [Suz80, Suz82, Suz83]. In this approach the effective hamiltonian is given by

$$H_{eff} = PX^{-1}HXP = PX^{-1}\left[T + \sum_{i<j}^{A} V_{ij}\right]XP, \tag{4.26}$$

where $V_{eff} = PX^{-1}\left[\sum_{i<j}^{A} V_{ij}\right] XP$ is the effective interaction. Note that the effective hamiltonian acts only in the P-space and contains the influence of the Q-space through the action of the transformation operator $X = e^{\omega}$, which is responsible of the reprojection of the information contained in the Q-space into the model space. Namely, it is defined such that that $\omega = Q\omega P$. The representation of the original hamiltonian and of the transformed one, after the application of the similarity transformation, is the following

$$H = \left(\begin{array}{c|c} H_{PP} & H_{QP} \\ \hline H_{PQ} & H_{QQ} \end{array}\right) \rightarrow \tilde{H} = X^{-1}HX = \left(\begin{array}{c|c} \tilde{H}_{PP} & 0 \\ \hline \tilde{H}_{PQ} & \tilde{H}_{QQ} \end{array}\right) \tag{4.27}$$

and the effective hamiltonian is clearly $H_{eff} = \tilde{H}_{PP}$. The condition that the operator ω has to satisfy in order to yield $\tilde{H}_{QP} \equiv 0$ is

$$Q(H + [H, \omega] - \omega H \omega)P = 0, \tag{4.28}$$

which can be obtained using the fact that the transformation admits the following expansion $X = 1 + \omega$, since $\omega^2 = \omega^3 = .. = 0$ (it can be seen from the form of the operator $\omega = Q\omega P$). One can calculate the eigenvectors of the effective hamiltonian H_{eff}, which are contained in the P-space, i.e. one can construct the space $\tilde{\epsilon}_P = \{|\tilde{\Psi}_\mu\rangle : \tilde{H}|\tilde{\Psi}_\mu\rangle = \epsilon_\mu|\tilde{\Psi}_\mu\rangle \quad \text{with} \quad |\tilde{\Psi}_\mu\rangle = P|\tilde{\Psi}_\mu\rangle\}$. With the help of the transformation X one can also construct the corresponding space for the true hamiltonian, i.e. $\epsilon_P = \{|\Psi_\mu\rangle : |\Psi_\mu\rangle = X|\tilde{\Psi}_\mu\rangle \quad \text{with} \quad |\tilde{\Psi}_\mu\rangle \in \tilde{\epsilon}_P\}$. Clearly any element of this last space has components also in the Q-space. The important fact is that any vector belonging to ϵ_P is eigenvector of the true hamiltonian with the same eigenvalue as for the effective hamiltonian. Namely, it holds that $H|\Psi_\mu\rangle = HX|\tilde{\Psi}_\mu\rangle = XX^{-1}HX|\tilde{\Psi}_\mu\rangle = X\tilde{H}|\tilde{\Psi}_\mu\rangle = \epsilon_\mu X|\tilde{\Psi}_\mu\rangle = \epsilon_\mu|\Psi_\mu\rangle$.

It can be proven that, knowing only the space ϵ_P, one can construct the similarity transformation via the matrix element of the operator ω from

$$\langle\alpha|\omega|\beta\rangle = \sum_{\mu} \langle\beta|\Psi_\mu\rangle (A^{-1})_{\mu\alpha}, \tag{4.29}$$

where $(A)_{\alpha\mu} = \langle\alpha|\Psi_\mu\rangle$ and $|\alpha\rangle$ and $|\beta\rangle$ are basis states for the P-space and Q-space, respectively. The solution for ω given in (4.29) satisfies the condition required in Eq. (4.28) for the effective interaction. It is clear that, within this approach, in order to construct the effective interaction one has to be able to build not only the P-space, but also the Q-space.

An equivalent hermitian effective interaction can be constructed through the transformation [Suz82]

$$H_{eff} = \frac{P+\omega}{\sqrt{P(1+\omega^{\dagger}\omega)P}} H \frac{P+\omega}{\sqrt{P(1+\omega^{\dagger}\omega)P}}, \tag{4.30}$$

where the operator ω is the same as in (4.29).

Since the effective interaction contains the whole A-body information of the Q space, the calculation of the A-body effective interaction is as difficult as finding the full space solutions. Furthermore, in general, the effective interaction appearing in Eq. (4.26) is an A-body effective interaction, also if one starts from a two-body NN potential. This makes the exact solution of the Eq. (4.26) very difficult and the difficulty increases with increasing A. The idea is then to build an approximate effective interaction, with the requirement that

$$V_{eff}^{app} \rightarrow V \;\text{ if }\; P \rightarrow \mathbb{1},$$

i.e., enlarging the dimension of the model P-space with increasing K_{max} and n_{ρ}^{max}, the approximated effective interaction should converge to the exact one.

One method to find an approximate effective interaction was already proposed in the context of shell model calculations, where the harmonic oscillator basis functions are defined in terms of the Jacobi coordinates, the so called "No Core Shell Model" (NCSM) calculations [Nav96, Nav98, Nav99]. It consists in substituting the A-body effective interaction with a sum of two-body effective interactions

$$V_{eff} = PX^{-1}\left[\sum_{i<j}^{A} V_{ij}\right] XP \;\rightarrow\; V_{eff}^{app} = \sum_{i<j}^{A} V_{eff,\,ij}^{(2)},$$

where the two-body effective interaction is derived from a two-body hamiltonian

$$H^{(2)} = H_0 + V^{(2)},$$

with $[H_0, P] = [H_0, Q] = 0$ and $PH_0Q = QH_0P = 0$. The two-body effective interaction is obtained calculating exactly the Lee-Suzuki transformation for a two body problem in the presence of $A-2$ non-interacting nucleons. Practically, one constructs the two-body hermitian effective interaction as

$$H_{eff}^{(2)} = \frac{P_2+\omega_2}{\sqrt{P_2(1+\omega_2^{\dagger}\omega_2)P_2}} H^{(2)} \frac{P_2+\omega_2}{\sqrt{P_2(1+\omega_2^{\dagger}\omega_2)P_2}}. \tag{4.31}$$

The index 2 in ω and in the projection operators refers to the fact that only two particles are interacting. The two-body effective interaction is then obtained subtracting H_0 as

$$V_{eff}^{(2)} = H_{eff}^{(2)} - PH_0P.$$

Clearly, for a two-body problem one can easily construct an effective interaction according to the Lee-Suzuki method, since it can be solved exactly. Therefore, defining a model space P_2 and a complementary Q_2 space one can obtain from Eq. (4.29) the operator ω_2 and thus the transformation operator. In effect this means we replace the original A interacting nucleons by an A-body system where only two particles interact, i.e. a two body system embedded into $A-2$ non-interacting nucleons as depicted in Fig. (4.3).

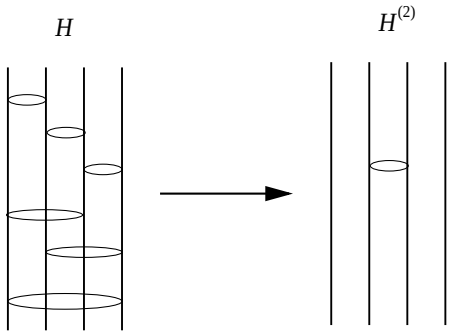

Figure 4.3: Representation of our reduction: the A-body system where all particles interact pairwise, described by H is substituted with an A-body system in which only two particle interact and the others are spectators, described by $H^{(2)}$. The interaction is depicted with an ellipse that connect the two involved nucleons in a four body-system, as an example.

Therefore the natural choice for the two-body hamiltonian is

$$H^{(2)} = \frac{1}{2m}\frac{\hat{K}^2}{\rho^2} + V_{A,A-1}, \tag{4.32}$$

which contains the total hyperspherical kinetic energy, defined through the grandangular operator[1] $\hat{K}^2$, and the interaction between the last two particles. It contains informations of the residual $A-2$ system via the kinetic energy and via the hyperradial coordinate, which has a collective character. Therefore we can say that the other non-interacting $A-2$ particle contribute to $H^{(2)}$ with a "medium correction".

[1]Note that, contrary to the notation used up to now, here the operator is denoted with the hat, since it is necessary to distinguish the operator from the eigenvalue.

The matrix element of $H^{(2)}$ between the A-body hyperspherical wave functions are

$$\begin{aligned}\langle [K]|\, H^{(2)}\, |[K']\rangle &= \delta_{S_2S_2'}\delta_{T_2T_2'}...\delta_{S_{A-2}S'_{A-2}}\delta_{T_{A-2}T'_{A-2}}\Bigg[\delta_{[K][K']}\delta_{ss'}\delta_{tt'}\frac{1}{2m}\frac{K(K+3A-5)}{\rho^2} \\ &+ \delta_{[K_{A-2}][K'_{A-2}]}V^{K_{A-2}j}_{K\ell st;K'\ell's't'}(\rho)\Bigg], \qquad (4.33)\end{aligned}$$

where one sees that $H^{(2)}$ is diagonal in the quantum numbers $[K_{A-2}]$. Furthermore, the kinetic energy is also diagonal in $[K]$. The matrix element $V^{K_{A-2}j}_{K\ell st;K'\ell's't'}(\rho)$ is diagonal in ℓ, s and t in case of a central interaction. This matrix element is like that in (4.15) in the sense that it consists in an integral that can be solved with a two-dimensional Gauss quadrature integration.

Thus, from the last expression it is clear that the effective interaction depends on the residual states, since due to the hyperangular integration it depends on K_{A-2} (see (4.18)). This medium correction results in a faster convergence of the effective interaction compared to the bare one [Bar01, Bar01a], but the price one has to pay is that for each state one has to calculate a different effective interaction, resulting in a so called "state dependent effective interaction". In fact, for every fixed value of K_{A-2} of the model space P one can determine the matrix elements of $H^{(2)}$. Then one can diagonalize it in order to construct the ϵ_P space and the similarity transformation, according to the Lee-Suzuki method [Suz80]. In our case the model P_2-space is made of $\{[K] : K \leq K_{max} \text{ with fixed } K_{A-2}\}$ with $P_2 \subset P$, and the Q_2-space is obtained by $\{[K] : K_{max} \leq K \leq K_{MAX} \text{ with fixed } K_{A-2}\}$. The value of K_{MAX} is chosen to be about 60 for purely S-wave interaction and about 180 for P-wave potentials. We recall that the relation between K and K_{A-2} is always $K = 2n + K_{A-2} + \ell$. The P_2- and Q_2-spaces clearly depend on K_{A-2} and therefore we will have as many of them as the number of K_{A-2} values in the P-space. For simplicity, however, we do not indicate this dependence in our notation. At this point one can solve Eq. (4.29), going through the inversion of the matrix $A_{\alpha\mu}$ with dimension n_P, where n_P is the number of HH basis functions in the P-space that belong to the subspace $[K_{A-2}]$, and consequently to the corresponding P_2. Therefore, for every K_{A-2} value one has an effective interaction, which is obtained subtracting the kinetic energy from the effective hamiltonian

$$V^{(2)}_{eff\ A,A-1} = H^{(2)}_{eff} - \frac{1}{2m}\frac{\hat{K}^2}{\rho^2}. \qquad (4.34)$$

Finally one can use this two-body effective interaction to solve the A-body problem. Namely, using an antisymmetrized basis state one can relate the matrix element of

the approximate effective interaction to the matrix element of the last pair

$$\langle V_{eff}^{app} \rangle = \frac{A(A-1)}{2} \left\langle V_{eff\ A,A-1}^{(2)} \right\rangle ,$$

where in the last matrix element only one Jacobi coordinate is involved, with the relative distance $\mathbf{r}_{A,A-1} = \sqrt{2}\boldsymbol{\eta}_{A-1} = \left(\sqrt{2}\rho \sin\varphi, \hat{\eta}_{A-1}\right)$ in hyperspherical coordinates. This is exactly the matrix element of the two-body effective interaction we have calculated where only particle A interacts with particle $A-1$. Note that only the effective interaction $V_{eff\ A,A-1}^{(2)}$ is actually needed in this method, and not all the different $V_{eff\ ij}^{(2)}$, which makes "natural" the choice of the starting hamiltonian in (4.32).

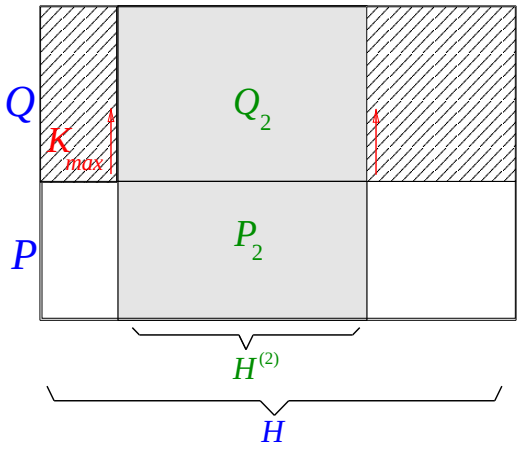

Figure 4.4: Schematization of the EIHH method: a two-body effective interaction is constructed starting form $H^{(2)}$ and then it is used in the solution of the A-body Schrödinger equation.

In order to understand better why this approximated effective interaction should converge to the exact one, we present in Fig. 4.4 a schematization of the approximation performed. This picture is only meant to visualize things in a figurative manner, with no pretension of completeness, for which we refer to the literature, e.g. [Suz80, Nav96, Nav98, Bar01, Bar01a]. In the picture, the total A-body Hilbert space is separated in the model P-space and in the complementary Q-space. Within the A-body Hilbert space we isolate the "two-body interaction" space, defining a P_2 and a Q_2 space for every K_{A-2}, in which only two particles interact with each other, while the others are frozen. Working in these spaces one constructs the effective interaction, that clearly includes the information of the Q_2 space. Therefore, with enlarging the P-space (which in our case means increasing K_{max}) also

the space P_2 is consequently enlarged. This means the effective interaction used to solve the A-body problem contains almost all the information of the Q space, since the not considered contributions (marked with bars in Fig. 4.4) tends to zero when $P \to \mathbb{1}$ $(K_{max} \to \infty)$. Therefore, the approximate effective interaction has to converge to the exact A-body effective interaction and therefore to the bare one.

The effective interaction method in conjunction with the hyperspherical formalism has revealed to be a very good bound state technique, since it enables one to obtain a fast convergence in the hyperspherical harmonics basis expansion, and the matrix elements required are at most two-dimensional numerical matrix elements, while all the rest can be performed analytically. This last property cannot be obtained using the correlation method, where, via the Jastrow factor, all the Jacobi coordinates are mixed and usually one has to calculate the $3(A-1)$-dimensional integrals with a Monte Carlo method, which is numerically very time consuming.

With the EIHH it has been possible indeed to obtain bound state properties for nuclei with $4 \leq A \leq 7$ with great success, as will be shown also in this work. Clearly, in increasing the mass number A, the number of hyperspherical harmonics states for a given K_{max} value becomes very large, and at some point it constitutes a bottleneck, if all states are kept and no selection of basis states is made, i.e. eliminating certain states with no influence.

Since the EIHH is a very good bound state technique that enables one to calculate wave functions, it can also be used to solve the Schrödinger-like equation one ends up with the LIT method. Quite a few examples of reactions studied with the combination of these two methods are already available in the literature (see e.g. [Bar01b, Bac02, Bac04, Bac04b, Gaz04]), and some of them will be presented in the present work.

Chapter 5

Application to Photodisintegration

In this chapter the first microscopic calculation of the total photoabsorption cross sections of six- and seven-body nuclei is presented. The final state interaction is completely taken into account with the LIT method. The discussion of the results follows a general description of the calculation.

5.1 Description of the Calculation

In an inclusive photodisintegration reaction, $\gamma + A \to X$, a real photon γ with momentum $\mathbf{q}$ and energy $\omega = |\mathbf{q}|$ is absorbed by an A-body nucleus that makes a transition from the ground state with energy and momentum $(E_0, \mathbf{P}_0)$ to a final state described by $(E_f, \mathbf{P}_f)$, that is not measured. The cross section of the process (Eq. (3.38)) is proportional to the response function of the transverse current (see Eq. (3.39)). As already mentioned, below pion production only the E1 multipole of the current has to be taken into account, because it is well known that the dipole approximation is excellent for describing the total photoabsorption cross section of nuclei, see e.g. [Eis70, Are91]. Using the Siegert theorem, the operator to consider in the response function takes, in the long wave range limit[1], the simple form of

$$D_z = \sum_{k=1}^{A} \frac{\tau_k^3 z'_k}{2}. \tag{5.1}$$

Here τ_k^3 and z'_k represent the third component of the isospin operator and of the coordinate of the k-th particle in the center of mass reference frame, respectively. The response function $R(\omega)$ is calculated according to the LIT method by solving

[1] The Bessel function is approximated as $j_1(qr) \sim \frac{qr}{3}$ for $qr \ll 1$.

the following "Schrödinger-like" equation

$$(H - E_0 + \sigma)|\widetilde{\Psi}\rangle = D_z|\Psi_0\rangle. \tag{5.2}$$

The first step to solve Eq. (5.2) is to find the solution Ψ_0 for the ground state, which is then used as input for the generalized eigenvalue problem (5.2) for $\tilde{\Psi}$. Our method consists in expanding Ψ_0 and $\tilde{\Psi}$ in terms of the A-body symmetrized HH [Bar97b, Bar98]. The expansion is performed up to maximal values of the HH grand-angular momentum quantum number K^0_{max} for Ψ_0 and K_{max} for $\widetilde{\Psi}$. The number of HH states for a given grand-angular momentum depends on the A-body system considered. We improve the convergence of the HH expansion using the EIHH method [Bar01, Bar01a]. In case of Ψ_0 the basis states are constructed with the quantum numbers of the ground state. For $\tilde{\Psi}$ the basis functions possess the quantum numbers selected by the isovector dipole transition. The specific quantum numbers of the nuclei being studied will be shown later in the presentation of the results.

In order to evaluate the LIT we calculate the quantity $\langle\widetilde{\Psi}|\widetilde{\Psi}\rangle$ using the Lanczos algorithm [Mar03]. It can be proven that the use of the Lanczos algorithm is equivalent to solving Eq. (5.2) by a matrix inversion, which is quite time consuming. The advantage of this algorithm is that it is very fast, since only multiplications of matrices with vectors are required, as will be explained later.

In case of semirealistic interactions the total orbital angular momentum L_0 and the total spin S_0 are good quantum numbers of the ground state $|\Psi_0(M_0^L, M_0^S)\rangle$, with projections M_0^L and M_0^S, respectively. Then, one can rewrite the LIT of the response as (see [Mar03, Bac01])

$$\begin{aligned}\mathcal{L}(\sigma_R, \sigma_I) &= \frac{1}{2L_0+1}\,\frac{1}{2S_0+1}\frac{1}{\sigma_I}\sum_{M_0^L, M_0^S} \\ &\times\ \mathrm{Im}\{\langle\Psi_0(M_0^L, M_0^S)|D_z^\dagger\frac{1}{H - E_0 - \sigma_R - i\sigma_I}D_z|\Psi_0(M_0^L, M_0^S)\rangle\},\end{aligned} \tag{5.3}$$

The transform $\mathcal{L}(\sigma_R, \sigma_I)$ is evaluated by inserting a complete set of projection operators

$$\sum_{C, M^L, M^S} |\Psi_C(M^L, M^S)\rangle\langle\Psi_C(M^L, M^S)| \equiv \sum_{C, M^L, M^S} P_{C, M^L, M^S},$$

where $C = \{L, S, T, T^z, \pi\}$ stands for the quantum numbers characterizing the channels (angular momentum, spin, isospin, isospin projection and parity, respectively), while M^L and M^S are the third components of angular momentum and spin. In the

sum only the channels allowed by the dipole selection rules need to be considered and, since the dipole operator does not depend on spin, we do not need to average over the initial spin projections (M_0^S), neither to sum over M^S. Therefore one obtains

$$\mathcal{L}(\sigma_R,\sigma_I) = \frac{1}{2L_0+1}\frac{1}{\sigma_I}\sum_{C,M^L,M_0^L}|\langle\Psi_C|D_z|\Psi_0\rangle|^2\mathrm{Im}\{\langle\Psi_C|\frac{1}{H-E_0-\sigma_R-i\sigma_I}|\Psi_C\rangle\}, \tag{5.4}$$

where

$$|\Psi_C\rangle = \frac{P_C D_z|\Psi_0\rangle}{\sqrt{\langle\Psi_0|D_z P_C D_z|\Psi_0\rangle}}. \tag{5.5}$$

To simplify the notation, in the last two equations the dependence on M^L and M_0^L has been omitted, as will be done in the following.

It can be shown [Mar03] that one can use the Lanczos algorithm to calculate the (5.4). The recursion relation to use is

$$b_{n+1}|\varphi_{n+1}\rangle = H|\varphi_n\rangle + a_n|\varphi_n\rangle - b_n|\varphi_{n-1}\rangle\,, \tag{5.6}$$

$$a_n = \langle\varphi_n|H|\varphi_n\rangle,\quad b_n = ||b_n|\varphi_n\rangle||, \tag{5.7}$$

where $\{|\varphi_n\rangle; n\geq 0\}$ is an orthonormal set and a_n and b_n are the Lanczos coefficients, starting with a given $|\varphi_0\rangle$ and $b_0=0$. Taking (5.5) as starting Lanczos vector, the imaginary part in the LIT becomes a continued fraction in terms of the Lanczos coefficients as

$$F_C = \mathrm{Im}\left\{\langle\Psi_C|\frac{1}{H-E_0-\sigma_R-i\sigma_I}|\Psi_C\rangle\right\} = \mathrm{Im}\left\{\frac{1}{(z-a_0)-\frac{b_1^2}{(z-a_1)-\frac{b_2^2}{(z-a_2)-b_3^2\cdots}}}\right\}_C, \tag{5.8}$$

where $z = E_0+\sigma_R+i\sigma_I$. In Ref. [Mar03] it is shown that a rapid convergence of the continued fraction is reached. Note that in the recursion (5.6) only products of matrices with vectors are needed. Furthermore, in this way, once one has calculated the Lanczos coefficients for every channel, the LIT for different σ_R and σ_I can be easily evaluated, while using the method of matrix inversion one would need to repeat the inversion procedure for every value of σ.

In this way the total LIT can be written as sum of the Lorentz transforms of the

individual channels

$$\mathcal{L}(\sigma_R, \sigma_I) = \sum_C \mathcal{L}_C(\sigma_R, \sigma_I)\,, \tag{5.9}$$

where for every channel one has $\mathcal{L}_C(\sigma_R, \sigma_I) = \mathcal{N}_C^2 F_C$. Here $\mathcal{N}_C$ is connected to the norm of $P_C D_z|\Psi_0\rangle$,

$$\mathcal{N}_C^2 = \frac{1}{2L_0+1} \sum_{M^L, M_0^L} |\langle \Psi_C | D_z | \Psi_0 \rangle|^2 = \frac{1}{2L_0+1} \sum_{M^L, M_0^L} \langle \Psi_0 | D_z P_C D_z | \Psi_0 \rangle. \tag{5.10}$$

This formalism will be used in the discussion of the results.

5.2 Results for ^{6}Li and ^{6}He Photoabsorption

For the first six-body photoabsorption calculations we have made use of simple nucleon-nucleon (NN) potentials, the so-called semirealistic interactions. We have used three different models: the Malfliet-Tjon (MTI-III) [Mal69] and Minnesota (MN) [Tho77] potentials, acting in (L =even) states only, and the AV4' [Pie02], that includes also (L=odd)-wave interactions. The MTI-III model contains Yukawa-type potentials and has a strong short range repulsion, while the MN consists of Gauss-type potentials and has a rather soft core. The MTI-III potential is fitted to the NN scattering S-wave phase-shifts, ^{1}S$_0$ and ^{3}S$_1$, up to the pion threshold, whereas the MN potential is fitted to low-energy two- and three-body data. The AV4' is a simplified version of the AV18 potential where only the first central terms are kept and no tensor force is included. The prime indicates that it is not simply a truncated version of the AV18, but the parameters are refitted to reproduce the binding energy of the deuteron. These potentials are all called semirealistic, because, despite their simple structure, they "effectively" include partially the influence of the tensor force.

As a first step one has to solve the Schrödinger equation to find the solution for the ground state, making sure that convergence in K^0_{max} is reached. With a central interaction no coupling between spin and angular momentum is required, and therefore the good quantum numbers to use for the construction of the wave functions for ^{6}He (and ^{6}Li) are: angular momentum $L_0 = 0$ (0), spin $S_0 = 0$ (1), isospin $T_0 = 1$ (0) with third component T^z=-1 (0). In Table 5.1 we present the values for binding energies that we have obtained with the three different potential models. The values reported in Table 5.1 correspond to a calculation with $K^0_{max} = 10$ for the dominant S-wave potentials and with $K^0_{max} = 14$ for the AV4'. In fact,

Table 5.1: Binding energies of ^{6}Li and ^{6}He obtained with EIHH for the three potentials and the GFMC results for AV4' [Pie02] in comparison with experimental data. The error bars of the experimental data are not presented since they are smaller than the second digit. In the calculations the Coulomb force is always included.

	MTI-III	MN	AV4'	AV4'-GFMC	EXP
B.E.(^{6}Li) [MeV]	-35.88(20)	-34.89(10)	-36.44(10)	-35.81(3)	-31.99
B.E.(^{6}He) [MeV]	-31.87(10)	-30.48(10)	-32.87(10)	-32.22(3)	-29.27

the addition of the (L=odd)-wave interactions leads to a slower convergence in the grandangular momentum. The binding energies are compared to those obtained from the Green Function Monte Carlo (GFMC) calculation with the AV4' potential [Pie02], and to the experimental values. It is clear that the EIHH results for AV4' do not agree completely with the GFMC values, since there is a difference of 2%. One should mention that there are other calculations, with the No Core Shell Model (NCSM) [Bac05], that give an energy of -36.78 (12) MeV for ^{6}Li with AV4' which is closer to the EIHH value. For the MN potential without the Coulomb force the result of NCSM for the binding energy of ^{6}Li, -36.50(8) MeV, is compatible with that of EIHH, -36.64(10) MeV (the difference with the value in Table 5.1 is due to the Coulomb force). Unfortunately, no GFMC calculations with this potential are available. The origin of this discrepancy is still not understood, but detailed studies by the various groups are under way [Bac05]. Nevertheless, it is known that a small difference in the binding energy of a nucleus does not lead to a dramatic difference in the absorption cross section. Thus, in the following we will describe in greater details the calculation of the LIT and of the photoabsorption cross section.

To evaluate the LIT one uses the ground state as input in the Schrödinger-like equation (5.2). Since the dipole carries angular momentum 1 and isospin 1 the good quantum numbers for $\tilde{\Psi}$ in case of ^{6}He (^{6}Li) are: $L = 1$ (1), $S = 0$ (1), $T = 1$ and 2 (1), T_z=-1 (0). Note that in case of ^{6}He there are two different final isospin channels, T=1 and 2, since the third possibility T=0 is not possible because of the conservation of the third component of the isospin, which is T_z=-1.

With respect to the convergence of the LIT as a function of K^0_{max} and K_{max}, it was sufficient, in case of the AV4' potential, to consider the bound state calculated with $K^0_{max} = 12$, yielding as binding energy $E_0 = -32.90$ MeV for ^{6}He and $E_0 = -36.47$ MeV for ^{6}Li (note that the small difference with respect to the values presented in Table 5.1 is due to the different K^0_{max} used). Since $\widetilde{\Psi}$ depends on Ψ_0 one has also to check whether the norm $\langle\widetilde{\Psi}|\widetilde{\Psi}\rangle$, i.e. $\mathcal{L}(\sigma_R, \sigma_I)$, converges for $K^0_{max} = 12$.

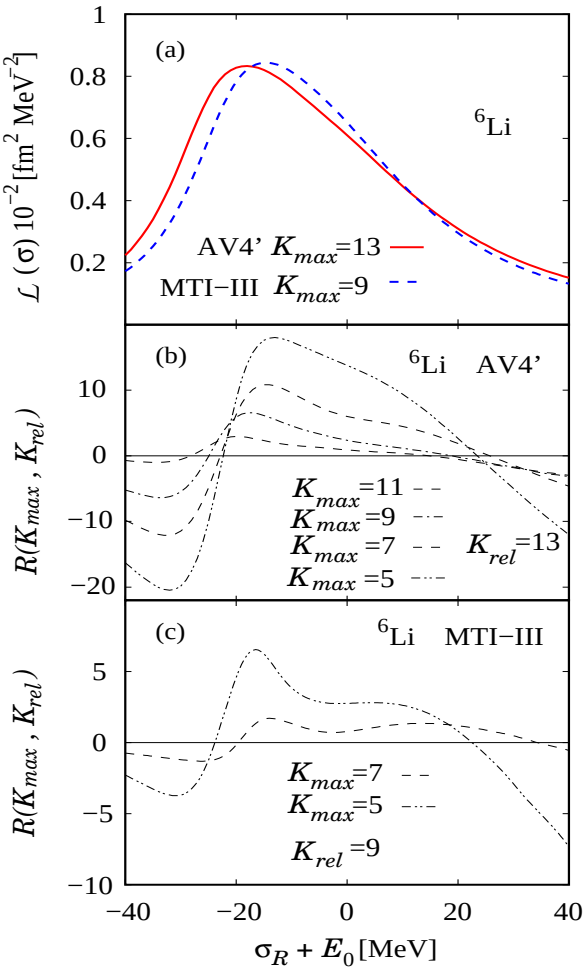

Figure 5.1: (a) LIT for ^{6}Li ($\sigma_I = 10$ MeV) with AV4' and MTI-III potentials; HH convergence of LIT as function of K_{max} with $K_{rel} = 13$ for the AV4' (b) and $K_{rel} = 9$ for the MTI-III (c) potential (see definition of R in the text).

Indeed the transforms $\mathcal{L}(\sigma_R, \sigma_I = 10$ MeV) obtained with $K^0_{max} = 12$ and 14 at fixed K_{max} differ by less than 1%.

In case of the MTI-III and MN potentials the calculations of the LIT are performed with a bound state expansion up to $K^0_{max} = 10$, which has been found to be sufficient. In Fig. 5.1 we show the convergence of the LIT for ^{6}Li for the AV4' and the MTI-III potentials. In the upper panel the two LIT results obtained with the highest considered K_{max} are presented, while in the two lower panels we show the relative error R in percent, for the two potentials separately. The quantity R is defined as

$$R(K_{max}, K_{rel}) = \frac{\mathcal{L}(K_{max}) - \mathcal{L}(K_{rel})}{\mathcal{L}(K_{rel})} \times 100\,. \tag{5.11}$$

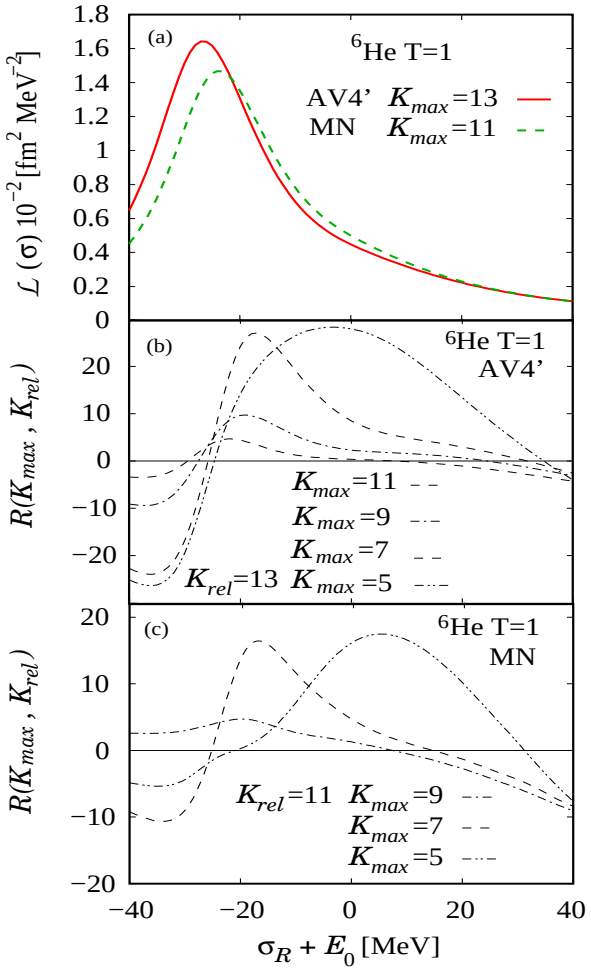

Figure 5.2: (a) LIT for ^{6}He ($\sigma_I = 10$ MeV), in the isospin channel $T = 1$, with AV4' and MN potentials; HH convergence of LIT as function of K_{max} with $K_{rel} = 13$ for the AV4' (b) and $K_{rel} = 11$ for the MN (c) potential.

One can clearly see quite a nice convergence pattern with increasing K_{max}.

In Fig. 5.2 we present an analogous picture for ^{6}He with the AV4' and the MN potentials. One finds rather satisfactory results, but compared to ^{6}Li the AV4' case exhibits a slower convergence, e.g., in the lower σ_R range, where mainly strength from the threshold region is sampled, one has $R(K_{max} = 11) \simeq 1\%$ in case of ^{6}Li and $R(K_{max} = 11) \simeq 3\%$ in case of ^{6}He. Figures 5.1 and 5.2 also illustrate that the convergence is better for the dominant S-wave potentials, with interaction in (L=even)-waves only. Thus addition of (L=odd)-wave interactions seems to lead to a slightly slower convergence of the HH expansion, as already mentioned. In fact performing LIT calculations with a modified AV4' potential, namely with switched off (L=odd)-wave interaction, one gets a convergence pattern similar to those of MN

or MTI-III potentials.

Here one has to mention the fact that these calculations have been performed on a parallel machine[2]. In fact, the dimensionality of the problem to solve is rather big, since the number of hyperspherical states used in the solution of the Schrödinger (and Schrödinger-like) equation increases dramatically with K in case of a six-body system, see e.g. Table 5.2. The impossibility to perform such calculations on a

Table 5.2: Number N_{HH} of hyperspherical harmonics at a given K^0_{max} value for the six-body problem. The total number of states to use in the expansion is obtained multiplying N_{HH} with the number of Laguerre polynomials ~ 30.

K^0_{max}	4	6	8	10	12	14
N_{HH}	8	42	186	695	2278	6664

simple PC could only be overcome by parallelizing the code and then by running the programs on more powerful machines[3].

Another way to overcome the problem of the increasing number of states consists in performing a cut on those states which do not contribute in the expansion. In fact the present results were obtained by eliminating such states. The details of this technical aspect are described in [Bac04].

In the following the results of the photoabsorption cross section are discussed. They are obtained using Eq. (3.38), where $R(\omega)$ is taken from the inversion of the best calculated LIT.

In Fig. 5.3 we show our final results for the three potentials [Bac02, Bac04]. The three interactions show a qualitatively similar behavior of $\sigma(\omega)$ differing only slightly in the position, height and width of the curves. There is one single giant dipole resonance peak for ^{6}Li and two well separated peaks for ^{6}He. For the latter one finds a low-energy peak at about ω=8 MeV (present only in the T=1 channel), which is due to the breakup of the halo part of ^{6}He and a second bump, at about ω=32 MeV (with contributions of about 60% from T=1 and 40 % form T=2 channels), which is caused by the breakup of the α-core of the nucleus. This requires higher photon energies, since in order to have a T=2 final state one has to break the core. The ^{6}Li total cross section does not show such a substructure. This is probably due to the fact that the breakup in two three-body nuclei, ^{3}He + ^{3}H, fills the gap between the halo and the α-core peaks. Note that in case of ^{6}He a corresponding

[2]IBM SP4 at CINECA (Bologna, Italy).

[3]The parallelization of the code has been part of the present PhD work, but will not be discussed further, since it is too technical.

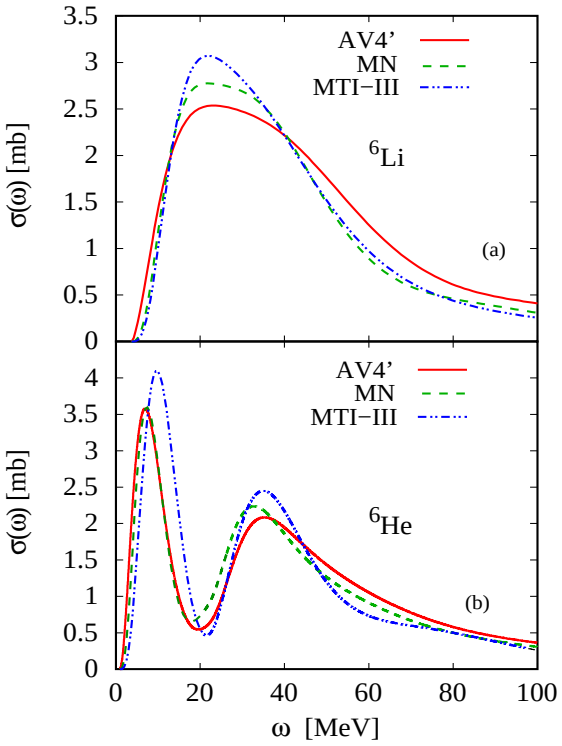

Figure 5.3: Total photoabsorption cross sections for the six-body nuclei with AV4', MN and MTI-III potentials: (a) ^{6}Li, (b) ^{6}He.

breakup in two identical nuclei, ^{3}H + ^{3}H, can not be induced by the dipole operator.

The two peaks of the ^{6}He can also have another interpretation, namely the low

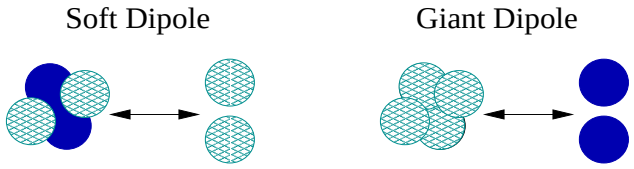

Figure 5.4: Soft mode and giant dipole mode of ^{6}He.

energy peak may represent a "soft mode" in which the two neutrons of the *skin* of the nucleus oscillate against the α-core, whereas the second peak describes an usual giant dipole resonance, in which all protons move against all neutrons in a collective motion, as depicted in Fig. 5.4. In the framework of "halo-nuclei" research, this low-energy peak has been foreseen and it has been called "pigmy resonance" since it was expected to be small. It is interesting to note that this microscopic calculation for ^{6}He leads to a soft mode peak which is actually much higher than the so-called

"giant" dipole resonance. Namely, the separation energy of the two neutrons is very low (0.975 MeV), which means that they can easily be knocked out by the photon.

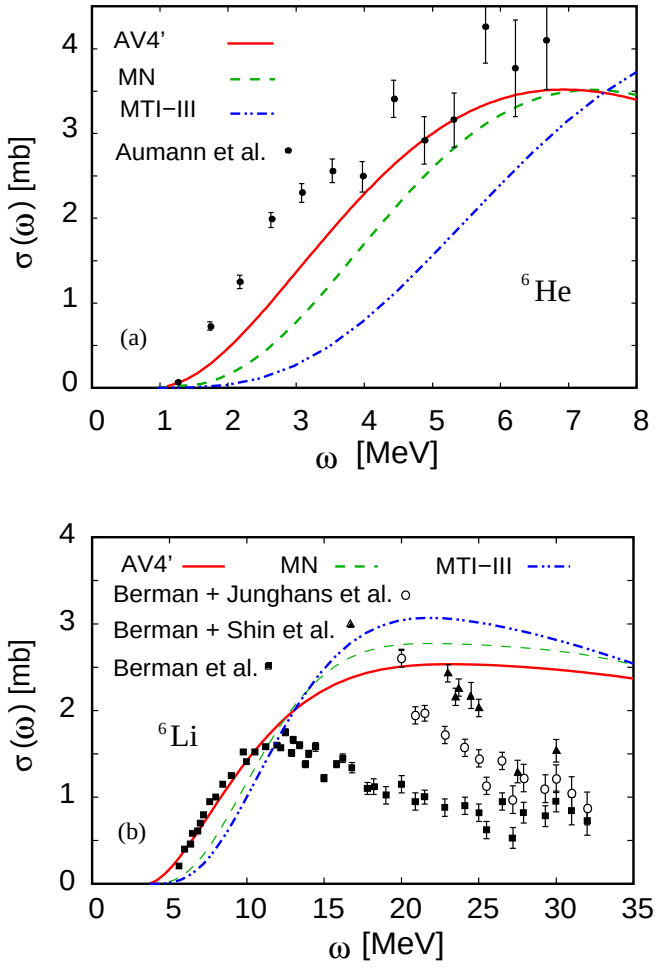

Figure 5.5: Theoretical and experimental photoabsorption cross section results (see also text): (a) ^{6}He with data from [Aum98, Aum01] (theoretical results convoluted with instrumental response function); (b) ^{6}Li with experimental data from [Ber65, Jun79, Shi75].

At this point it is interesting to compare the results obtained with available experimental data. In Fig. 5.5 we show the results of a recent low-energy experiment by Aumann et al. [Aum98, Aum01] on ^{6}He in comparison with our curves. The experimental cross section was extracted from Coulomb excitation of ^{6}He using a secondary radioactive ^{6}He beam. It is evident that our theoretical results have a similar shape, but are shifted by about 1 to 3 MeV towards higher energies, depending on the potential used.

In case of ^{6}Li the experimental situation is a bit more complex. The semi-inclusive channel $^6\mathrm{Li}(\gamma, \sum_n)$ measured by Berman *et al.* [Ber65] corresponds to the

total $\sigma(\omega)$ below $\omega = 15.7$ MeV. At higher energy channels not involving neutrons open up (^{3}He + ^{3}H, ^{3}H + p +d), which are not measured in [Ber65]. Regarding these last two channels we show two experimental data sets: Junghans *et al.* [Jun79] and Shin *et al.* [Shi75] (for both it is not clear whether ^{3}H + d + p is measured or not). In order to make the comparison simpler, we have summed these data with the Berman data. At low energies, up to 10 MeV, the comparison of theoretical and experimental results is similar to the ^{6}He case with a shift of the theoretical cross section to somewhat higher energies. At higher energies the data indicate a faster fall-off of the cross section than the theory. On the other hand the experimental situation is clearly not settled as one can note from the different results of Refs. [Jun79] and [Shi75]. Figure 5.5 shows also that for the AV4' potential one finds an enhancement of strength in the threshold region and lower strength at higher energies compared to the dominant S-wave potentials. It is evident that the inclusion of the P-wave interaction improves the agreement with experimental data considerably. This is particularly the case for ^{6}Li. In fact with the AV4' potential one has quite a good agreement with experimental data up to about 12 MeV. In case of ^{6}He the increase of low-energy strength is not sufficient, there is still some discrepancy with data. Probably, in order to describe the halo structure of this nucleus, more refined potentials are needed. In particular the spin-orbit (LS) component of the NN potential could play a role in the determination of the soft dipole resonance. In fact in a single particle picture of ^{6}He the two halo neutrons will mainly stay in a p-state and can interact with one of the core nucleons via the LS-force. Another reason for the discrepancy could be the convergence. As already pointed out, our HH convergence is quite satisfactory for ^{6}Li, whereas it is still not yet fully complete in case of ^{6}He. The pronounced halo structure of this nucleus could make the HH expansion more difficult.

In conclusion one can say that further investigations, both in theory and experiment, are needed: experimental data are too few (^{6}He) or do not present a clear picture (^{6}Li), and from the theoretical point of view, more effort has to be addressed to the inclusion of additional parts in the NN potential.

5.3 Results for ^{7}Li Photodisintegration

For the total photoabsorption of ^{7}Li again the Argonne potential AV4' [Pie02] was used, since it has resulted in a better description of experimental data in case of ^{6}He and ^{6}Li photodisintegration. One would expect the addition of the P-wave

interaction to play a role in all P-shell nuclei, therefore also in ^{7}Li.

The ground state of ^{7}Li has total angular momentum and parity $J^\pi = \frac{3}{2}^-$, and isospin $T_0 = \frac{1}{2}$ with projection $T_0^z = -\frac{1}{2}$. Using central forces, one has ground state orbital angular momentum $L_0 = 1$ and spin $S_0 = \frac{1}{2}$.

For the ground state calculation of ^{7}Li good convergence is reached with $K^0_{max} = 9$ with a binding energy of $-45.28(10)$ MeV. Further increase to $K^0_{max} = 11$ leads only to a small change of the binding energy by 0.05 MeV. In Figure 5.6 we show the convergence pattern of the binding energy of ^{7}Li with the AV4' potential as a function of K^0_{max}, where one can see that a good convergence plateau is reached. In

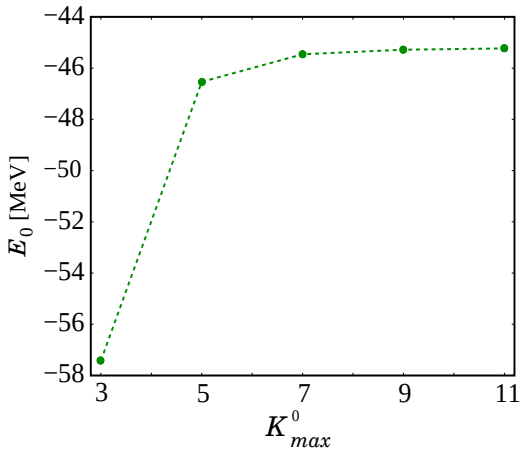

Figure 5.6: Binding energy of ^{7}Li with the AV4' potential as function of the grandangular momentum K^0_{max}.

Table 5.3 the number of hyperspherical functions for each K^0_{max} value is presented. As one can see, this number is increasing dramatically. Actually, the calculation of the binding energy with $K^0_{max} = 11$ has been performed with a reduction of the hyperspherical harmonics from 9888 to 4512, cutting those states which did not contribute to the binding energy at lower K^0_{max}. Although the convergence pattern is rather good, the obtained result for the ground state energy is not in agreement with the one obtained with a GFMC calculation [Pie02], which is $-43.9(1)$ MeV. Again, as in case of the six-body calculations, the origin of this discrepancy is not yet understood.

Considering then the dipole transition, there are six different channels allowed by the selection rules corresponding to angular momenta $L = L_0 - 1, L_0, L_0 + 1$, spin $S = S_0$ and isospins $T = T_0, T_0 + 1$ with isospin projection conserved $T^z = T_0^z$. In Table 5.4 the good quantum numbers of these channels are listed. This means that one has to calculate six different LITs, according to what has been discussed above,

Table 5.3: Number N_{HH} of hyperspherical harmonics as function of K^0_{max} for ^{7}Li. The total number of states to use in the expansion is obtained multiplying N_{HH} with the number of Laguerre polynomials ~ 30.

K^0_{max}	3	5	7	9	11
N_{HH}	2	37	325	2016	9888

in order to obtain the total photoabsorption cross section.

Table 5.4: Good quantum numbers for the channels $|\Psi_C\rangle$ with $C = 1, ..., 6$ allowed by the dipole selections rules for ^{7}Li.

	$\|\Psi_1\rangle$	$\|\Psi_2\rangle$	$\|\Psi_3\rangle$	$\|\Psi_4\rangle$	$\|\Psi_5\rangle$	$\|\Psi_6\rangle$
L	0	0	2	2	1	1
S	$\frac{1}{2}$	$\frac{1}{2}$	$\frac{1}{2}$	$\frac{1}{2}$	$\frac{1}{2}$	$\frac{1}{2}$
T	$\frac{1}{2}$	$\frac{3}{2}$	$\frac{1}{2}$	$\frac{3}{2}$	$\frac{1}{2}$	$\frac{3}{2}$
T^z	$-\frac{1}{2}$	$-\frac{1}{2}$	$-\frac{1}{2}$	$-\frac{1}{2}$	$-\frac{1}{2}$	$-\frac{1}{2}$

At this point, one can also say that, because of the dipole selection rule $K = K_0 \pm 1$ between states with hyperangular momenta K and K_0, an expansion of the ground state up to a certain K^0_{max} implies that in $|\Psi_C\rangle$ only states with hyperangular momentum $K \leq K_{max} = K^0_{max} + 1$ contribute to the LIT. Thus it is expected that for sufficiently high K^0_{max} a further increase of K_{max} beyond $K^0_{max}+1$ will not result in a significant change. For this reason one has to consider calculations of the LIT with K^0_{max} for the ground state and $K^0_{max} + 1$ for the transform, and consequently, the convergence in K^0_{max} has to be investigated.

In the present work, the best calculation of the LIT corresponds to a final state with $K_{max} = 10$. In this case the number of HH-basis states to be included becomes quite large, especially for the channels with $L_C = 1$ and 2. For example, for channel $C = 3$ and $K_{max} = 10$ one has already 6348 hyperspherical states. This number has to be multiplied by the number of hyper-radial states, about 30, to obtain the total number N of states needed in the expansion. Therefore, also in case of the $|\Psi_C\rangle$ it is desirable to discard those HH states which give only negligible contributions to the LIT. To this end one can study the importance of the HH states according to their spatial symmetry. One finds that quite a few of them can safely be neglected (for more details see [Bac04b]). The validity of the approximation can be checked by performing calculations with the complete set of states for lower values of K_{max} and comparing the results with those using a truncated set.

In this way one can accomplish for $K_{max} = 10$ a sizable reduction from $N = 190\,440$ to $N = 111\,900$ total basis functions, for $C = 3$. A similar reduction has been done also for $C = 4, 5, 6$, whereas for $C = 1$ and 2 all hyperspherical harmonics have been considered in the calculation, since with $L_C = 0$ the number of states is still not critical. The estimated error introduced by these truncations is of the order of 0.5%.

The error introduced by the symmetry truncation can also be checked in a second way. Considering the sum over the norms $\mathcal{N}_C^2$ defined in (5.10) and using completeness, one finds

$$\sum_C \mathcal{N}_c^2 = \frac{1}{2L_0+1} \sum_{C,M^L,M_0^L} |\langle \Psi_C | D_z | \Psi_0 \rangle|^2 = \frac{1}{2L_0+1} \sum_{M_0^L} \langle \Psi_0 | D_z^\dagger D_z | \Psi_0 \rangle \,, \quad (5.12)$$

where the last expression is nothing else than the mean expectation value of the operator $D_z^\dagger D_z$ in the ground state, that can be easily calculated (see Ref. [Bac02]). With respect to Eq. (5.12) we obtained 1.877 [fm^2] for the ground state expectation value with $K_{max}^0 = 9$, while using a symmetry truncated expansion for $|\Psi_C\rangle$ up to $K_{max} = 10$ we get 1.871 [fm^2]. The small difference of 0.3% reflects the small error introduced by the symmetry truncation.

As next point we address the quality of convergence of the LIT with respect to the HH expansion. The best calculations we could perform for the LIT are those with $K_{max}^0 = 9$ and $K_{max} = 10$, which are denoted by $\mathcal{L}_C(9/10)$ (note that in this case the selection rule of the dipole for the grandangular momentum is fulfilled). It is likely, that a further increase to $K_{max}^0 = 11$ and $K_{max} = 12$, $\mathcal{L}_C(11/12)$ would lead to an improvement of the convergence, and a comparison between $\mathcal{L}_C(9/10)$ and $\mathcal{L}_C(11/12)$ could give the order of magnitude of the numerical accuracy of the calculations. Although the calculation of the ground state for $K_{max}^0 = 11$ can be performed, the corresponding calculation of the final state with $K_{max} = 12$, i.e. $\mathcal{L}_C(11/12)$, is beyond our present technical capabilities, whereas it can be done for $K_{max} = 10$, i.e. $\mathcal{L}_C(11/10)$ can be calculated (in this case the dipole selection rule is not exhausted). Thus the question now is, how much is the convergence improved in going from $\mathcal{L}_C(9/10)$ to $\mathcal{L}_C(11/10)$. The answer to this question can be taken as estimation of the error in the calculation. Therefore, we define the relative percentage error by

$$R_C = \frac{\mathcal{L}_C(11/10) - \mathcal{L}_C(9/10)}{\mathcal{L}_C(11/10)} \times 100, \quad (5.13)$$

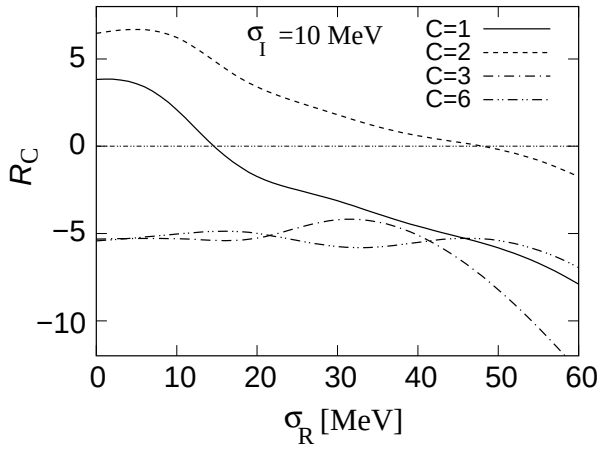

Figure 5.7: Relative error in percent of the calculation of the LITs ($\sigma_I = 10$ MeV) for some channel C (see text for details).

and study the behavior of R_C for the different channels. In Fig. 5.7 the convergence pattern of R_C is shown for four channels. One can readily see that the relative error is of about 5% for the presented channels in the energy range of interest. Assuming that the other two channels behave similarly, one can estimate a total uncertainty of about 5%.

Now results for photodisintegration of ^{7}Li will be discussed. In Fig. 5.9 we show both the calculated total cross section and the contributions of the separate channels. The energetically lowest open channel is the $T = \frac{1}{2}$ channel associated with the reaction $^7\text{Li} + \gamma \rightarrow {}^4\text{He} + {}^3\text{H}$ with a threshold of 2.47 MeV (the theoretical threshold obtained with the AV4' potential is 4.17 MeV), whereas the lowest open $T = \frac{3}{2}$ channel corresponds to $^7\text{Li} + \gamma \rightarrow {}^6\text{He} + \text{p}$, whose threshold is 9.975 MeV (the theoretical value is 12.41 MeV). In Fig. 5.8 the theoretical thresholds have been used. For the $T = 1/2$ channels in Fig. 5.8 (a) one readily sees that by far the largest contribution comes from channel 3 rising steeply above threshold, reaching a maximum around 17 MeV and falling off only slowly. Channel 5 is the next in importance rising only slowly above 10 MeV with a maximum near 33 MeV and becoming then comparable in size to channel 3. Only in the very near threshold region channel 1 is dominant but then becomes much smaller than the other two channels. In Fig. 5.8 (b) the $T = 3/2$ channels have two dominant contributions, almost similar in size. Channel 4 is slightly larger showing also a steep rise at threshold and slow fall-off with a maximum near 23 MeV whereas the second in importance, channel 6, shows a slow rise and a peak around 40 MeV. Compared to these two channels, the remaining channel 2 appears quite marginal.

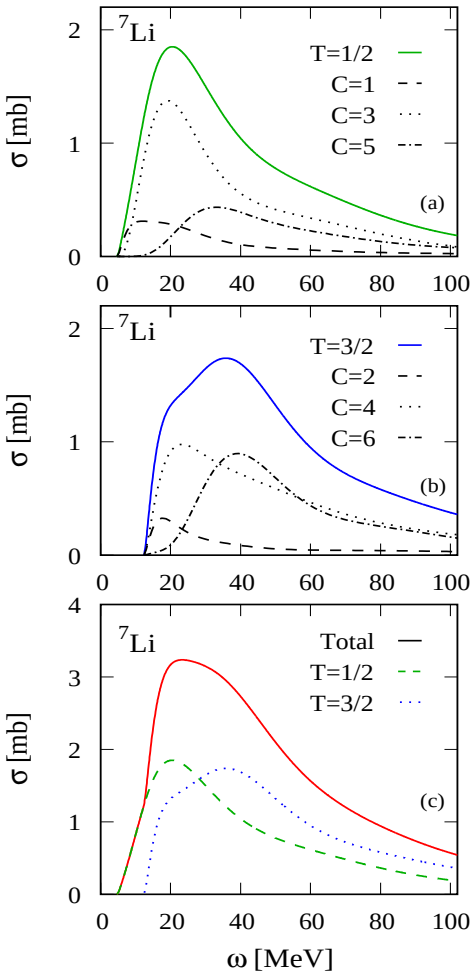

Figure 5.8: Contribution of various channels to the total cross section. Panels (a) and (b) show the separate contributions of the different channels and their sum for $T = 1/2$ and $T = 3/2$, respectively. Panel (c) shows again the $T = 1/2$ and $T = 3/2$ contributions and the total cross section.

In view of the two maxima of almost equal height with a separation by about 17 MeV the total $T = 3/2$-contribution exhibits a broader distribution than the $T = 1/2$-contribution with a shoulder on the low-energy side. The maxima of both contributions have about the same size but are separated by about 20 MeV. Thus, the resulting total cross section in Fig. 5.8 (c) shows also a broad distribution with a steep rise right above threshold, a slight shoulder above the maximum and a slow fall-off at higher energies. This characteristic behavior is indeed exhibited by the experimental data on ^{7}Li in Fig. 5.9 where we show a comparison of the theoretical result to experimental data from [Ahr75]. Note that the theoretical cross section is shifted here from the theoretical threshold to the experimental one. One readily notes that the gross properties of the data, steep rise, broad maximum and slow

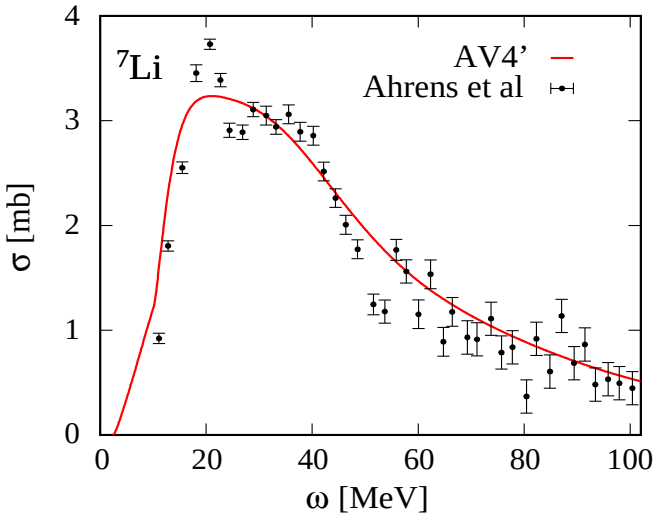

Figure 5.9: Comparison of the theoretical photoabsorption cross section calculated with AV4' potential with experimental data from [Ahr75].

fall off, are very well reproduced quantitatively over the whole energy region by the theory. It is worthwhile to emphasize that this result is based on an ab initio calculation in which the complicated final state interaction of the 7-body system is rigorously taken into account by application of the LIT method. No adjustable parameters were used, the sole ingredient being the AV4' NN potential model. It remains to be seen whether the slight variation of the data near and above the maximum will also be found in an experiment with improved accuracy. Therefore, a new measurement of the total cross section with a higher precision, especially in energy resolution, would be very desirable. Furthermore, in order to clarify the question whether a simple semi-realistic potential like the AV4' model is sufficient for an accurate theoretical description of this reaction, one should perform calculations with more realistic nuclear forces including a 3N-force.

Chapter 6

Application to Electron Scattering

In this chapter we present the results obtained for the longitudinal and transverse response functions of ^{4}He with a microscopic calculation performed via the LIT method in conjunction with the EIHH. In the discussion two main sections are presented, where the longitudinal and transverse response functions and the corresponding charge and current operators, are treated separately.

6.1 Longitudinal Response Function

In an inclusive electron scattering experiment it is possible to disentangle the longitudinal response function form the transverse response via a Rosenbluth separation as shown in Chapter 3. We recall that the longitudinal response function, given in (3.42), is defined by means of the charge operator $\tilde{\rho}(\mathbf{q})$ as

$$R_L(\omega, \mathbf{q}) = \sum\!\!\!\!\!\!\int_f |\langle \Psi_f | \, \tilde{\rho}(\omega, \mathbf{q}) \, |\Psi_0\rangle|^2 \, \delta(E_f - E_0 - \omega), \tag{6.1}$$

where in the present case Ψ_0 is the ground state of ^{4}He with binding energy E_0 and Ψ_f is an unmeasured final state with energy E_f. The complication of the explicit calculation of all final states in the (6.1) is circumvented via the LIT method, where one has to solve the bound state equation

$$(H - E_0 + \sigma)|\widetilde{\Psi}\rangle = \tilde{\rho}(\omega, \mathbf{q})|\Psi_0\rangle. \tag{6.2}$$

We use a non-relativistic dynamical model and we take the single-particle form of the electromagnetic charge operator as in Eq. (3.34). Our purpose is to study the longitudinal response $R_L(\omega, \mathbf{q})$ as a function of the energy transfer ω and for

a fixed value of the three-momentum modulus $q = |\mathbf{q}|$. We are mainly interested in exploring the region of the quasi-elastic peak, from the lowest disintegration threshold up to pion-production.

The longitudinal response function $R_L(\omega, \mathbf{q})$ has already been calculated for ^{4}He with the LIT method [Efr97a] using as NN interaction the simple semirealistic TN potential [Efr97a, Efr99a], that provides a very good description of the S-wave phase shift up to pion threshold. A very good agreement with the experimental data from [Dyt88, Zgh94] was obtained in the quasi-elastic region for three values of momentum transfer q = 300, 400 and 500 MeV/c. In the calculation presented in [Efr97a] a hyperspherical harmonics expansion of the wave function was implemented. A correlation method was used to accelerate the convergence and the matrix elements were evaluated with the help of a Monte Carlo calculation.

At present, we are interested in doing an analogous calculation, however using the EIHH method, since it is numerically much faster and the convergence pattern has been proven to be better [Bar01b].

The charge operator we use for solving the (6.2) has the following form

$$\tilde{\rho}_{(1)}(\omega, \mathbf{q}) = \sum_k \left(\frac{1+\tau_k^3}{2} G_E^p(q_\mu^2) + \frac{1-\tau_k^3}{2} G_E^n(q_\mu^2) \right) e^{i\mathbf{q}\cdot\mathbf{r}'_k}, \tag{6.3}$$

where we have taken the one-body charge of (3.34), expressed in momentum space, and the electric nucleon form factors $G_E^{p/n}(q_\mu^2)$ have been introduced. The τ_k^3 is the third component of the isospin and $\mathbf{r}'_k$ is the coordinate in the center of mass frame corresponding to particle k. Note that we have separated the electric charge e, since it is customary to incorporate it in the Mott cross section appearing in the expression of the inclusive cross section, as shown in (3.40). We use the usual dipole fit for the Sachs form factors $G_E^{p/n}(q_\mu^2)$ [Gal71]. Since they depend on the squared four-momentum transfer $q_\mu^2 = \omega^2 - q^2$, we insert their contribution only after the inversion of the LIT, where we have the information of the energy ω in the response function. This means, we first separate the charge operator into an isoscalar (s) and in an isovector (v) part, for a fixed value of the momentum $\mathbf{q}$, as

$$\begin{aligned} \tilde{\rho}_{(1)}(\omega, \mathbf{q}) &= \big(G_E^p(q_\mu^2) + G_E^n(q_\mu^2)\big)\rho^s_{(1)}(\mathbf{q}) \\ &+ \big(G_E^p(q_\mu^2) - G_E^n(q_\mu^2)\big)\rho^v_{(1)}(\mathbf{q}), \end{aligned} \tag{6.4}$$

where the form factors are factorized in front and are not anymore included in the

isoscalar and isovector charge operators, defined as

$$\begin{aligned} \rho^{s}_{(1)}(\mathbf{q}) &= \sum_k \frac{1}{2} e^{i\mathbf{q}\cdot\mathbf{r}'_k}, \\ \rho^{v}_{(1)}(\mathbf{q}) &= \sum_k \frac{\tau^3_k}{2} e^{i\mathbf{q}\cdot\mathbf{r}'_k}, \end{aligned} \tag{6.5}$$

which do not depend on the energy ω. The difference between the isoscalar and isovector charge is in the isospin part of the operator, which is simply $\frac{1}{2}$ times an unit operator for the isoscalar part and $\frac{\tau^3_k}{2}$ for the isovector part.

We firstly solve the Schrödinger-like equation with the two operators in (6.5), providing the two solutions for $\langle\widetilde{\Psi}|\widetilde{\Psi}\rangle$ with the Lanczos method, as discussed in Chapter 5. Only after the inversion of the LIT, where we obtain an isoscalar and an isovector response function, depending on the energy ω, we can add the information of the form factors. This is done at the very end, as will be shown later.

In the calculation of the matrix elements of the one-body operators in (6.5) we will make use of the antisymmetrization of the wave function as in Eq. (4.13), such that the real matrix element one has to consider corresponds to the operator acting only on the coordinate of the last particle. This means that we can practically consider the following form for our isoscalar and isovector charge operators

$$\begin{aligned} \rho^{s}_{(1)}(\mathbf{q}) &\equiv A e^{i\mathbf{q}\cdot\mathbf{r}'_A} \frac{1}{2}, \\ \rho^{v}_{(1)}(\mathbf{q}) &\equiv A e^{i\mathbf{q}\cdot\mathbf{r}'_A} \frac{\tau^3_A}{2}. \end{aligned} \tag{6.6}$$

We perform a multipole expansion of (6.6) by means of the isoscalar and isovector Coulomb multipoles. A detailed description of the calculation of these multipoles is presented in Appendix C. Choosing the direction of $\mathbf{q}$ to be along the $\hat{z}$ axis, the multipole expansion reads

$$\rho^{s/v}_{(1)}(q) = \sum_J \tilde{C}^{s/v}_J(q), \tag{6.7}$$

where $\tilde{C}^{s/v}_J(q)$ are the isoscalar (s) and isovector (v) Coulomb multipoles. The expansion in multipoles is performed up to convergence in J, which depends on the value of momentum transfer q considered. This means that we solve a Schrödinger-like equation for every multipole. Obviously, the LIT of the response of the isoscalar charge operator in (6.5) is given by the sum of the LIT for every $\tilde{C}^{s}_J(q)$, and the same for the isovector part.

We have performed the calculation using two semirealistic interactions, the TN potential [Efr99a], yielding for ^{4}He a ground state energy of $E_0 = -31.34$ MeV, and the Malfliet-Tjon potential [Mal69], yielding $E_0 = -30.56$ MeV. We have studied the response $R_L(\omega, \mathbf{q})$ as function of the energy ω, for two fixed values of $q = 300$ and 500 MeV/c along $\hat{z}$; for this reason we will write from now only $R_L(\omega)$.

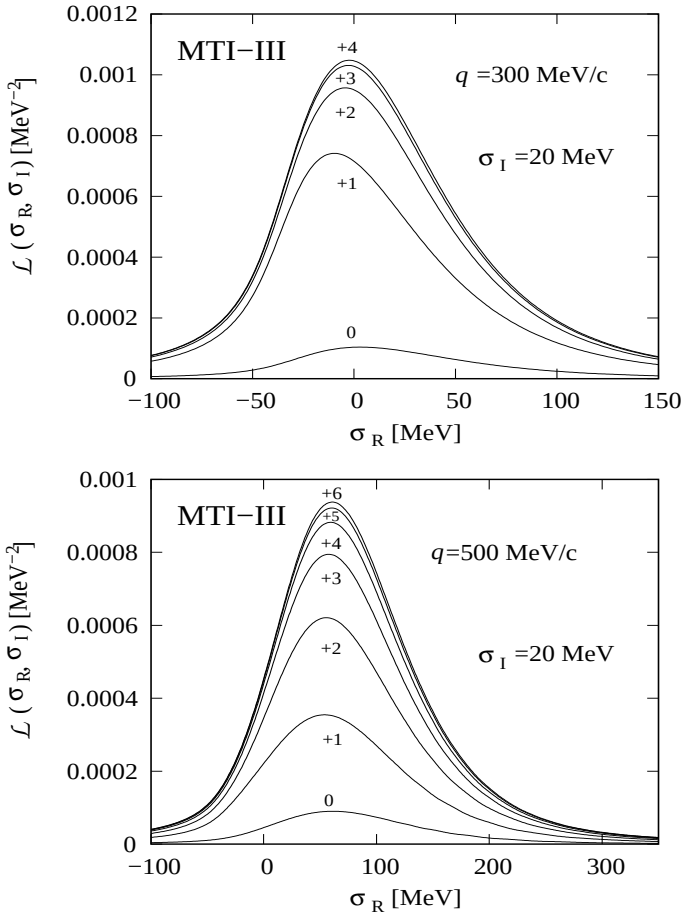

Figure 6.1: The Lorentz integral transform of the various isovector Coulomb multipoles, consecutively summed, as a function of the parameter σ_R with $\sigma_I = 20$ MeV fixed. The MTI-III potential is used and results for momentum transfer $q = 300$ MeV/c are shown in the upper panel and for $q = 500$ MeV/c in the lower panel.

In Figure 6.1 we firstly present the LIT for the various isovector multipoles for two values of momentum transfer $q = 300$ and $q = 500$ MeV/c, obtained with the MTI-III potential. We start from the transform $\mathcal{L}(\sigma_R, \sigma_I)$ of the first isovector Coulomb multipole $\tilde{C}_0^v$ and then we add the contribution of the transform of the next multipole, $\tilde{C}_1^v$, then $\tilde{C}_2^v$, etc., until convergence is reached. One readily sees that in case of momentum transfer $q = 300$ MeV/c a good convergence of the multipole expansion is reached with five Coulomb multipoles, up to $\tilde{C}_4^v$, whereas

for a momentum transfer $q = 500$ MeV/c two more multipoles are needed and the maximal Coulomb multipole considered is $\tilde{C}^v_6$.

The calculations of the LITs have been performed with an expansion of the grandangular momentum $K^0_{max} = 10$ for the ground state, $K_{max} = 9$ for the odd Coulomb multipoles and $K_{max} = 10$ for the even ones. A very good convergence in the HH expansion is reached, and the corresponding convergence error can be estimated to be below 0.5%. An analogous calculation is performed for the isoscalar Coulomb multipoles.

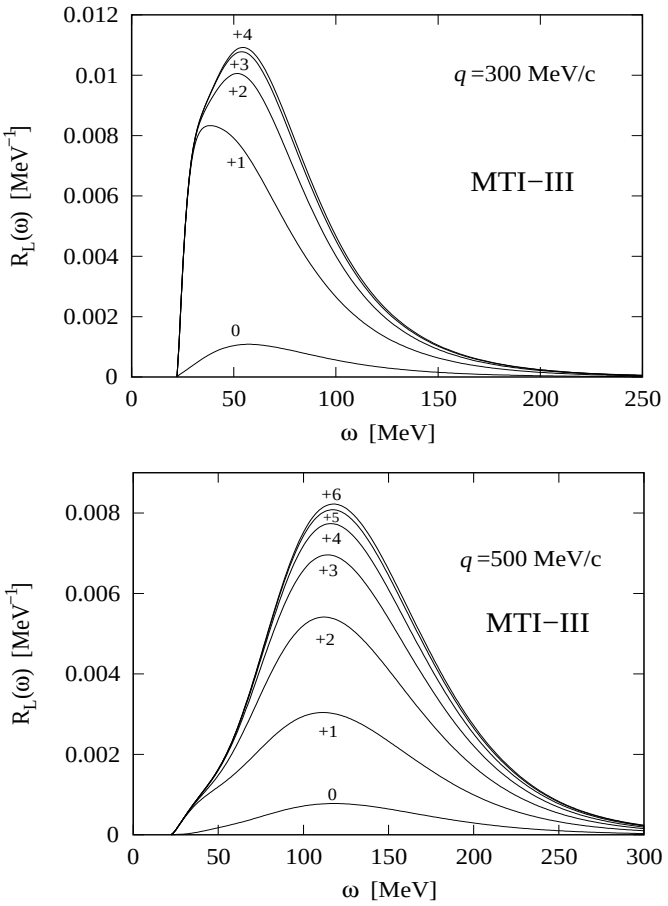

Figure 6.2: The response functions of the various isovector Coulomb multipoles, recursively summed, as a function of the center of mass energy ω obtained with the MTI-III potential: results for momentum transfer $q = 300$ MeV/c in the upper panel and for $q = 500$ MeV/c in the lower panel.

Inverting the various LITs, we get a convergence pattern for the longitudinal isovector response function, which is depicted in Figure 6.2. At this level, no nucleon form factors have been included yet. One recognizes the quasi-elastic regime, which is peaked at a center of mass energy ω of about 70 MeV in case of momentum

transfer $q = 300$ MeV/c, while at $q = 500$ MeV/c the broader peak is found at about 120 MeV. The presented threshold behavior is also very different: in case of momentum $q = 300$ MeV/c a very steep rise above threshold with a high shoulder is found, while for $q = 500$ MeV/c a much slower rise of the response function with a smaller shoulder is seen.

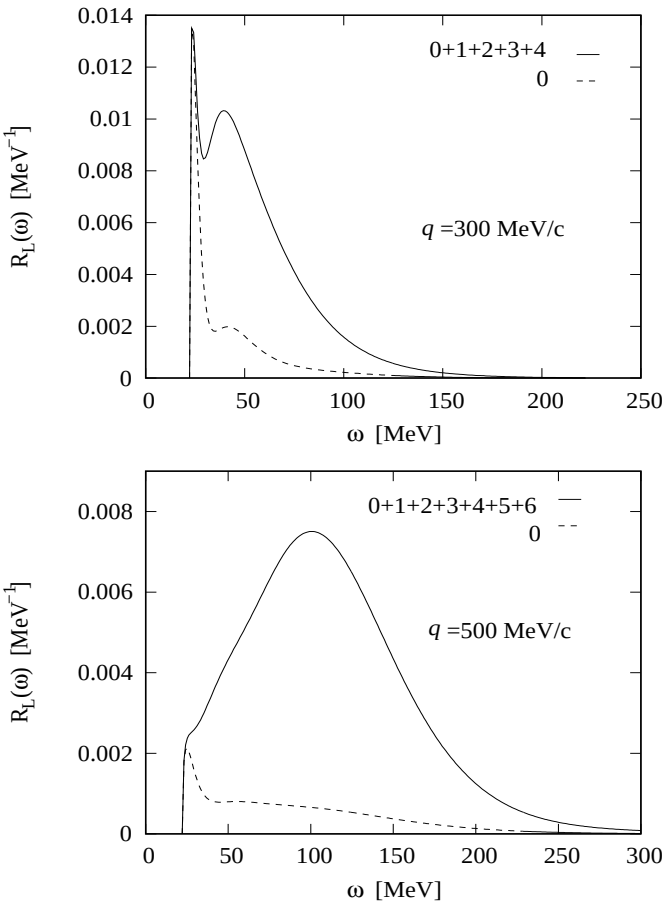

Figure 6.3: Response functions of the isoscalar Coulomb multipoles with the MTI-III: comparison of the $\tilde{C}_0^s$ contribution with the sum of all contributing multipoles. Results for momentum transfer $q = 300$ MeV/c in the upper panel and for $q = 500$ MeV/c in the lower panel.

The isoscalar multipoles show a very similar convergence pattern in the expansion in J with the difference that there is more strength in the multipole $\tilde{C}_0^s$, especially close to threshold. In Figure 6.3 we present the response of the multipole $\tilde{C}_0^s$ in comparison with the total isoscalar longitudinal response obtained from the sum of all Coulomb multipoles needed to reach convergence. One notes that in the low energy region the $\tilde{C}_0^s$ multipole presents a peak, which is very pronounced in case of momentum transfer $q = 300$ MeV/c, and less pronounced, but still relevant, for

the momentum value $q = 500$ MeV/c. We have to say that the response of the $\tilde{C}_0^s$ is obtained from an inversion of the LIT, where the elastic contribution has been taken out. In fact, the $\tilde{C}_0^s$ transition on ^{4}He nucleus can give rise to an elastic reaction in which the final state is the same as the initial one with total spin and parity $J^\pi = 0^+$. This contribution is present in the LIT and therefore it has to be subtracted in order to consider the pure inelastic response function above the disintegration threshold. This is obtained performing the inversion of the LIT with the usual basis state (see Chapter 2) and an additional elastic term like $c\delta(\omega)$. From the best fit of the inversion procedure, one gets the coefficient c, allowing one to remove this contribution from the total response.

In order to compare the theoretical results with experimental data one has to consider the response as a function of the energy in the laboratory system and not of the center of mass, therefore we have to consider the recoil energy shift as $\omega_{lab} = \omega + \frac{q^2}{2M}$. At this point we can also add the information of the form factors $\left(G_E^p + G_E^n\right)$ and $\left(G_E^p - G_E^n\right)$ for the isoscalar and isovector part, respectively, with $G_E^{p/n}(\omega_{lab}^2 - q^2)$.

Our theoretical curves obtained with the MTI-III and TN potential are shown in Figure 6.4 in comparison with the available experimental data form Bates [Dyt88], Saclay [Zgh94] and finally with a world data fit from [Car02, Jou04]. The total longitudinal response is dominated by the isoscalar response close to threshold, where one recognizes a peak in case of $q = 300$ MeV and a shoulder in case of $q = 500$ MeV due to the $\tilde{C}_0^s$ multipole. This structure is not present in the data as regarding the $q = 300$ MeV measurements, while a similar threshold behavior is seen at $q = 500$ MeV in the data. Furthermore, one notes that for the lower momentum value the theoretical results tend to overestimate the data from Bates and from the world data set, but also at some point the higher Saclay data. The same happens in case of $q = 500$ MeV, where our curve reproduces pretty well the shape of the data, but it is a bit higher. This is probably due to the fact that no relativistic corrections have been included. In fact, in [Efr97a] where a relativistic correction, the Darwin Foldy term, has been accounted for via a modification of the form factors [DeF84], the agreement with data at the higher momentum transfer value was better. From Figure 6.4 one can also see that the two semirealistic potentials, the MTI-III [Mal69] and the TN [Efr99a] lead to a very similar description of the longitudinal response function of ^{4}He, although for the MTI-III results one always finds slightly more strength than for the TN potential.

Finally, the effect of the tensor force and of other terms of the NN interaction on

this observable could be investigated only by performing a microscopic calculation with realistic interactions.

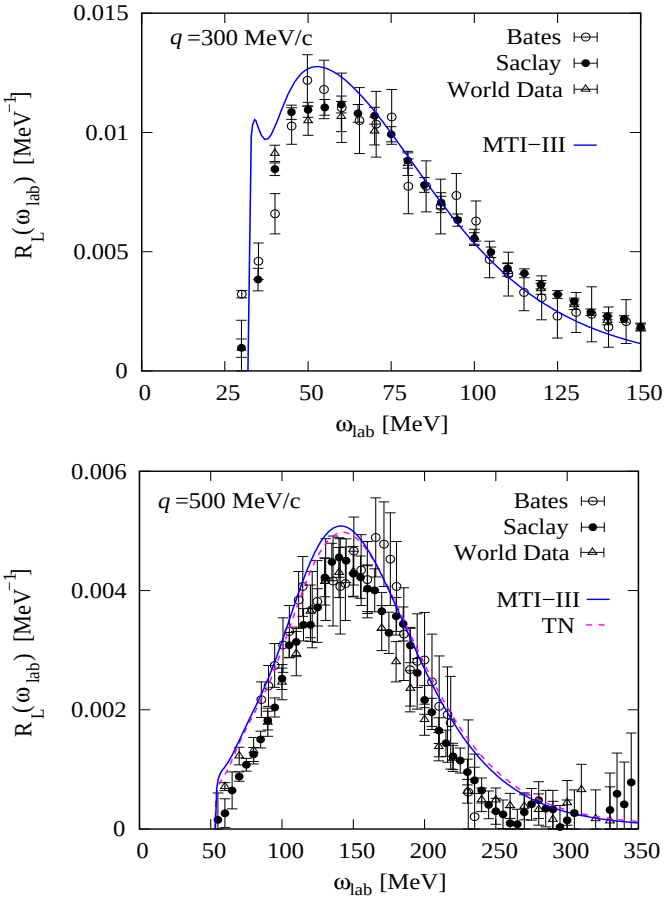

Figure 6.4: Comparison of the theoretical results obtained with the MTI-III and TN potential for the longitudinal response with the available experimental data form Bates [Dyt88], Saclay [Zgh94] and a world data fit from [Car02, Jou04]. Results for momentum transfer $q = 300$ MeV/c in the upper panel and for $q = 500$ MeV/c in the lower panel.

Comparing these results with the standard plane wave impulse approximation (PWIA) calculations in the literature, see e.g. [Cio91, Lag91], we can see that the inclusion of the FSI leads to a much better description of the experimental data. The PWIA predicts namely 40% strength more than a full calculation, while at $q = 500$ MeV the overestimation is of the order of 10% [Car92, Efr98].

6.2 Transverse Response Function

For the inclusive electron scattering we recall that the transverse response is given by

$$R_T(\omega,\mathbf{q}) = \sum\!\!\!\!\!\!\int_f \left[|\langle \Psi_f | J_+(\omega,\mathbf{q}) | \Psi_0 \rangle|^2 + |\langle \Psi_f | J_-(\omega,\mathbf{q}) | \Psi_0 \rangle|^2 \right] \delta(\omega - E_f - E_0) \quad (6.8)$$

where the operators $J_\pm(\omega,\mathbf{q})$ are the components of the transverse current $\mathbf{J}(\omega,\mathbf{q})$ in the spherical basis and the energy dependence is due to the presence of form factors for the nucleons as in case of the charge operator. In an inclusive unpolarized reaction the two projections of the transverse components of the current give the same contribution, i.e.

$$\sum\!\!\!\!\!\!\int_f |\langle \Psi_f | J_+(\omega,\mathbf{q}) | \Psi_0 \rangle|^2 = \sum\!\!\!\!\!\!\int_f |\langle \Psi_f | J_-(\omega,\mathbf{q}) | \Psi_0 \rangle|^2 . \quad (6.9)$$

Therefore, it is sufficient to calculate one contribution and then use

$$R_T(\omega,\mathbf{q}) = \sum\!\!\!\!\!\!\int_f 2 |\langle \Psi_f | J_+(\omega,\mathbf{q}) | \Psi_0 \rangle|^2 \delta(\omega - E_f - E_0). \quad (6.10)$$

In the literature one finds several calculations of the above quantity in the plane wave impulse approximation (PWIA) for different nuclei, e.g. [Cio91, Lag91], which slightly underestimate the transverse response shown by data in the quasi-elastic region. The transverse response function of a nucleus has not yet been calculated with the LIT and the EIHH methods and at present our emphasis lies on the calculation of $R_T(\omega,\mathbf{q})$ in case of ^{4}He. As discussed in Chapter 3, in a non-relativistic approach the current operator is given by a one-body and a two-body contribution as

$$\mathbf{J}(\omega,\mathbf{q}) = \mathbf{J}_{(1)}(\omega,\mathbf{q}) + \mathbf{J}_{(2)}(\omega,\mathbf{q}) = \sum_i \mathbf{J}_i(\omega,\mathbf{q}) + \sum_{i<j} \mathbf{J}_{ij}(\omega,\mathbf{q}). \quad (6.11)$$

The one-body current operator consists in the spin current $\mathbf{J}^s_{(1)}(\omega,\mathbf{q})$ and in the convection current $\mathbf{J}^c_{(1)}(\omega,\mathbf{q})$, whereas the two-body operator $\mathbf{J}_{(2)}(\omega,\mathbf{q})$ is the already mentioned meson exchange current (MEC), which depends on the interaction model used.

The lack of transverse strength found by the theory was usually attributed to the contribution of the two-body current to the response function, which was missing or not completely taken into account. However, different calculations which include

two-body currents have found different effects, between 10% and 40%, such that the picture is not yet clear. Our aim consists in the calculation of the exact transverse response function of ^{4}He, where the FSI is completely taken into account and a gauge invariant model for the current is constructed. For this purpose, we will consider firstly a simple semirealistic interaction model, to start to tackle the problem.

In the region of the quasi-elastic peak it is well known from standard PWIA calculations, that the dominant term of the current is the one-body spin part. For this reason we will start to investigate the transverse spin current response. Then, we will also treat the convection current and finally the consistent MEC.

In analogy to what done in case of the longitudinal response, in order to study $R_T(\omega, \mathbf{q})$ with the full FSI we use the fact that the energy dependence of the excitation operators is included in the form factors and we solve the Schrödinger-like equation

$$(H - E_0 + \sigma)|\widetilde{\Psi}\rangle = \sqrt{2} J_+(q)|\Psi_0\rangle, \tag{6.12}$$

where on the right-hand-side we have now the current operator as a function of the momentum only. We add the energy dependence after the inversion of the transform.

In the following we present three sections where we discuss the calculation of the matrix elements of $J_+(q)$ and of the corresponding responses in case of the three current operators, $\mathbf{J}^s_{(1)}$, $\mathbf{J}^c_{(1)}$ and $\mathbf{J}_{(2)}$.

6.2.1 The Spin Current

The spin current has already been defined in Eq. (3.35). It has a purely transverse contribution and in the momentum space it assumes the form

$$\mathbf{J}^s_{(1)}(\omega, \mathbf{q}) = \frac{i}{2m} \sum_k \left(G^p_M(q^2_\mu) \frac{1 + \tau^3_k}{2} + G^n_M(q^2_\mu) \frac{1 - \tau^3_k}{2} \right) (\boldsymbol{\sigma}_k \times \mathbf{q}) e^{i\mathbf{q}\mathbf{r}'_k}, \tag{6.13}$$

where the charge e has not been written, since it is included in the Mott cross section (Eq. (3.40)). In the above expressions the magnetic form factors of proton and neutron $G^{p/n}_M(q^2_\mu)$ are defined through the electric form factors and the magnetic moments as $G^{p/n}_M(q^2_\mu) = \mu_{p/n} G^p_E(q^2_\mu)$, where $\mu_p = 2.793\ \mu_N$ and $\mu_n = -1.913\ \mu_N$. The $\boldsymbol{\sigma}_k$ are the Pauli spin matrices, τ^3_k is the third component of the isospin and finally $\mathbf{r}'_k$ are the coordinates of particle k in the center of mass frame.

In analogy to what has been done for the charge operator, the spin current can

be separated in isoscalar (s) and isovector (v) part as

$$\begin{aligned} \mathbf{J}^{s}_{(1)}(\omega,\mathbf{q}) &= \big(G^p_M(q^2_\mu)+G^n_M(q^2_\mu)\big)\mathbf{J}^{s(s)}_{(1)}(\mathbf{q}) \\ &+ \big(G^p_M(q^2_\mu)-G^n_M(q^2_\mu)\big)\mathbf{J}^{s(v)}_{(1)}(\mathbf{q}), \end{aligned} \tag{6.14}$$

where the form factors are kept in front and thus are not anymore included in the isovector and isoscalar spin current operators, defined as

$$\begin{aligned} \mathbf{J}^{s(s)}_{(1)}(\mathbf{q}) &= \frac{i}{2m}\sum_k \frac{1}{2}(\boldsymbol{\sigma}_k\times\mathbf{q})e^{i\mathbf{q}\mathbf{r}'_k} \\ \mathbf{J}^{s(v)}_{(1)}(\mathbf{q}) &= \frac{i}{2m}\sum_k \frac{\tau^3_k}{2}(\boldsymbol{\sigma}_k\times\mathbf{q})e^{i\mathbf{q}\mathbf{r}'_k}, \end{aligned} \tag{6.15}$$

which do not depend on the energy ω. As in case of the charge operator, we firstly provide the solutions of $\langle\widetilde{\Psi}|\widetilde{\Psi}\rangle$ for the two operators in Eq. (6.15) with a fixed value of momentum transfer $|\mathbf{q}|=q$. The contribution of the form factors, which are functions of $q^2_\mu=\omega^2-q^2$, will be included at the very end, after the inversion of the Lorentz transforms, where we have a response as function of the energy ω.

In the calculation of the matrix elements of the one-body operators in (6.15) we will make use of the antisymmetrization of the wave function as in Eq. (4.13), such that one has to consider only the operator acting on the last coordinate. This means we can use the following redefinition of the isoscalar and isovector spin currents as

$$\begin{aligned} \mathbf{J}^{s(s)}_{(1)}(\mathbf{q}) &\equiv A\,\frac{i}{2m}(\boldsymbol{\sigma}_A\times\mathbf{q})e^{i\mathbf{q}\mathbf{r}'_A}\frac{1}{2} \\ \mathbf{J}^{s(v)}_{(1)}(\mathbf{q}) &\equiv A\frac{i}{2m}(\boldsymbol{\sigma}_A\times\mathbf{q})e^{i\mathbf{q}\mathbf{r}'_A}\frac{\tau^3_A}{2}. \end{aligned} \tag{6.16}$$

These last operators can be decomposed into multipoles yielding following expansion for the components of the isoscalar and isovector spin currents with $\mathbf{q}\parallel\hat{z}$

$$J^{s(s/v)}_{(1)+}(q)=\sum_J\big(E^{s/v}_J(q)+M^{s/v}_J(q)\big), \tag{6.17}$$

where $E^{s/v}_J(q)$ are the electric and $M^{s/v}_J(q)$ the magnetic isoscalar (s) and isovector (v) multipoles, respectively. A detailed derivation of the multipole decomposition of the spin current and the description of the corresponding matrix elements is presented in Appendix C.

The expansion in multipoles is performed up to convergence in J, which depends on the value of momentum transfer q considered. As for the longitudinal response, we

solve a Schrödinger-like equation for every multipole and the LIT of the response of the isoscalar spin current operator in (6.13) is given by the sum of the LIT for every $E^s_J(q)$ and $M^s_J(q)$ multipoles, and analogously for the isovector part. No interference between electric and magnetic moments exists, since they have different parity.

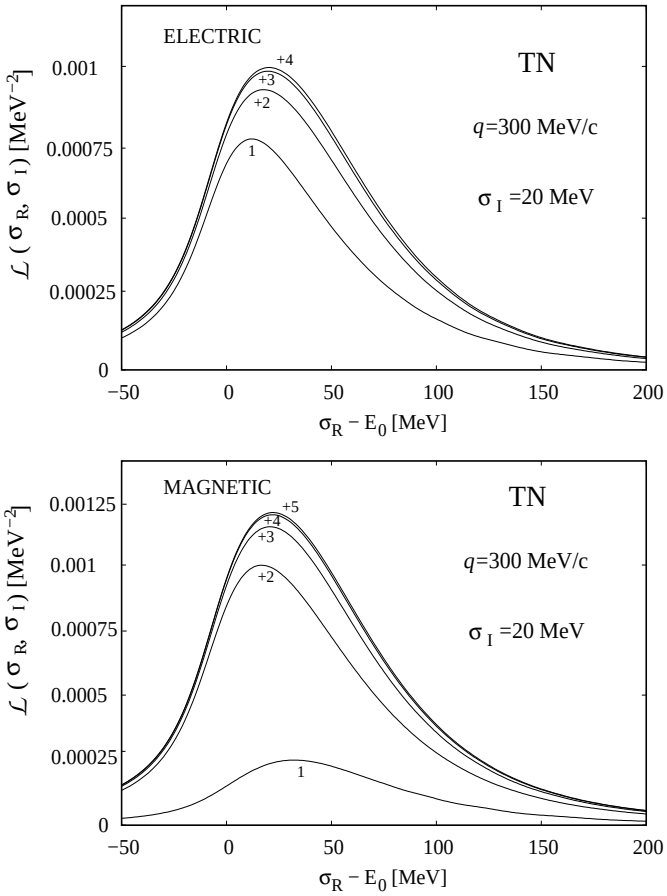

Figure 6.5: The Lorentz integral transform of the various isovector electric and magnetic multipoles, consecutively summed, as a function of the parameter $\sigma_R - E_0$ with $\sigma_I = 20$ MeV fixed. The TN potential is used ($E_0 = -31.34$ MeV) and the momentum transfer is $q = 300$ MeV/c.

We have performed the calculation using two semirealistic interactions, the TN potential [Efr99a] and the Malfliet-Tjon potential [Mal69]. We have studied the contribution of the spin current to $R_T(\omega, \mathbf{q})$ for two fixed values of $q = 300$ and 500 MeV/c along $\hat{z}$; for this reason we will write from now only $R_T(\omega)$.

In Figure 6.5 we firstly present the LIT for the various isovector electric and magnetic multipoles for the value of momentum transfer $q = 300$ MeV/c obtained with the TN potential. We start from the transform $\mathcal{L}(\sigma_R, \sigma_I)$ of the first isovector multipole $E^v_1(q)$ and $M^v_1(q)$, respectively, and then we add the contribution of the

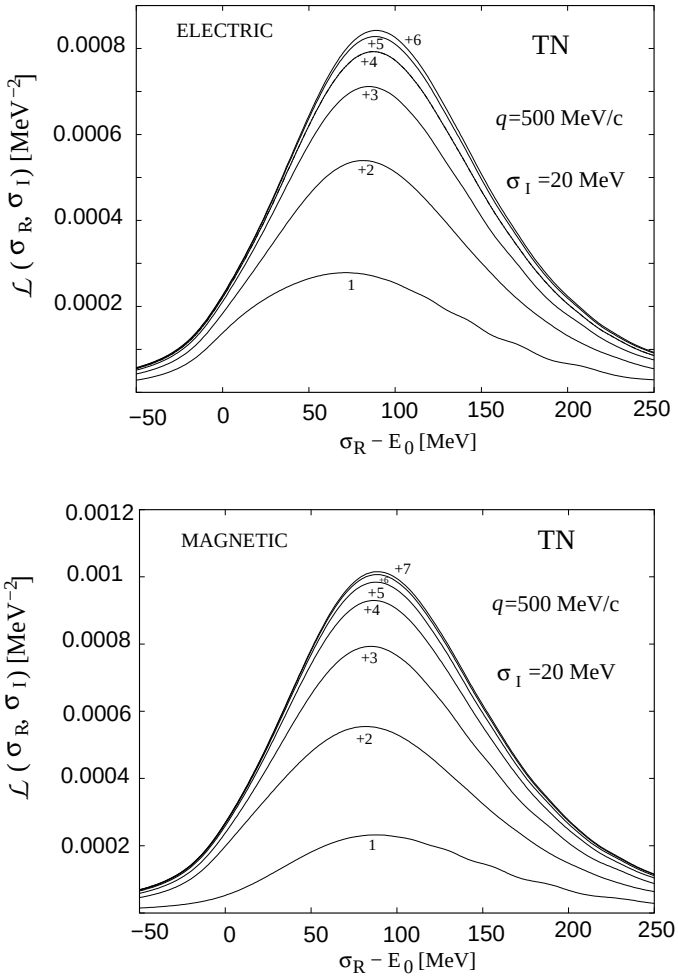

Figure 6.6: The Lorentz integral transform of the various isovector electric and magnetic multipoles, consecutively summed, as a function of the parameter $\sigma_R - E_0$ with $\sigma_I = 20$ MeV fixed. The TN potential is used ($E_0 = -31.34$ MeV) and the momentum transfer is $q = 500$ MeV/c.

transform of the next multipoles, $E_2^v(q)$ and $M_2^v(q)$ and so on, until convergence is reached. One readily sees that in case of the electric multipoles a good convergence of the expansion is reached considering all multipoles up to $J = 4$, whereas for the magnetic multipole one more contribution ($J = 5$) has been added. This is due to the fact that the strength of the multipole strongly depends on the order of the Bessel function appearing in the multipole expression (see (C.24)). In case of the electric multipoles $E_J^{s/v}(q)$ one deals with the Bessel function of order J, whereas in case of $M_J^{s/v}(q)$ two Bessel functions contribute, the $J-1$ and the $J+1$, among which the lower one dominates. In the light of the fact that the $E_J^{s/v}(q)$ and the $M_{J+1}^{s/v}(q)$ contain the same Bessel function $j_J(qr')$, the convergence pattern shown

in Fig. 6.5 should be clear. A similar picture is obtained for the MTI-III potential.

In case of the momentum transfer $q = 500$ MeV/c the convergence of the multipole expansion is clearly slower than for $q = 300$ MeV/c and two more multipoles have to be considered, as shown in Fig. 6.6. For the momentum transfer $q = 500$ MeV/c the LITs present some small oscillation in the tail, as one can see from Fig. 6.6. This is due to the fact that in the calculation of the matrix elements we have kept the same parameters for the hyper-radial and hyperangular quadrature integration as in case of $q = 300$ MeV/c. Since the momentum transfer here is higher, the numerical integrations are not anymore as accurate as in Fig. 6.5. This effect can be easily removed increasing for example the number of Laguerre polynomials used in the expansion of the wave function and accordingly the number of grid-points used in the quadrature integration. Looking at Fig. 6.6 one can see that such oscillations compensate each other in the sum of all multipole, where they are much less pronounced. Nevertheless, they do not have any effect on the inversion procedure, which is stable to such regular small oscillations in the tail [Efr99a]. We have verified it, performing some calculations of the LIT with an improved numerical integration, which is clearly more time consuming.

We have calculated the transforms with an expansion of the grandangular momentum $K^0_{max} = 10$ for the ground state, $K_{max} = 9$ for the odd electric multipoles and $K_{max} = 10$ for the even electric ones. In case of the magnetic multipole we have used on the contrary $K_{max} = 10$ for the odd and $K_{max} = 9$ for the even multipoles, due to the opposite parity. A very good convergence in the HH expansion is reached, and the corresponding convergence error can be estimated to be below 0.5%.

In order to compare the theoretical results with experimental data we have to invert the transforms of the multipoles and then to consider the responses as a function of the energy in the laboratory system $\omega_{lab} = \omega + \frac{q^2}{2M}$. At this level the information of the form factors $\left(G^p_M + G^n_M\right)$ and $\left(G^p_M - G^n_M\right)$ for the isoscalar and isovector part, respectively, can be added using $G^{p/n}_M(\omega^2_{lab} - q^2)$.

As in case of the longitudinal response [Efr97a], one can invert the transform of every multipole and then sum the inversions or, on the contrary, one can firstly sum the LITs and then invert the sum of the transforms. These two procedures have to give the same result, up to a small numerical error, if the inversions are stable. We prefer to invert the single multipoles, since in this case one can judge the stability of each inversion, especially if the different multipoles present different structures. Nevertheless, the percentage difference of the two methods is about 1%.

In Fig. 6.7 we show the total transverse response to the spin current obtained

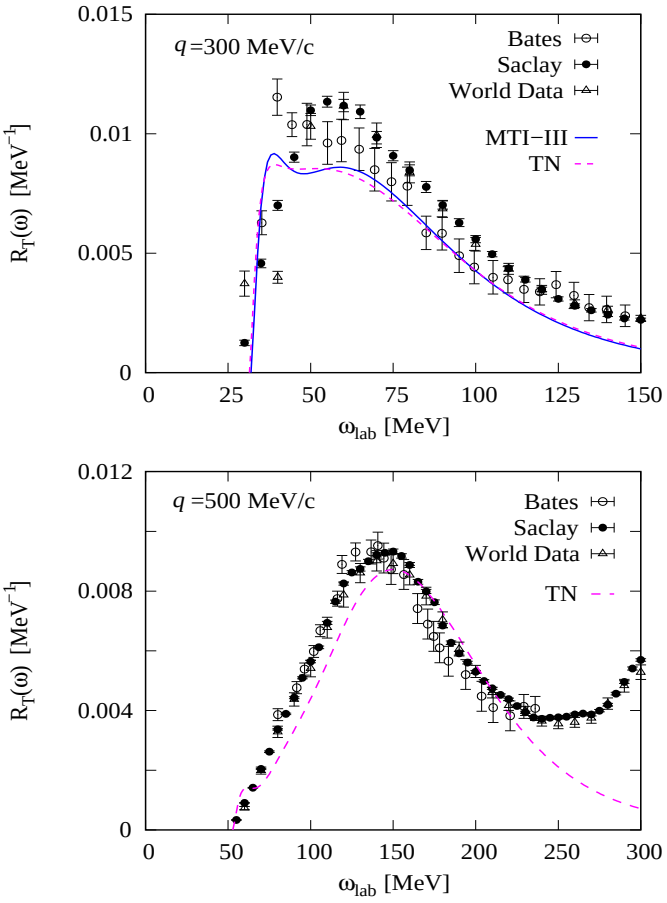

Figure 6.7: Comparison of the theoretical results obtained with the MTI-III and TN potential for the transverse response of the spin current with the available experimental data form Bates [Dyt88], Saclay [Zgh94] and a world data fit from [Car02, Jou04]. Results for momentum transfer $q = 300$ MeV/c in the upper panel and for $q = 500$ MeV/c in the lower panel.

with the MTI-III and TN potentials in comparison with the available experimental data form Bates [Dyt88], Saclay [Zgh94] and finally with a world data fit from [Car02, Jou04]. As in case of the longitudinal response, also $R_T(\omega)$ deriving from $\mathbf{J}^s_{(1)}(\mathbf{q})$ is dominated by the quasi-elastic peak for both the momentum transfer values $q = 300$ MeV/c and $q = 500$ MeV/c. One can see that for the lower momentum value the two potentials lead to a very similar description of the response, although the MTI-III presents a slightly more pronounced structure at low energy. This substructure is found also in case of $q = 500$ MeV/c, close to threshold and it is mainly due to the effect of E_1 and M_1 excitations.

From Fig. 6.7 it is clear that the theoretical curves miss some strength, especially in the peak region. It is very likely that part of the missing strength will be provided

by the not yet included current contributions of $\mathbf{J}^c_{(1)}(\omega,\mathbf{q})$ and $\mathbf{J}_{(2)}(\omega,\mathbf{q})$. On the other hand, we have to remember that we are using simple semirealistic interactions, whose capability to give a detailed description of the nuclear dynamics can only be tested comparing their results with calculations obtained with realistic potentials. The first question, whether the missing strength is due to the missing parts of the current can be answered adding also the contribution of the convection current and of the MEC to the transverse response.

6.2.2 The Convection Current

First of all we recall that the convection current, as already defined in Eq. (3.35), is given by

$$\mathbf{j}^c_{(1)}(\mathbf{x}) = \frac{1}{2m}\sum_k \frac{1+\tau_k^3}{2}\{\mathbf{p}_k, \delta(\mathbf{x}-\mathbf{r}_k)\} \tag{6.18}$$

where we have omitted the charge e, since as usual it is already included in the Mott cross section. Note that the convection current is written as function of the coordinates $\mathbf{r}_k$ of a generic reference frame and of the corresponding conjugate variables $\mathbf{p}_k = -i\boldsymbol{\nabla}_k$.

In the momentum space, applying a Fourier transform, it becomes

$$\mathbf{J}^c_{(1)}(\omega,\mathbf{q}) = \frac{1}{2m}\sum_k \{\mathbf{p}_k, e^{i\mathbf{q}\cdot\mathbf{r}_k}\}\left(G_E^p(q_\mu^2)\frac{1+\tau_k^3}{2} + G_E^n(q_\mu^2)\frac{1-\tau_k^3}{2}\right),$$

where we have added the electric form factors of the proton and of the neutron functions of the four-momentum squared q_μ^2. Writing explicitly the anticommutator, one can separate the convection current into two terms as

$$\begin{aligned}
\mathbf{J}^c_{(1)}(\omega,\mathbf{q}) &= \mathbf{J}^{c,a}_{(1)}(\omega,\mathbf{q}) + \mathbf{J}^{c,b}_{(1)}(\omega,\mathbf{q}) \\
&= \frac{\mathbf{q}}{2m}\sum_k e^{i\mathbf{q}\cdot\mathbf{r}_k}\left(G_E^p(q_\mu^2)\frac{1+\tau_k^3}{2} + G_E^n(q_\mu^2)\frac{1-\tau_k^3}{2}\right) \\
&+ \frac{1}{m}\sum_k e^{i\mathbf{q}\mathbf{r}_k}\ \mathbf{p}_k\left(G_E^p(q_\mu^2)\frac{1+\tau_k^3}{2} + G_E^n(q_\mu^2)\frac{1-\tau_k^3}{2}\right),
\end{aligned} \tag{6.19}$$

where the first part is purely longitudinal with respect to the direction of $\mathbf{q}$, while the second one contains a longitudinal and a transverse part.

Now we would like to have the intrinsic convection current as a function of the coordinates in the center of mass frame as in case of the charge and spin current where we wrote the operators as functions of the coordinates $\mathbf{r}'_k$. If the operators

depend on the coordinates $\mathbf{r}_k$ only, as for the charge, the spin current and the purely longitudinal convection current, one can simply apply the transformation (4.1) to the relative coordinates $\mathbf{r}'_k$. In the center of mass frame clearly $\mathbf{r}'_k = \mathbf{r}_k$, such that the operators remain the same in the relative coordinate system. On the other hand, in case of the second part of the convection current, $\mathbf{J}^{c,b}_{(1)}(\omega, \mathbf{q})$, we also have a dependence on the conjugate momenta $\mathbf{p}_k$, which have to be written as a function of the relative and center of mass momenta. However, the relative momenta are not a set of A independent variables and we cannot simply define the conjugate variable $\mathbf{p}'_k = -i\boldsymbol{\nabla}'_k$, since the usual commutation relation is not satisfied, but it holds $[\mathbf{r}'_{k\alpha}, \mathbf{p}'_{j\beta}] = i(\delta_{kj} - \frac{1}{A})\delta_{\alpha\beta}$. In fact, as for the coordinates $\mathbf{r}'_k$, also the gradients $\boldsymbol{\nabla}'_k \equiv \frac{d}{d\mathbf{r}'_k}$ are not linearly independent, which means that the derivative on a certain internal coordinate involves all the other coordinates, since $\sum_k \mathbf{r}'_k = 0$. For this reason it is always preferable to work with independent coordinates in order to have conjugate momenta which are defined as usual through the simple derivative. Thus, we will firstly make use of the antisymmetrization of the wave function and then we will relate the coordinate $\mathbf{r}_A$ and the momentum $\mathbf{p}_A$ to the Jacobi coordinates which are linearly independent and where the conjugate momenta are well defined via the corresponding gradients. Therefore, concerning the convection current $\mathbf{J}^{c,b}_{(1)}(\omega, \mathbf{q})$, we firstly separate it in isoscalar and isovector parts as

$$\mathbf{J}^{c,b}_{(1)}(\omega, \mathbf{q}) = \left(G^p_E(q^2_\mu) + G^n_E(q^2_\mu)\right)\mathbf{J}^{c,b(s)}_{(1)}(\mathbf{q}) + \left(G^p_E(q^2_\mu) - G^n_E(q^2_\mu)\right)\mathbf{J}^{c,b(v)}_{(1)}(\mathbf{q}), \quad (6.20)$$

where the isoscalar and isovector operators do not depend on the energy ω anymore and are defined as

$$\begin{aligned} \mathbf{J}^{c,b(s)}_{(1)}(\mathbf{q}) &\equiv A\frac{1}{m}e^{i\mathbf{q}\mathbf{r}_A}\mathbf{p}_A\frac{1}{2} \\ \mathbf{J}^{c,b(v)}_{(1)}(\mathbf{q}) &\equiv A\frac{1}{m}e^{i\mathbf{q}\mathbf{r}_A}\mathbf{p}_A\frac{\tau^3_A}{2}. \end{aligned} \quad (6.21)$$

At this point, using the transformation (4.2) to Jacobi coordinates, one finds

$$\mathbf{r}_A = \sqrt{\frac{A-1}{A}}\boldsymbol{\eta}_{A-1} + \frac{1}{\sqrt{A}}\boldsymbol{\eta}_0, \quad (6.22)$$

where $\boldsymbol{\eta}_0 = \sqrt{A}\mathbf{R}_{cm}$. Calling the Jacobi conjugate coordinates $\boldsymbol{q}_i = -i\frac{d}{d\boldsymbol{\eta}_i}$, one has

$$\mathbf{p}_A = \sqrt{\frac{A-1}{A}}\mathbf{q}_{A-1} + \frac{1}{\sqrt{A}}\mathbf{q}_0. \quad (6.23)$$

In the center of mass frame we have $\boldsymbol{\eta}_0 \equiv 0$ and furthermore the contribution of $\mathbf{q}_0$ can be neglected, since it does not act on the intrinsic wave function we are interested in. This means we can simply consider the following expressions

$$\mathbf{r}'_A = \sqrt{\frac{A-1}{A}}\boldsymbol{\eta}_{A-1} \quad \text{and} \quad \mathbf{p}'_A = \sqrt{\frac{A-1}{A}}\mathbf{q}_{A-1}. \tag{6.24}$$

If we now want to write the operators as a function of the internal coordinate $\mathbf{r}'_A$, as done for the charge and spin current, we can write

$$\sqrt{\frac{A-1}{A}}\mathbf{q}_{A-1} = -i\sqrt{\frac{A-1}{A}}\frac{d}{d\boldsymbol{\eta}_A} = -i\frac{A-1}{A}\frac{d}{d\mathbf{r}'_A}. \tag{6.25}$$

Finally, the operators in (6.21) become

$$\mathbf{J}^{c,b(s/v)}_{(1)}(\mathbf{q}) = -i\frac{A-1}{m}e^{i\mathbf{q}\mathbf{r}'_A}\frac{d}{d\mathbf{r}'_A}O^{\mathcal{T}T_z}_{s/v}(t_A) \tag{6.26}$$

as function of the internal coordinate $\mathbf{r}'_A$, where the isospin operator $O^{\mathcal{T}T_z}_{s/v}(t_A)$ is simply $\frac{1}{2}$ and $\frac{\tau^3_A}{2}$ for the isoscalar and isovector part, respectively. Note that they contain a derivative that will act on the wave functions on the right in the matrix elements. The treatment of such a derivative term is discussed in Appendix C.

In analogy to what has been done for the spin current, also the $J_+(q)$ component of the transverse convection current can be expanded in isoscalar and isovector electric and magnetic multipoles. Namely, considering that the transverse component of the convection current is included in the operator $\mathbf{J}^{c,b(s/v)}_{(1)}(\mathbf{q})$, we can write

$$J^{c,b(s/v)}_{(1)+}(q) = \sum_J \left(E^{s/v}_J(q) + M^{s/v}_J(q)\right). \tag{6.27}$$

The explicit derivation of the multipole expansion of the convection current is presented in Appendix C. Clearly the multipole expansion has to be considered up to convergence in J and the effect on the response function can be studied. It is well known from the literature, that the contribution of the convection current to the transverse response function is very small with respect to that of the spin current at medium momentum transfer. This can already be seen from the fact that the spin current in (6.13) is proportional to $\mathbf{q}$, while this is not the case of the transverse convection current, as in $\mathbf{J}^{c,b}_{(1)}$ of (6.19). This means that with increasing momentum transfer $\mathbf{q}$ the effect of the convection current on the response function becomes smaller with respect to the spin part.

Furthermore, since we are considering as NN interactions the TN [Efr99a] and the MTI-III [Mal69] potential, for which $[V, \rho(\mathbf{x})] \neq 0$ holds, also the MEC contribute to the transverse response. The effect of the convection and of the two-body current to the first electric multipole E_1 will be discussed in the section on the Siegert test presented in this Chapter. In the following we firstly discuss the meson exchange current in case of the MTI-III potential.

6.2.3 The Meson Exchange Current

Since our final aim is to study exactly the transverse response function of the electro-disintegration of ^{4}He including all current contributions, we have also to deal with the already mentioned MEC. In Chapter 3 we stressed the fact that the explicit form of the two-body current depends on the potential model used and can be recovered using the minimal coupling method. In this section we will apply the latter to the case of the MTI-III potential. We choose to work with the MTI-III since it has the simple form of a scalar meson exchange and therefore the construction of the corresponding MEC is straightforward (see also Appendix A), since it consists only in meson in flight terms, as depicted in Fig. 6.8. This is not the case of the TN

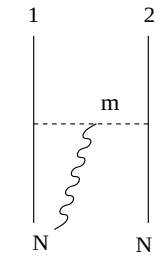

Figure 6.8: Diagram of the meson-in-flight two-body current.

interaction, where one would firstly have to rewrite the r-space part of the potential as a superposition of meson propagators and then to build the corresponding MEC. In the following we present a detailed derivation of the two-body current in case of the MTI-III.

The Malfliet-Tjon potential is defined as

$$V(r) = V_{13}(r)P_{13} + V_{31}(r)P_{31}, \tag{6.28}$$

where $r = |\mathbf{r}| = |\mathbf{r}_1 - \mathbf{r}_2|$, the radial functions are

$$\begin{aligned} V_{13}(r) &= A\frac{e^{-m_1 r}}{r} - B\frac{e^{-m_2 r}}{r}, \\ V_{31}(r) &= C\frac{e^{-m_1 r}}{r} - D\frac{e^{-m_2 r}}{r}, \end{aligned} \tag{6.29}$$

and the projectors are given by

$$\begin{aligned} P_{13} &= \left(\frac{1-\boldsymbol{\sigma}_1\cdot\boldsymbol{\sigma}_2}{4}\right)\left(\frac{3+\boldsymbol{\tau}_1\cdot\boldsymbol{\tau}_2}{4}\right) \\ P_{31} &= \left(\frac{3+\boldsymbol{\sigma}_1\cdot\boldsymbol{\sigma}_2}{4}\right)\left(\frac{1-\boldsymbol{\tau}_1\cdot\boldsymbol{\tau}_2}{4}\right). \end{aligned} \tag{6.30}$$

The constants A, B, C, D and the masses m_1, m_2 can be found also in [Bar01]. If we call the radial quantity

$$J_{m_{1/2}}(r) = \frac{e^{-m_{1/2}r}}{4\pi r}, \tag{6.31}$$

and we recognize it to be a propagator of a scalar meson with mass $m_{1/2}$, we get the following expression for the Malfliet-Tjon potential

$$\begin{aligned} V(r) &= \frac{12\pi}{16}\Big(AJ_{m_1}(r) - BJ_{m_2}(r) + CJ_{m_1}(r) - DJ_{m_2}(r)\Big) \\ &+ \frac{4\pi}{16}\Big(-3AJ_{m_1}(r) + 3BJ_{m_2}(r) + CJ_{m_1}(r) - DJ_{m_2}(r)\Big)\,\boldsymbol{\sigma}_1\cdot\boldsymbol{\sigma}_2 \\ &+ \frac{4\pi}{16}\Big(AJ_{m_1}(r) - BJ_{m_2}(r) - 3CJ_{m_1}(r) + 3DJ_{m_2}(r)\Big)\,\boldsymbol{\tau}_1\cdot\boldsymbol{\tau}_2 \\ &+ \frac{4\pi}{16}\Big(-AJ_{m_1}(r) + BJ_{m_2}(r) - CJ_{m_1}(r) + DJ_{m_2}(r)\Big)\,(\boldsymbol{\sigma}_1\cdot\boldsymbol{\sigma}_2)\,(\boldsymbol{\tau}_1\cdot\boldsymbol{\tau}_2). \end{aligned} \tag{6.32}$$

In the last expression one recognizes that the first term consists of the purely central part of the potential, the second part contains only a spin dependence, the third only an isospin dependence and finally the last term is the spin-isospin part. For our purpose, the only parts of the potential that need to be considered are those which do not commute with the charge operator $\rho(\mathbf{x}) = e\frac{1+\tau_1^3}{2}\delta(\mathbf{x}-\mathbf{r}_1) + e\frac{1+\tau_2^3}{2}\delta(\mathbf{x}-\mathbf{r}_2)$, therefore the part of the potential containing an isospin dependence. We will write this part as non-commuting (NC) potential

$$V^{\mathrm{NC}}(r) = 4\pi\,\boldsymbol{\tau}_1\cdot\boldsymbol{\tau}_2\Big(\alpha J_{m_1}(r) + \beta J_{m_2}(r) + \big(\gamma J_{m_1}(r) + \delta J_{m_2}(r)\big)\,\boldsymbol{\sigma}_1\cdot\boldsymbol{\sigma}_2\Big), \tag{6.33}$$

where the new constants are defined as

$$\alpha = \frac{1}{16}(A - 3C), \qquad \beta = -\frac{1}{16}(B - 3D)$$
$$\gamma = -\frac{1}{16}(A + C), \qquad \delta = \frac{1}{16}(B + D).$$

The corresponding meson exchange current is very easily recovered. In fact, applying the minimal coupling to the non commuting potential we will get only meson in flight terms, since the only momentum dependence is in the propagators $J_{m_{1/2}}(r)$. Therefore, the consistent meson exchange current will have the following form

$$\mathbf{j}_2^{\mathrm{MTI-III}}(\mathbf{x}, \mathbf{r}_1, \mathbf{r}_2) = \tag{6.34}$$
$$4\pi(\boldsymbol{\tau}_1 \times \boldsymbol{\tau}_2)^3 \Big[\alpha J_{m_1}(|\boldsymbol{r}_1 - \boldsymbol{x}|) \overleftrightarrow{\boldsymbol{\nabla}}_x J_{m_1}(|\mathbf{x} - \mathbf{r}_2|) + \beta J_{m_2}(|\mathbf{r}_1 - \mathbf{x}|) \overleftrightarrow{\boldsymbol{\nabla}}_x J_{m_2}(|\boldsymbol{x} - \boldsymbol{r}_2|)$$
$$+ \Big(\gamma J_{m_1}(|\mathbf{r}_1 - \mathbf{x}|) \overleftrightarrow{\boldsymbol{\nabla}}_x J_{m_1}(|\mathbf{x} - \mathbf{r}_2|) + \delta J_{m_2}(|\boldsymbol{r}_1 - \boldsymbol{x}|) \overleftrightarrow{\boldsymbol{\nabla}}_x J_{m_2}(|\mathbf{x} - \mathbf{r}_2|) \Big) \boldsymbol{\sigma}_1 \cdot \boldsymbol{\sigma}_2 \Big],$$

where the derivatives $\overleftrightarrow{\boldsymbol{\nabla}}_x$ act only on the propagatos $J_{m_{1/2}}$ and not on the wave function in the matrix element. Since there is no momentum dependence in the Malfliet-Tjon potential, no contact term is present in the corresponding meson exchange current (see also Appendix A).

It can be verified that the continuity equation

$$\boldsymbol{\nabla} \cdot \mathbf{j}_2^{\mathrm{MTI-III}}(\mathbf{x}, \mathbf{r}_1, \mathbf{r}_2) = -i \left[V^{\mathrm{NC}}(|\mathbf{r}_1 - \mathbf{r}_2|), \rho(\mathbf{x}) \right] \tag{6.35}$$

holds.

Due to the presence of the isospin operator $(\boldsymbol{\tau}_1 \times \boldsymbol{\tau}_2)^3$ in Eq. (6.34), the contribution of the MEC is purely isovector. Furthermore, we can see that this two-body operator is in general a function of both particle coordinates $\mathbf{r}_1$ and $\mathbf{r}_2$ and not only of the difference of the two $\mathbf{r} = \mathbf{r}_1 - \mathbf{r}_2$ as for the potential itself.

At this point, if we want to proceed in the calculation of the effect of the MEC on the transverse response function, in analogy to what done for the spin and convection current, we have to consider the two-body current in momentum space $\mathbf{J}_{(2)}^{\mathrm{MTI-III}}(\mathbf{q}, \mathbf{r}_1, \mathbf{r}_2)$. We firstly note that the meson in flight current appearing in Eq. (6.34) consist in a linear combination of terms like

$$\mathbf{j}_{(2)}(\mathbf{x}, \mathbf{r}_1, \mathbf{r}_2) = J_m(|\mathbf{r}_1 - \mathbf{x}|) \overleftrightarrow{\boldsymbol{\nabla}}_x J_m(|\mathbf{x} - \mathbf{r}_2|) =$$
$$= \frac{1}{(4\pi)^2} \frac{e^{-m(|\mathbf{r}_1 - \mathbf{x}|)}}{|\mathbf{r}_1 - \mathbf{x}|} \overleftrightarrow{\boldsymbol{\nabla}}_x \frac{e^{-m(|\mathbf{x} - \mathbf{r}_2|)}}{|\mathbf{x} - \mathbf{r}_2|}, \tag{6.36}$$

where we omit the isospin parts for simplicity and write only one mass m. In order to work in momentum space we have to consider the Fourier transform as

$$\begin{aligned}
\mathbf{J}_{(2)}(\mathbf{q},\mathbf{r}_1,\mathbf{r}_2) &= \frac{1}{(4\pi)^2}\int d^3x\; e^{i\mathbf{q}\cdot\mathbf{x}}\;\frac{e^{-m(|\mathbf{r}_1-\mathbf{x}|)}}{|\mathbf{r}_1-\mathbf{x}|}\overleftrightarrow{\boldsymbol{\nabla}}_x\frac{e^{-m(|\mathbf{x}-\mathbf{r}_2|)}}{|\mathbf{x}-\mathbf{r}_2|} \\
&= \frac{1}{(4\pi)^2}\int d^3x\; e^{i\mathbf{q}\cdot\mathbf{x}}\;\frac{e^{-m(|\mathbf{r}_1-\mathbf{x}|)}}{|\mathbf{r}_1-\mathbf{x}|}\left(\boldsymbol{\nabla}_x\frac{e^{-m(|\mathbf{x}-\mathbf{r}_2|)}}{|\mathbf{x}-\mathbf{r}_2|}\right) \\
&- \frac{1}{(4\pi)^2}\int d^3x\; e^{i\mathbf{q}\cdot\mathbf{x}}\left(\boldsymbol{\nabla}_x\frac{e^{-m(|\mathbf{r}_1-\mathbf{x}|)}}{|\mathbf{r}_1-\mathbf{x}|}\right)\frac{e^{-m(|\mathbf{x}-\mathbf{r}_2|)}}{|\mathbf{x}-\mathbf{r}_2|}.
\end{aligned}$$

After some steps (writing the propagators with the integral representation as in Eq. (A.2) and using the symmetry property between $\mathbf{x}$ and $\mathbf{r}_{1/2}$), this operator becomes

$$\mathbf{J}_{(2)}(\mathbf{q},\mathbf{r}_1,\mathbf{r}_2) = \frac{1}{(2\pi)^3}(\boldsymbol{\nabla}_1-\boldsymbol{\nabla}_2)\int d^3p\frac{e^{i(\mathbf{r}_1-\mathbf{r}_2)\cdot\mathbf{p}}\;e^{i(\mathbf{r}_1+\mathbf{r}_2)\cdot\frac{1}{2}\mathbf{q}}}{[(\mathbf{p}+\frac{1}{2}\mathbf{q})^2+m^2][(\mathbf{p}-\frac{1}{2}\mathbf{q})^2+m^2]}.$$

We can now perform a transformation in the two nucleon system, going from the two coordinates $\mathbf{r}_1$ and $\mathbf{r}_2$ to a new set of coordinates, the center of mass of the two-body system and the relative coordinate as

$$\mathbf{R} = \frac{\mathbf{r}_1+\mathbf{r}_2}{2},\quad \mathbf{r} = \mathbf{r}_1-\mathbf{r}_2.$$

In these coordinates we have that

$$\boldsymbol{\nabla}_1-\boldsymbol{\nabla}_2 = 2\boldsymbol{\nabla}_{\mathbf{r}},$$

such that the two-body current operator becomes

$$\mathbf{J}_2(\mathbf{q},\mathbf{r},\mathbf{R}) = \frac{1}{4\pi^3}e^{i\mathbf{R}\cdot\mathbf{q}}\;\boldsymbol{\nabla}_{\mathbf{r}}\int d^3p\frac{e^{i(\mathbf{r}_1-\mathbf{r}_2)\cdot\mathbf{p}}}{[(\mathbf{p}+\frac{1}{2}\mathbf{q})^2+m^2][(\mathbf{p}-\frac{1}{2}\mathbf{q})^2+m^2]}.$$

Calling the quantity

$$I_m(\mathbf{q},\mathbf{r}) = \int d^3p\frac{e^{i\mathbf{r}\cdot\mathbf{p}}}{[(\mathbf{p}+\frac{1}{2}\mathbf{q})^2+m^2][(\mathbf{p}-\frac{1}{2}\mathbf{q})^2+m^2]},$$

which depends only on the relative coordinate and contains the mass m of the meson, the current is finally simply

$$\mathbf{J}_2(\mathbf{q},\mathbf{r},\mathbf{R}) = \frac{1}{4\pi^3}e^{i\mathbf{R}\cdot\mathbf{q}}\big(\boldsymbol{\nabla}_{\mathbf{r}}I_m(\mathbf{q},\mathbf{r})\big). \tag{6.37}$$

In case of the Malfliet-Tjon potential the consistent two-body current in Eq. (6.34) is a linear combination of terms like those shown in the last equation with two different masses m_1 and m_2 in the functions $I_{m_{1/2}}(\mathbf{q},\mathbf{r})$. Note that in a matrix element calculation the gradient in the last expression acts only on $I_{m_{1/2}}$ and not on the wave functions, as in case of the convection current.

As already mentioned the two-body current operator does not depend on the relative coordinate $\mathbf{r}$ only, but it also includes a dependence on the center of mass of the two-body system, i.e. $\mathbf{R}$. In Chapter 4 we have stressed that the calculation of such a general two-body matrix element with the symmetrized hyperspherical harmonics is much more complicated than the calculation of a one-body operator matrix element, since one has to consider a further generation of the coefficient of fractional parentage and one has to integrate on the last two coordinates. Nevertheless, we have also said that the calculation of the matrix element of a two-body operator that simply depends on the relative coordinate $\mathbf{r}$ is analogous to the calculation of a one-body matrix element, and therefore much simpler. For this reason, we will neglect in the following the center of mass dependence in the two-body current of (6.37) and we will concentrate on the function $I_m(\mathbf{q},\mathbf{r})$ which depends only on the relative motion, i.e. we will consider an approximate two-body current as

$$\mathbf{J}_{(2)}(\mathbf{q},\mathbf{r},\mathbf{R}) \backsimeq \mathbf{J}^a_{(2)}(\mathbf{q},\mathbf{r}) = \frac{1}{4\pi^3}\boldsymbol{\nabla}_{\mathbf{r}} I_m(\mathbf{q},\mathbf{r}). \tag{6.38}$$

This approximation is certainly good in case of low momentum transfer $\mathbf{q}$, where the quantity $e^{i\mathbf{q}\cdot\mathbf{R}} \backsimeq 1$, but its effect for high momentum transfer cannot be judged a priori. The question whether such an approximation makes sense in a calculation with momentum transfer $q = 300$ or 500 MeV/c, as we would like to do, could be answered only performing a full calculation, without any approximations. Nevertheless, we will perform for the moment this approximation and we will try to estimate its effect.

Our purpose is then to consider the MEC in case of the MTI-III potential as in Eq. (6.34) with the above mentioned approximation, which in momentum space is

$$\mathbf{J}^{\mathrm{MTI-III,a}}_{(2)}(\omega,\mathbf{q}) = \frac{1}{\pi^2}(G^p_E(q^2_\mu) - G^n_E(q^2_\mu)) \sum_{i<j} (\boldsymbol{\tau}_i \times \boldsymbol{\tau}_j)^3 \Big[\alpha \boldsymbol{\nabla}_{\mathbf{r}_{ij}} I_{m_1}(\mathbf{q},(\mathbf{r}_i - \mathbf{r}_j)) +$$
$$\beta \boldsymbol{\nabla}_{\mathbf{r}_{ij}} I_{m_2}(\mathbf{q},(\mathbf{r}_i - \mathbf{r}_j)) + \Big(\gamma \boldsymbol{\nabla}_{\mathbf{r}_{ij}} I_{m_1}(\mathbf{q},(\mathbf{r}_i - \mathbf{r}_j)) + \delta \boldsymbol{\nabla}_{\mathbf{r}_{ij}} I_{m_1}(\mathbf{q},(\mathbf{r}_i - \mathbf{r}_j))\Big)\boldsymbol{\sigma}_i \cdot \boldsymbol{\sigma}_j\Big], \tag{6.39}$$

where we have now written the operator acting on pairs of particles of an A-body system and we have included the isovector form factor as usual.

At this point, in analogy to what was done for the spin and convection currents also the $J_+(q)$ component of the meson exchange current can be expanded in multipoles, neglecting the form factors dependence, whose information is added later, as usual. Actually, it turns out that all magnetic multipoles vanish for such a two-body current operator (see Appendix C) and therefore the multipole expansion reads simply

$$J^{\mathrm{MTI-III,a}(v)}_{(2)+}(q) = \sum_J E^v_J(q) = -\sqrt{2\pi}\sum_J \hat{J} T^{el}_{J1}(q). \tag{6.40}$$

Calculating this multipoles and taking into account the interference between convection and MEC currents one can study the effect of the latter on the transverse response function for ^{4}He.

However, another way to perform a calculation of the transverse response function consists in making use of the Siegert theorem, as introduced in Chapter 3. In fact each transverse electric multipole can be separated into two terms like

$$T^{el}_{J\mu}(q) = S^{el}_{J\mu}(q) + K^{el}_{J\mu}(q),$$

where the first one, $S^{el}_{J\mu}(q)$, is the so called Siegert operator, which is proportional to the Coulomb multipole as in Eq. (3.32), and the second one is the correction to the Siegert operator. In case of the Siegert operator the effect of the MEC is automatically taken into account without any need to explicitly write the form of the two-body current. Therefore it serves as method to understand the effect of the meson exchange current with respect to the convection current in the electric multipoles. On the other hand, depending on the value of the momentum transfer q under study, the effect of the correction $K^{el}_{J\mu}(q)$ can be small or sizable with respect to the Siegert operator itself. Usually, in case of low momentum transfer $qr \ll 1$, the Siegert operator is enough to correctly describe the electric transverse multipole. This is not the case for higher momentum transfers like $q = 300$ and 500 MeV/c. The effect of the correction $K^{el}_{J\mu}(q)$ is in any case smaller than $S^{el}_{J\mu}(q)$, since the it contains a higher Bessel function. For this reason, one can use the Siegert operator to relate the dominant term of the electric multipole to the Coulomb one, where no explicit MEC is needed, and then one can study the effect of the MEC only on the correction $K^{el}_{J\mu}(q)$. This would be in our case the preferable strategy, since we do not know a priori the effect of the approximation done on the MEC for the MTI-III

potential. Namely, its effect can be reduced if it is included only in the correction to the Siegert operator and not directly into all transverse multipoles $T^{el}_{J\mu}(q)$, since it would be a "correction to a correction". We should also remember that the error of this procedure is smaller only because of the fact that no magnetic multipole exist for this current. In a different situation, the only way to study the effect of the MEC on the magnetic multipole is to calculate explicitly the M_J, considering also the interference with other current terms, since no Siegert theorem exists for the magnetic part.

In the following we will show how we have used the Siegert theorem to estimate the effect of the MEC in the electric dipole and to check the correctness of the numerical evaluation of the convection current multipoles. Finally, we use again the Siegert test to understand the effect of the approximation made in the MEC for the MTI-III potential.

6.2.4 The Siegert Test

In Chapter 3 we have seen that the Siegert operator is written in terms of Coulomb multipoles, making use of the continuity equation, as

$$S^{el}_{J\mu}(q) = -\sqrt{\frac{J+1}{J}}\frac{\omega}{q} i^J C_{J\mu}(q). \tag{6.41}$$

The Siegert operator has to be the same as the first part of the electric multipole in Eq. (3.27)

$$T'^{el}_{J\mu}(q) = -\frac{1}{4\pi}\sqrt{\frac{J+1}{J}} \int d\hat{q}' \; \hat{\mathbf{q}}' \cdot \mathbf{J}(\mathbf{q}') \; Y^J_\mu(\hat{q}') \tag{6.42}$$

where all terms of the electromagnetic current are explicitly considered. Since there is a scalar product in the definition, it is clear that the spin current, which is purely transverse, does not contribute to $T'^{el}_{J\mu}(q)$, while the convection and the two-body current both contribute to it. Therefore, if one calculates the electric multipole $T'^{el}_{J\mu}(q)$ using the convection current $\mathbf{J}^c_{(1)}$ plus the consistent MEC current $\mathbf{J}_{(2)}$, the identity $S^{el}_{J\mu}(q) = T'^{el}_{J\mu}(q)$ has to hold. On the other hand, it is clear that if one compares the Siegert operator in (6.42), where the convection current and the MEC are implicitly included, with the $T'^{el}_{J\mu}(q)$ including only the convection current, one can estimate the influence of MEC on the corresponding multipole.

We have done such a comparison in case of the electric dipole, $J = 1$, which we will call E1. In Fig. 6.9 we show the Siegert operator of (6.41) in comparison with $T'^{el}_{1\mu}(q)$ of (6.42) obtained with $\mathbf{J}^c_{(1)}$ only; the momentum transfer $q = 300$ MeV/c

has been chosen and the calculation is performed with the MTI-III potential. The Siegert part of the electric multipole for the convection current is derived in detail in Appendix C, where also the calculation of the corresponding matrix element is discussed. One readily sees that the convection current alone covers only about

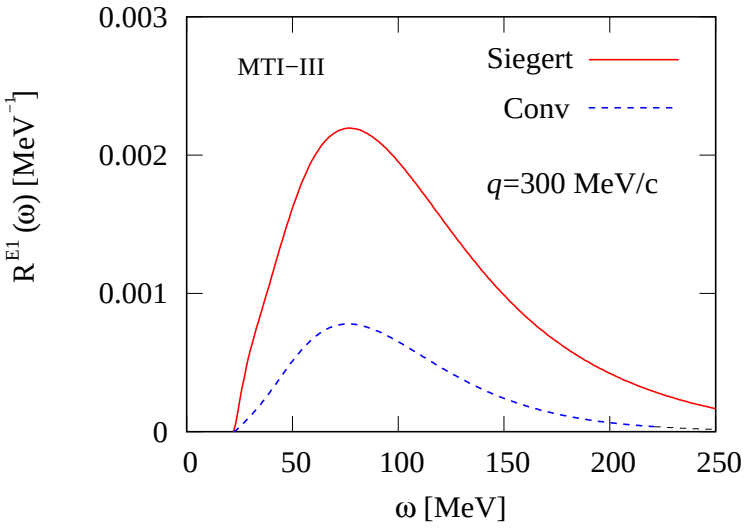

Figure 6.9: Comparison of the Siegert operator $S^{el}_{1\mu}(q)$, which includes implicitly the MEC effect, with the dipole electric multipole $T'^{el}_{1\mu}(q)$ of the convection current for the MTI-III potential and for the momentum transfer $q = 300$ MeV/c. The multipoles are divided by $\frac{\sqrt{2}}{4\pi}$ with respect to formulas.

40% of the total dipole strength of the Siegert operator in the quasi-elastic peak region. For this reason we can say that in case of this high momentum transfer the MEC have a relevant effect, which is about 60% of the total dipole strength. A similar comparison can be done for all multipoles of the current. A more detailed explanation of these calculations is presented in the following paragraphs.

A good check of the numerical evaluation of the convection current matrix element, that contains a derivative operator which acts on the wave function, can be done using the Siegert theorem in case of an interaction that satisfies the commutation relation $[V, \rho(\mathbf{x})] = 0$. This is certainly the case of a purely central potential with no spin-isospin dependence. For this reason we have chosen to work with the central version of the Malfliet-Tjon (MTV) potential, wich is simply

$$V(r) = A' \frac{e^{-m'_1 r}}{r} - B' \frac{e^{-m'_2 r}}{r} \tag{6.43}$$

with parameters A', B' and m'_1, m'_2 as given in [Bar01]. With this MTV we obtain a

ground state energy for ^{4}He which is -31.36 MeV, but we also see a dipole resonance below the disintegration threshold. This creates a very similar situation for the LIT as that found in case of the Coulomb multipole C_0^s for the longitudinal response. The difference is that here we do not have an elastic channel but a bound state dipole excitation. This excitation corresponds to a metastable resonance, peaked below the disintegration threshold, that will decay again into the ground state. This contribution is present in the LIT and can be subtracted calculating the energy E^* of the metastable state and then performing the inversion of the LIT with the usual basis state (see Chapter 2) and an additional term like $c\delta(\omega-\omega^*)$ with $\omega^* = E^*-E_0$. To simplify further the calculation we have decided to work with another potential, which has been obtained starting from the MTV and modifying the amplitudes A' and B' in order to move the resonance to the continuum. Taking new amplitudes, defined as the 80% of those in [Bar01], we have obtained a ground state energy of -12.56 MeV, but the bound resonance has disappeared. We call this potential MTV' and we will use it as a toy potential to perform a faster Siegert test. The name "toy" is ment to underline the fact that the obtained binding energy is far away from being semirealistic.

Using the MTV' potential we have performed the Siegert test only for the dipole multipole E1. The test, if done properly, has to show that the Siegert operator coincides with the convection current dipole, since no MEC exists for this potential model. The Siegert operator for the dipole is clearly

$$S^{el}_{1\mu}(q) = -i\sqrt{2}\frac{\omega}{q}C_{1\mu}(q). \tag{6.44}$$

Since it contains a dependence on the energy ω, that is factorizable, in order to calculate the response function of the system to the excitation of such an operator, we firstly calculate the LIT for the Coulomb operator $C_{1\mu}$, we invert it, i.e. we get $R^{C_1}(\omega)$ and then we obtain the response to $S^{el}_{1\mu}$ as

$$R^{S_1}(\omega) = 2\left(\frac{\omega}{q}\right)^2 R^{C_1}(\omega). \tag{6.45}$$

Concerning the contribution of the convection current to the Siegert part of the electric multipoles, an explicit derivation of it is presented in Appendix C. Both parts of the convection current in (6.19), the purely longitudinal $\mathbf{J}^{c,a}_{(1)}$ and also $\mathbf{J}^{c,b}_{(1)}$,

which contains a transverse and a longitudinal term, contribute to $T'^{el}_{1\mu}(q)$, such that

$$T'^{el}_{1\mu}(q) = T'^{el(a)}_{1\mu}(q) + T'^{el(b)}_{1\mu}(q). \tag{6.46}$$

Using Eq. (C.48) and (C.52) we get the form of $T'^{el(a/b)}_{J\mu}(q)$ for the dipole ($J = 1$), which are, omitting the isospin structure,

$$T'^{el(a)}_{1\mu}(q) = -\frac{iq}{\sqrt{2}m} C_{1\mu}(q) = -\frac{Aiq}{\sqrt{2}m} j_1(qr'_A) Y^1_\mu(\hat{r}'_A), \tag{6.47}$$

$$T'^{el(b)}_{1\mu}(q) = \frac{i\sqrt{2}(A-1)}{m}\left[\frac{1}{\sqrt{3}} j_0(qr'_A)[Y^0(\hat{r}'_A) \times \boldsymbol{\nabla}'^1_A]^1_\mu + \sqrt{\frac{2}{3}} j_2(qr'_A)[Y^2(\hat{r}'_A) \times \boldsymbol{\nabla}'^1_A]^1_\mu\right].$$

Since the parity of these operators is the same and they both lead to transitions with a final angular momentum $J_f = 1$ in case of ^{4}He ($J_0 = 0$), they can interfere whith each other. This means that the response of the system to the operator (6.46) is not simply the sum of the responses of the two operators in (6.47), but one has to consider also the interference term. We have firstly calculated the LIT for the two operators in (6.47) separately, solving two Schrödinger-like equations. Then, from the inversions of the two we get the separate responses of $T'^{el(a)}_{1\mu}$ and $T'^{el(b)}_{1\mu}$. In order to calculate the response of the total convection current with the LIT we have simply summed the two right-hand-sides of the Schrödinger-like equations solved before, i.e. $T'^{el(a)}_{1\mu}|\Psi_0\rangle$ and $T'^{el(b)}_{1\mu}|\Psi_0\rangle$, and then we have used it as source term of a third Schrödinger-like equation. Inverting the corresponding LIT one gets obviously the response of the total convection current. Clearly, this is analogous as writing directly one single operator $T'^{el}_{1\mu}$ as the sum of the two terms in (6.47) and calculating only one right-hand-side for the Schrödinger-like equation. The only advantage of the procedure we have used is that one can study separately the effect of the single parts of the operator, with the corresponding interference. In Fig. 6.10 we show the Siegert test in case of the isovector dipole for the momentum values $q = 3$, 100 and 300 MeV/c. The response function of the Siegert operator is compared with the response of the dipole $T'^{el}_{1\mu}$ in case of the convection current. The separated contributions of $T'^{el(a)}_{1\mu}$, containing the Bessel function j_1, and $T'^{el(b)}_{1\mu}$, including the Bessel functions j_0 and j_2, are also presented in the picture. One can see that for the lowest momentum value, i.e. $q = 3$ MeV/c, only the component proportional to the Bessel j_0 plays a role, while the others are negligible.

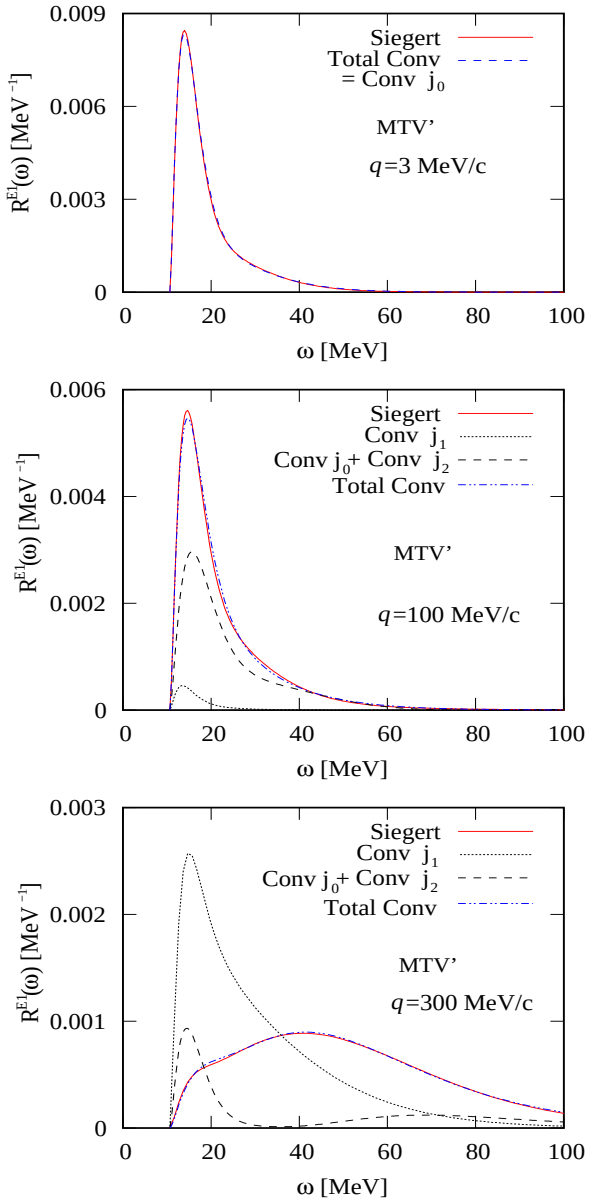

Figure 6.10: Comparison of the isovector dipole Siegert operator and the isovector electric dipole of the convection current in case of the MTV' potential for various momentum transfers. We also show the two separate contributions of the convection current, one containing the Bessel functions j_0 and j_2, and the other containing the Bessel function j_1. The multipoles are divided by $\frac{\sqrt{2}}{4\pi}$ with respect to formulas.

In case of $q = 100$ MeV/c the $T'^{el(b)}_{1\mu}$ dominates over the $T'^{el(a)}_{1\mu}$ component, but their combined contribution agrees quite well with the Siegert operator. Finally, in case of momentum transfer $q = 300$ MeV/c one can see how $T'^{el(a)}_{1\mu}$ and $T'^{el(b)}_{1\mu}$ interfere destructively to give a total contribution which again agrees quite well with the Siegert dipole response. The small deviations between Siegert and total convection current response reflect the size of the numerical error, which is certainly below a few percent. The numerical error comes from the fact that the matrix elements of the two operators are calculated in a very different way, leading to two different LITs. Furthermore, they derive from two different inversions. Note that such a comparison cannot be done at a transform level, since the information on the energy ω in the Siegert operator can be added only after the inversion procedure. Since such numerical error is clearly small, we can say that the Siegert test of the convection current in case of the MTV' potential shows that the numerical integration of the convection current has been performed correctly.

Performing an analogous calculation in case of the MTI-III potential one can estimate the influence of the MEC in the dipole response and study its dependence on the energy ω and momentum transfer q. However, our final aim is also to include explicitly in the transverse response function the effect of the MEC for the MTI-III potential. Since we have introduced an approximation in the two-body current neglecting the center of mass motion $\mathbf{R}$ of the two-particle system, we can again use the Siegert test to check the validity of this assumption. For this purpose we have calculated the Siegert part of the dipole operator in (6.42) in case of the $\mathbf{J}^{\mathrm{MTI-III,a}}_{(2)}$ of Eq. (6.39). The explicit derivation of the Siegert part of the electric multipole for the MEC is presented in Appendix C. In case of the dipole the main structure of the operator is, up to some factor and omitting the isospin isovector structure,

$$T'^{el}_{1\mu}(q) = \frac{4\pi}{\sqrt{3}}\big[\Phi^1_{1,0}(q, r_{A,A-1}) - \sqrt{2}\Phi^1_{1,2}(q, r_{A,A-1})\big]Y^1_\mu(\hat{r}_{A,A-1}), \tag{6.48}$$

where the radial functions are defined in (C.56) of Appendix C. Note that, considering also the MEC, we have to perform the Siegert test in case of the isovector dipole, since no isoscalar contribution of the MEC is present. Furthermore, we have again to consider the interference between convection current and MEC, since they both contribute to the dipole excitation.

In Fig. 6.11 we present the Siegert test for the isovector dipole operator in case of the MTI-III potential for three values of momentum transfer $q = 3$ MeV/c, 100 MeV/c and 300 MeV/c.

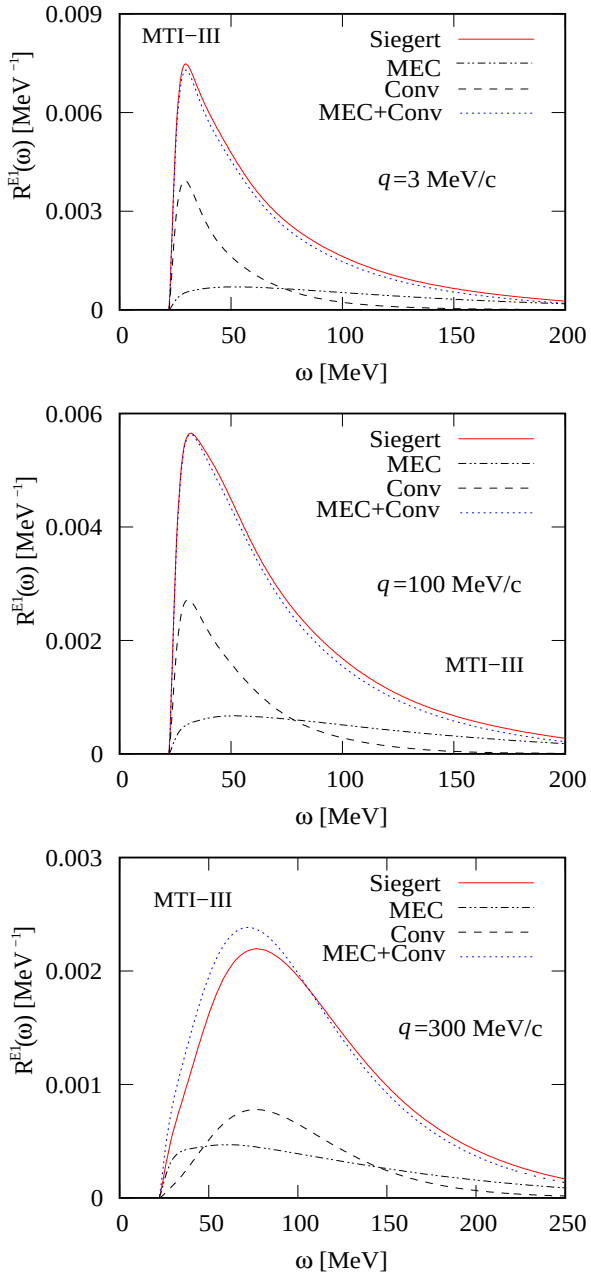

Figure 6.11: Comparison of the isovector dipole Siegert operator with the isovector electric dipole induced by the MEC, by the convection current and finally by the sum of the two currents. The calculations are performed with the MTI-III potential for various momentum transfers. The multipoles are divided by $\frac{\sqrt{2}}{4\pi}$ with respect to formulas.

We see the comparison between the response function of the Siegert operator in (6.44), of $T'^{el}_{1\mu}$ of Eq. (6.42) in case of the total convection current, in case of the MEC, and in case where both contributions with the relative interference are taken into account. From Fig. 6.11 one can see that the convection current shows a similar shape as the Siegert result although of smaller size for all three different momentum values, while the response of the MEC presents a rather flat behavior over the whole energy spectrum.

One can note that the relative effect of the MEC alone with respect to the total dipole strength of the Siegert operator increases with increasing q, moving from about 9% in case of $q = 3$ MeV/c up to about 20% in case of $q = 300$ MeV/c. Considering also the interference part, namely comparing the Siegert operator with the convection current alone, one can estimate the total effect of the MEC on the dipole, which appears important, reaching about 60% in case of $q = 300$ MeV/c. From the last figure we can also see that we do not get perfect agreement between the Siegert response and the combined response of convection current and MEC. We note a small constant deviation in the tail of the response, which is present in all three momentum transfer values. In case of $q = 300$ MeV/c we find a deviation also in the low energy region, where the convection current with MEC give a higher contribution to the dipole than the Siegert operator itself. This second last disagreement is certainly due to the approximation we have done in the two-body current, since it is found only for the highest momentum value. We can therefore conclude that the performed approximation has an effect which depends on the momentum value, as expected. This effect seems not to be present or to be negligibly small up to the 100 MeV/c of momentum transfer, while it reaches about 10% on the peak in case of $q = 300$ MeV/c.

The fact that we do not get the same accuracy in the Siegert test in case of MTV' and MTI-III potential for low momentum values, where the approximation of the MEC should not have an effect, can be due to numerical error or still to a wrong implementation of the MEC multipole. The numerical error could be bigger in the presence of the MEC, since we are summing two different calculations, where a one-body and a two-body matrix element are evaluated. Nevertheless, this question should be investigate further, for example performing the Siegert test also for other multipoles. Another possible source of error is the fact that within an effective interaction method one should use the similarity transformation also on the excitation operators, i.e. on the charge and currents. Up to now we have not used these effective operators, since in convergence this is not necessary. However,

it could be possible that the MEC is more sensitive to such fine corrections than a simple Coulomb multipole, since it is introduced to ensure consistency and gauge invariance. This point has to be analyzed further by studying the LIT at higher K_{max} values.

Furthermore, if the effect of the approximation done in the MEC turns out to be of about 10% one could calculate the effect of the MEC in the transverse response function using the Siegert theorem and considering the explicit form of the two-body current only to the correction $K^{el}_{J\mu}(q)$ to the Siegert operator in the electric multipole, see Eq. (3.31). This would certainly limit the error of the approximation under 10%, since $K^{el}_{J\mu}(q)$ is of second order with respect to the Siegert operator in the total electric multipole.

Concluding, we can say that we have calculated for the first time the transverse response function for ^{4}He with the LIT and EIHH methods, using semirealistic potentials. The effect of the spin current is dominant in comparison to the other current parts, but it is clearly not enough to reach the experimental data for $R_T(\omega)$.

The convection current operator, which contains a derivative acting on the wave function, has been implemented in the HH formalism without difficulties. Its effect is however small on the total transverse response.

The effect of the two-body current has been estimated to be of about 60% of the total dipole strength in case of $q = 300$ MeV/c. A consistent MEC has been built for the MTI-III potential, but an approximation has been done in order to simplify the more complicated calculation of a two-body operator matrix element. The first checks on the correctness of the implementation of the MEC and of the validity of the performed approximation have been carried on. Further investigation is necessary to finally answer the question about the total effect of the MEC on the transverse response of ^{4}He in case of semirealistic potentials.

Chapter 7

Conclusions and Outlook

In the following two sections, one on the photoabsorption on $A > 4$ nuclei and the other on electron scattering off ^{4}He, we briefly summarize the results obtained, focusing the attention on the goals achieved and on the remaining open questions. We also present an overview on possible future developments of these studies.

7.1 Photoabsorption Reactions on $A > 4$ Nuclei

In this thesis we have presented the first microscopic calculation of the total photodisintegration cross section for six- and seven-body nuclei with complete inclusion of the FSI. We have used the dipole approximation for the excitation operator and simple semirealistic potentials as NN interaction.

The cross sections of ^{6}Li and ^{6}He show a rather different structure. While ^{6}Li exhibits a single broad giant dipole resonance, one clearly distinguishes two well separated peaks for ^{6}He. The low-energy peak is due to the breakup of the ^{6}He neutron halo, whereas the second peak corresponds to the breakup of the α core. Unfortunately, in case of ^{6}Li no inclusive experiment exists to the best of our knowledge and the comparison with data obtained from different exclusive experiments is quite unclear. In case of ^{6}He new data at low energy obtained with radioactive beams are available and the agreement of the calculations is qualitatively satisfactory, while the second peak at higher energies still waits experimental confirmation. The addition of a P-wave interaction, which is achieved using the AV4' potential, improves substantially the agreement with data. It is evident that further experimental activities are necessary in order to shed more light on the six-nucleon photoabsorption cross sections.

For the ^{7}Li a single broad giant dipole resonance is found with the AV4' potential

and a good agreement with the available experimental data is obtained. From the theoretical point of view the question whether a semirealistic interaction is enough to describe the reaction mechanism can be answered only by performing calculations with full realistic two-body and three-body potentials.

For the future, the possible developments of this project are:

- Go beyond the dipole approximation in the total photoabsorption cross section to understand whether the effect of other multipoles is appreciable and improves the comparison with data;
- Use more realistic interactions to finally confirm or disprove the results obtained from semirealistic potentials;
- Study systematically the effect of the various interaction terms, such as spin-orbit and tensor force, on observables in the continuum;
- Find a way to discard those states in the HH expansion which do not contribute, since at some point the increasing number of basis states constitutes the main technical bottleneck;
- Push finally the method up to $A = 8$ nuclei, where other halo nuclei, e.g. ^{8}He, are present or other reactions of astrophysical interest could be investigated.

7.2 Electron Scattering off ^{4}He

We have presented a calculation of the longitudinal and transverse response functions for inclusive electron scattering off ^{4}He. The quasi-elastic region has been investigated at medium momentum transfer. A non-relativistic model for the electromagnetic charge and current excitation operators has been used. The calculations have been performed again with semirealistic interactions and a gauge invariant model has been build by construction of a consistent meson exchange current for the MTI-III potential.

The longitudinal response is compared with the available experimental data and with the already existing calculation performed with the LIT and the correlation method [Efr97a]. We obtained an overall reasonable agreement with experimental data, although our curves are slightly high also with respect to the previous calculation [Efr97a], where a relativistic corrections (Darwin-Foldy term) were included, which reduces the strength. With the MTI-III potential we see a substructure in the longitudinal response at $q = 300$ MeV, which is not shown by data.

Concerning the transverse response, the dominant one-body spin current has been treated and its response has been compared with data, finding some missing strength, which is probably due to the not yet present convection current and MEC. The one-body convection current has been implemented and checked via the Siegert test for the dipole contribution at various momentum transfers. We have also investigated the effect of the meson exchange currents for the MTI-III on the transverse response function. For this purpose an approximation has been made on the consistent MEC in order to treat it as an operator that simply depends on the relative distance between particles. The first estimations of the accuracy of this approximation are discussed. The effect of the MEC has been found to be of about 60% of the total dipole strength for a momentum transfer of $q = 300$ MeV/c.

Further studies are needed to finally calculate exactly the transverse response with all current parts. For the future the following points remain to be investigated:

- Perform the Siegert test for the various multipoles beyond the dipole to investigate the relative importance of the convection current and of the MEC;
- Calculate explicitly the contribution of the MEC to the correction to the Siegert operator. The Siegert operator alone is probably not enough for describing the electric dipole transition at medium momentum transfer;
- Treat the MEC exactly without any approximation, generalizing the calculation of the two-body operator matrix element in the HH formalism (actually it turns out that this is as difficult as considering a three-body nuclear force as done in [Bar04]);
- Once one finally has calculated the transverse response function of ^{4}He with the FSI and with a consistent MEC for the MTI-III potential, one can investigate the effect of more realistic interactions;
- Study the effect of relativistic contributions at medium and high momentum transfer;
- Extend the study of electron scattering with the LIT and EIHH methods on heavier nuclei ($A > 4$).

Appendix A

One Pion Exchange Current

In the following a short didactic example of a meson exchange current is presented. The one-pion exchange current is formally derived from the one-pion exchange potential using the minimal coupling method.

If one constructs a simple model of two non-relativistic nucleons interacting with a pion field, like in Figure A.1, one can derive by standard methods [Bjo64] the explicit form of the one pion exchange potential [Are82], which is given by

$$V^{\rm OPE}(\mathbf{r}_1-\mathbf{r}_2) = -\frac{f^2}{m_\pi^2}\boldsymbol{\tau}_1\cdot\boldsymbol{\tau}_2(\boldsymbol{\sigma}_1\cdot\boldsymbol{\nabla}_1)(\boldsymbol{\sigma}_2\cdot\boldsymbol{\nabla}_2)J_{m_\pi}(\mathbf{r}_1-\mathbf{r}_2), \tag{A.1}$$

where $\mathbf{r}_{1/2}, \boldsymbol{\tau}_{1/2},$ and $\boldsymbol{\sigma}_{1/2}$ are the coordinates, isospins and spins of nucleon 1 and 2, respectively. Here the function

$$J_{m_\pi}(\mathbf{r}_1-\mathbf{r}_2) = \int \frac{d^3p}{(2\pi)^3}\frac{e^{i(\mathbf{r}_1-\mathbf{r}_2)\cdot\mathbf{p}}}{\mathbf{p}^2+m_\pi^2} = \frac{1}{4\pi}\frac{e^{-m_\pi|\mathbf{r}_1-\mathbf{r}_2|}}{|\mathbf{r}_1-\mathbf{r}_2|} \tag{A.2}$$

is the propagator of the pion of mass m_π. Clearly, the gradients in the (A.1) act on the pion propagator.

Making use of the fact that $[\mathbf{p}, f(\mathbf{r})] = -i\boldsymbol{\nabla}f(\mathbf{r})$, for every function f of the coordinates, the OPE potential can be written as follows

$$V^{\rm OPE}(\mathbf{r}_1-\mathbf{r}_2) = \frac{f^2}{m_\pi^2}\Bigg[(\boldsymbol{\sigma}_1\cdot\mathbf{p}_1),\Bigg[(\boldsymbol{\sigma}_2\cdot\mathbf{p}_2),\sum_\mu(\tau_1^\mu)(\tau_2^\mu)^\dagger < \mathbf{r}_1\mu|\frac{1}{\mathbf{p}^2+m_\pi^2}|\mathbf{r}_2\mu>\Bigg]\Bigg], \tag{A.3}$$

which is a more convenient expression if one wants to construct a consistent meson exchange current using the minimal substitution, as will be explained later. Here

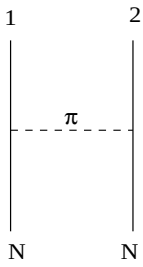

Figure A.1: Diagram of two nucleons exchanging a pion.

the pion propagator is represented by

$$J_{m_\pi}(\mathbf{r}_1 - \mathbf{r}_2) = < \mathbf{r}_1\mu | \frac{1}{\mathbf{p}^2 + m_\pi^2} | \mathbf{r}_2\mu >,$$

where with the notation $|\mathbf{r}_{1/2}\mu >$ a pion state at position $\mathbf{r}_{1/2}$ with charge μ is meant. Furthermore the quantity $\sum_\mu (\tau_1^\mu)(\tau_2^\mu)^\dagger$ is the scalar product $\boldsymbol{\tau}_1 \cdot \boldsymbol{\tau}_2$.

In order to recover the corresponding one pion exchange current we will now apply minimal coupling by the following substitution

$$\begin{aligned}
\mathbf{p}_1 &\rightarrow \mathbf{p}_1 - e_1 \mathbf{A}_1(\mathbf{r}), \\
\mathbf{p}_2 &\rightarrow \mathbf{p}_2 - e_2 \mathbf{A}_2(\mathbf{r}), \\
\mathbf{p} &\rightarrow \mathbf{p} - e_\pi \mathbf{A}_\pi(\mathbf{r}),
\end{aligned}$$

and then recover the exchange current from the functional derivative like in Eq. (3.2)

$$\hat{\mathbf{j}}_{(2)}^{\mathrm{OPE}}(\mathbf{x}, \mathbf{r}_1, \mathbf{r}_2) = -\frac{\delta V^{\mathrm{OPE}}(\mathbf{A})}{\delta \mathbf{A}}\bigg|_{\mathbf{A}=0}. \tag{A.4}$$

The minimal substitution in the potential leads to

$$\begin{aligned}
V^{\mathrm{OPE}}(\mathbf{r}_1 - \mathbf{r}_2, \mathbf{A}) = \frac{f^2}{m_\pi^2} \Bigg[(\boldsymbol{\sigma}_1 \cdot (\mathbf{p}_1 - e_1 \mathbf{A}_1)), \Bigg[(\boldsymbol{\sigma}_2 \cdot (\mathbf{p}_2 - e_2 \mathbf{A}_2)), \\
\sum_\mu (\tau_1^\mu)(\tau_2^\mu)^\dagger < \mathbf{r}_1\mu | \frac{1}{(\mathbf{p} - e_\pi \boldsymbol{A}_\pi)^2 + m_\pi^2} | \mathbf{r}_2\mu > \Bigg] \Bigg],
\end{aligned} \tag{A.5}$$

from which it is clear that the expression in Eq. (A.3) is useful because the pion momentum dependence is explicitly written, and therefore one can directly apply the minimal coupling.

For the derivative in Eq. (A.4) we then obtain

$$\begin{aligned}\hat{\mathbf{j}}^{\rm OPE}_{(2)}(\mathbf{x},\mathbf{r}_1,\mathbf{r}_2) &= -\frac{f^2}{m_\pi^2}\Big\{\big[-\boldsymbol{\sigma}_1 e_1\delta(\mathbf{x}-\mathbf{r}_1),\big[\boldsymbol{\sigma}_2\cdot\mathbf{p}_2,(\boldsymbol{\tau}_1\cdot\boldsymbol{\tau}_2)J_m(\mathbf{r}_1-\mathbf{r}_2)\big]\big]+\\ &+ \big[(\boldsymbol{\sigma}_1\cdot\mathbf{p}_1),\big[-\boldsymbol{\sigma}_2 e_2\delta(\mathbf{x}-\mathbf{r}_2),(\boldsymbol{\tau}_1\cdot\boldsymbol{\tau}_2)J_m(\mathbf{r}_1-\mathbf{r}_2)\big]\big]+\\ &+ \big[(\boldsymbol{\sigma}_1\cdot\mathbf{p}_1),\big[(\boldsymbol{\sigma}_2\cdot\mathbf{p}_2),\sum_\mu(\tau_1^\mu)(\tau_2^\mu)^\dagger\\ &\quad <\mathbf{r}_1\mu|\frac{1}{\mathbf{p}^2+m_\pi^2}\mu\big\{\mathbf{p},\delta(\mathbf{x}-\mathbf{r}_\pi)\big\}\frac{1}{\mathbf{p}^2+m_\pi^2}|\mathbf{r}_2\mu>\big]\big]\Big\}.\end{aligned} \tag{A.6}$$

The next step to do is to write the charges of the nucleons with the isospin formalism, as $e_{1/2}=\frac{1+\tau^3_{1,2}}{2}$ and to make use of the following commutation relation

$$[\boldsymbol{\tau}_1\cdot\boldsymbol{\tau}_2,\tau^3_{1/2}]=\pm 2i(\boldsymbol{\tau}_1\times\boldsymbol{\tau}_2)^3.$$

In this way, one gets from the first two lines of Eq. (A.6) the contact terms of the

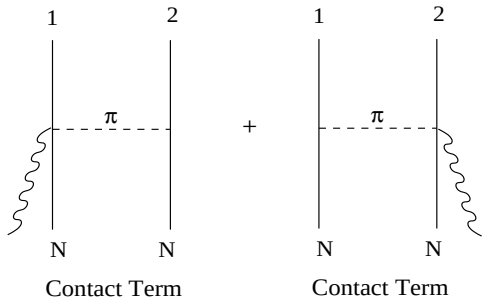

Figure A.2: Diagrams of the two contact terms of the one pion exchange current.

current, represented in Fig. A.2, which are formally

$$\hat{\mathbf{j}}^{\rm OPE}_{\rm cont}(\mathbf{x},\mathbf{r}_1,\mathbf{r}_2)=-\frac{f^2}{m_\pi^2}(\boldsymbol{\tau}_1\times\boldsymbol{\tau}_2)^3\boldsymbol{\sigma}_1(\boldsymbol{\sigma}_2\cdot\boldsymbol{\nabla}_2)J_{m_\pi}(\mathbf{r}_1-\mathbf{r}_2)\delta(\mathbf{x}-\mathbf{r}_1)+(1\leftrightarrow 2). \tag{A.7}$$

In order to derive the so called "pion in flight term", see Fig. A.3, we have to rewrite the two last lines of Eq. (A.6), using the following relation

$$\sum_\mu(\tau_1^\mu)(\tau_2^\mu)^\dagger\mu=i(\boldsymbol{\tau}_1\times\boldsymbol{\tau}_2)^3$$

and explicitly writing the anticommutator. The first term of the anticommutator,

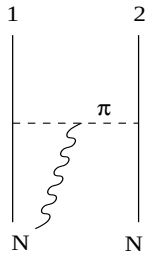

Pion in Flight Term

Figure A.3: Diagram of the pion in flight term for the one pion exchange current.

inserting two times a complete set $\int d^3r|\mathbf{r}><\mathbf{r}| = 1$, is then

$$
\begin{aligned}
&< \mathbf{r}_1\mu|\frac{1}{\mathbf{p}^2+m_\pi^2}\mathbf{p}\delta(\mathbf{x}-\mathbf{r}_\pi)\frac{1}{\mathbf{p}^2+m_\pi^2}|\mathbf{r}_2\mu >= \\
&= \int d^3r \int d^3r' < \mathbf{r}_1\mu|\frac{1}{\mathbf{p}^2+m_\pi^2}\mathbf{p}|\mathbf{r}><\mathbf{r}|\delta(\mathbf{x}-\mathbf{r}_\pi)|\mathbf{r}'><\mathbf{r}'|\frac{1}{\mathbf{p}^2+m_\pi^2}|\mathbf{r}_2\mu > \\
&= \int d^3r < \mathbf{r}_1\mu|\frac{1}{\mathbf{p}^2+m_\pi^2}\mathbf{p}|\mathbf{r}>\delta(\mathbf{x}-\mathbf{r})<\mathbf{r}|\frac{1}{\mathbf{p}^2+m_\pi^2}|\mathbf{r}_2\mu > \\
&=< \mathbf{r}_1\mu|\frac{1}{\mathbf{p}^2+m_\pi^2}\mathbf{p}|\mathbf{x}><\mathbf{x}|\frac{1}{\mathbf{p}_\pi^2+m_\pi^2}|\mathbf{r}_2\mu >= -i\big(\boldsymbol{\nabla}_x J_m(\mathbf{r}_1-\mathbf{x})\big)J_m(\mathbf{x}-\mathbf{r}_2)
\end{aligned}
$$

where we have used the fact that $< \mathbf{r} \mid \mathbf{r}' >= \delta(\mathbf{r}-\mathbf{r}')$ and we have integrated out the δ functions. The second part of the anticommutator will lead to

$$J_m(\mathbf{r}_1-\mathbf{x})i\boldsymbol{\nabla}_x J_m(\mathbf{x}-\mathbf{r}_2),$$

so that the total expression of the pion in flight current is

$$\hat{\mathbf{j}}^{\rm OPE}_{\rm pif}(\mathbf{x},\mathbf{r}_1,\mathbf{r}_2) = \frac{f^2}{m_\pi^2}(\boldsymbol{\tau}_1\times\boldsymbol{\tau}_2)^3(\boldsymbol{\sigma}_1\cdot\boldsymbol{\nabla}_2)(\boldsymbol{\sigma}_2\cdot\boldsymbol{\nabla}_2)J_{m_\pi}(\mathbf{r}_1-\mathbf{x})\overleftrightarrow{\boldsymbol{\nabla}}_x J_{m_\pi}(\mathbf{x}-\mathbf{r}_2), \tag{A.8}$$

whose Feynman diagram is shown in Fig. A.3.

The total OPE current is obviously the sum of the contact terms and of the pion in flight term as

$$
\begin{aligned}
\hat{\mathbf{j}}^{\rm OPE}_{(2)}(\mathbf{x},\mathbf{r}_1,\mathbf{r}_2) = -\frac{f^2}{m_\pi^2}(\boldsymbol{\tau}_1\times\boldsymbol{\tau}_2)^3\Big\{&\boldsymbol{\sigma}_1(\boldsymbol{\sigma}_2\cdot\boldsymbol{\nabla}_2)J_{m_\pi}(\mathbf{r}_1-\mathbf{r}_2)\delta(\mathbf{x}-\mathbf{r}_1)-(1\leftrightarrow 2) \\
-(\boldsymbol{\sigma}_1\cdot\boldsymbol{\nabla}_2)(\boldsymbol{\sigma}_2\cdot\boldsymbol{\nabla}_2)&J_{m_\pi}(\mathbf{r}_1-\mathbf{x})\overleftrightarrow{\boldsymbol{\nabla}}_x J_{m_\pi}(\mathbf{x}-\mathbf{r}_2)\Big\}.
\end{aligned} \tag{A.9}
$$

Appendix B

The Hyperspherical Formalism

In the following the definition of hyperspherical coordinates is presented. Then the form of the Laplace operator in these coordinates is discussed and finally the recursive construction of the A-body hyperspherical harmonics is shown as in [Bar97a].

B.1 Hyperspherical Coordinates

In order to define the hyperspherical coordinates it is necessary to start from a set of internal $A-1$ normalized Jacobi coordinates (see Eq. (4.2)). The (k−1)-th Jacobi coordinate is proportional to the position of the $k-$th particle relative to the center of mass of the $k-1$ particles ($i = 1, ..., k-1$). Each coordinate $\boldsymbol{\eta}_k$ consists of a radial part η_k and an angular part denoted with $\hat{\eta}_k \equiv (\theta_k, \phi_k)$. A two-body system is characterized by only one Jacobi coordinate $\boldsymbol{\eta}_1$, which of course has a radial part η_1 and an angular part $\hat{\eta}_1 \equiv (\theta_1, \phi_1)$.

A three-body systems is described by two Jacobi radial coordinates η_1, and η_2, and by two pairs of angular coordinates $\hat{\eta}_1 \equiv (\theta_1, \phi_1)$ and $\hat{\eta}_2 \equiv (\theta_2, \phi_2)$, which are the starting point for the construction of the hyperspherical coordinates. These are described by a hyper-radial coordinate ρ_2 and by a hyper-angular coordinate φ_2, defined as

$$\begin{aligned} \eta_1 = \rho_1 &= \rho_2 \cos\varphi_2, \\ \eta_2 &= \rho_2 \sin\varphi_2. \end{aligned} \tag{B.1}$$

The six dimensional volume element is given by

$$dV_6 = \rho_2^5 d\rho_2 dS_5 \equiv \rho_2^5 d\rho_2 \sin^2(\varphi_2) \cos^2(\varphi_2)\, d\varphi_2 d\hat{\eta}_1 d\hat{\eta}_2, \tag{B.2}$$

where dS_5 is the angular volume element associated the hypersphere in five dimensions and $d\hat{\eta}_1$ and $d\hat{\eta}_2$ are the volume elements associated to the angular part of the Jacobi coordinates $\hat{\eta}_1$ and $\hat{\eta}_2$, respectively. The hyperangle φ_2 assumes values in the range $\left[0, \frac{\pi}{2}\right]$.

Adding one particle, and therefore another Jacobi coordinate, one can define the hyper-radial coordinate, ρ_3, and the hyperangular one, φ_3, in the following way

$$\begin{aligned} \rho_2 &= \rho_3 \cos\varphi_3, \\ \eta_3 &= \rho_3 \sin\varphi_3. \end{aligned} \tag{B.3}$$

The hyperspherical coordinates of a four-body system with three Jacobi coordinates consist in a set of eight angular coordinates, the hyperspherical angles φ_2 and φ_3, the six spherical angles $\hat{\eta}_1$, $\hat{\eta}_2$, $\hat{\eta}_3$, and an hyper-radial coordinate ρ_3.

The nine dimensional volume element related to the four-body system is

$$dV_9 = \rho_2^8 d\rho_3 dS_8 \equiv \rho_3^8 d\rho_3 \sin^2(\varphi_3)\cos^5(\varphi_3)\, d\varphi_3 d\hat{\eta}_3 dS_5,$$

where dS_8 is the angular volume element associated to the eight dimensional hypersphere and dS_5 is defined in (B.2). The measure $d\hat{\eta}_3$ is the volume element associated with the angular coordinates $\hat{\eta}_3$ and the hyperangle φ_3 varies in the range $\left[0, \frac{\pi}{2}\right]$.

In general, having defined the hyper-radial coordinate ρ_{k-1}, one defines ρ_k and φ_k, such that

$$\begin{aligned} \rho_{k-1} &= \rho_k \cos\varphi_k, \\ \eta_k &= \rho_k \sin\varphi_k, \end{aligned} \tag{B.4}$$

where

$$\rho_k^2 = \rho_{k-1}^2 + \eta_k^2 = \sum_{i=1}^{k} \eta_i^2 = \frac{1}{k}\sum_{i<j}^{k+1} (\mathbf{r}_i - \mathbf{r}_j)^2 . \tag{B.5}$$

Here one can note that the hyper-radial coordinate is symmetric with respect to the permutation of the single particle coordinates. It also does not depend on the precise choice of the Jacobi coordinates.

The $3(A-1)$ internal coordinates of the A-body system are described by one hyper-radial coordinate, ρ_A, by $A-2$ hyper-angular coordinates, for wich we use the notation $\varphi_{(A-1)} \equiv \{\varphi_2, \varphi_3, ..., \varphi_{A-1}\}$, and finally by $2(A-1)$ angular coordinates, that are denoted with a collective symbol $\Omega_{(A-1)} \equiv \{\hat{\eta}_1, \hat{\eta}_2, ..., \hat{\eta}_{A-1}\}$.

These coordinates depend on the set of starting Jacobi coordinates, since, chang-

ing the indices of the particles a different set of hyperangular and angular coordinates is obtained (only the hyper-radius remains unchanged).

The volume element related to the $A-1$ Jacobi coordinates $\boldsymbol{\eta}_1, \boldsymbol{\eta}_2, ..., \boldsymbol{\eta}_{A-1}$ is

$$\begin{aligned} dV_{3(A-1)} &= \rho_{A-1}^{3A-4} d\rho_{A-1} dS_{3A-4} \\ &\equiv \rho_{A-1}^{3A-4} d\rho_{A-1} \sin^2(\varphi_{A-1}) \cos^{3A-7}(\varphi_{A-1}) \, d\varphi_{A-1} d\hat{\eta}_{A-1} dS_{3A-7}, \end{aligned} \tag{B.6}$$

where dS_{3A-7} and dS_{3A-4} are the volume elements associated to the hypersphere in $3A-7$ and $3A-4$ dimensions, respectively, and $d\hat{\eta}_{A-1}$ is the volume element associated to the angular part of the last Jacobi coordinate. Again, the hyperangle φ_{A-1}varies in the range $\left[0, \frac{\pi}{2}\right]$.

B.2 The Laplace Operator in Hyperspherical Coordinates

The internal kinetic energy operator for a two-body system is given by the three dimensional Laplace operator expressed in terms of the relative coordinate, i.e. the Jacobi coordinate $\boldsymbol{\eta}_1 = (\eta_1, \hat{\eta}_1)$,

$$\Delta_{(1)} = \Delta_{\boldsymbol{\eta}_1} = \Delta_{\eta_1} - \frac{1}{\eta_1^2} \hat{\ell}_1^2,$$

where the radial part is

$$\Delta_{\eta_1} = \frac{\partial^2}{\partial \eta_1^2} + \frac{2}{\eta_1} \frac{\partial}{\partial \eta_1}$$

and $\hat{\ell}_1$ is the relative angular momentum operator[1].

The internal kinetic energy of a three-particle system is described by the six dimensional Laplace operator, which is the sum of the three dimensional Laplace operators acting separately on the coordinates $\boldsymbol{\eta}_1$ and $\boldsymbol{\eta}_2$

$$\Delta_{(2)} = \Delta_{\boldsymbol{\eta}_1} + \Delta_{\boldsymbol{\eta}_2} = \Delta_{\eta_1} + \Delta_{\eta_2} - \frac{1}{\eta_1^2} \hat{\ell}_1^2 - \frac{1}{\eta_2^2} \hat{\ell}_2^2.$$

Using Eq. (B.1) one can transform the two coordinates η_1 and η_2 into the hyperradial coordinate ρ_2 and the hyperangular coordinate φ_2, by means of which the

[1]Note that we use the hat to denote the operator every time it is necessary to distinguish it from the corresponding eigenvalue.

Laplace operator becomes

$$\Delta_{(2)} = \Delta^2_{\rho_2} - \frac{1}{\rho_2^2}\hat{K}^2_2. \tag{B.7}$$

The radial part of Eq (B.7) depends only on the hyper-radial coordinate ρ_2,

$$\Delta^2_{\rho_2} = \frac{\partial^2}{\partial\rho_2^2} + \frac{5}{\rho_2}\frac{\partial}{\partial\rho_2},$$

whereas the hyperspherical angular momentum $\hat{K}^2_2$ is expressed in terms of the hyperangular coordinate φ_2 and of the two angular momenta $\hat{\ell}^2_1$ and $\hat{\ell}^2_2$, as

$$\hat{K}^2_2 = -\frac{\partial^2}{\partial\varphi_2^2} - 4\cot(2\varphi_2)\frac{\partial}{\partial\varphi_2} + \frac{1}{\cos^2(\varphi_2)}\hat{\ell}^2_1 + \frac{1}{\sin^2(\varphi_2)}\hat{\ell}^2_2. \tag{B.8}$$

The internal orbital angular momentum of the three-particle system is $\hat{L}_2 = \hat{\ell}_1 + \hat{\ell}_2$. It is to note that the operators $\hat{L}^2_2$ and $\hat{L}^z$ commute with $\Delta_{(2)}$, $\hat{\ell}^2_1$, $\hat{\ell}^2_2$ and $\hat{K}^2_2$.

The Laplace operator in $3(A-1)$ dimensions, that describes the internal kinetic energy of an A-body system, is given by the sum of the Laplace operators that act on the Jacobi coordinates $\boldsymbol{\eta}_1, \boldsymbol{\eta}_2, ..., \boldsymbol{\eta}_{A-1}$

$$\Delta_{(A-1)} = \sum_{i=1}^{A-1}\Delta_{\boldsymbol{\eta}_i} = \sum_{i=1}^{A-1}\left(\Delta_{\eta_i} - \frac{1}{\eta_i^2}\hat{\ell}^2_i\right).$$

From this expression follows a recursion relation for the Laplace operator of an A-body system

$$\Delta_{(A-1)} = \Delta_{(A-2)} + \Delta_{\boldsymbol{\eta}_{A-1}} = \Delta^{A-2}_{\rho_{A-2}} - \frac{1}{\rho^2_{A-2}}\hat{K}^2_{A-2} + \Delta_{\eta_{A-1}} - \frac{1}{\eta^2_{A-1}}\hat{\ell}^2_{A-1}.$$

With the help of Eq. (B.4) one can transform the coordinates ρ_{A-2} and η_{A-1} into hyper-radial coordinate ρ_{A-1} and hyperangular coordinate φ_{A-1}, such that the Laplace operator for $A-1$ Jacobi coordinates in terms of the hyperspherical coordinates becomes

$$\Delta_{(A-1)} = \Delta^{A-1}_{\rho_{A-1}} - \frac{1}{\rho^2_{A-1}}\hat{K}^2_{A-1}. \tag{B.9}$$

where the radial part is

$$\Delta^{A-1}_{\rho_{A-1}} = \frac{\partial^2}{\partial\rho^2_{A-1}} + \frac{3(A-1)-1}{\rho_{A-1}}\frac{\partial}{\partial\rho_{A-1}} \tag{B.10}$$

In Eq. (B.9) the operator $\hat{K}^2_{A-1}$ is the hyperspherical angular momentum associated

with the A particles and can be expressed in a recursive way as a function of $\hat{K}^2_{A-2}$, $\hat{\ell}^2_{A-1}$ and φ_{A-1} as follows

$$\hat{K}^2_{A-1} = -\frac{\partial^2}{\partial\varphi^2_{A-1}} + \frac{3A\text{–}9\text{–}(3A-5)\cos(2\varphi_{A-1})}{\sin(2\varphi_{A-1})}\frac{\partial}{\partial\varphi_{A-1}} + \frac{\hat{\ell}^2_{A-1}}{\sin^2\varphi_{A-1}} + \\ + \frac{\hat{K}^2_{A-2}}{\cos^2\varphi_{A-1}} \qquad \text{(B.11)}$$

where $\hat{K}^2_1 \equiv \hat{\ell}^2_1$. The internal orbital angular momentum of the A particles is $\hat{L}_{A-1} = \hat{L}_{A-2} + \hat{\ell}_{A-1}$. Furthermore, the operators $\hat{K}^2_{A-2}$, $\hat{\ell}^2_{A-1}$, $\hat{K}^2_{A-1}$, $\hat{L}^2_{A-1}$ and $\hat{L}^z_{A-1}$ commute with each other. Therefore the hyperspherical states are labelled with a set of good quantum numbers K_{A-1}, K_{A-2},..., K_2, corresponding to the hyperspherical angular momenta, with L_{A-1}, L_{A-2},..., L_2 corresponding to the spherical angular momenta of $A-1, A-2, ...,$ and 2 particles, with projection M_{A-1} of L_{A-1}, and finally with ℓ_{A-1}, ℓ_{A-2},..., ℓ_2, ℓ_1, corresponding to the angular part the Jacobi coordinates.

B.3 The Hyperspherical Harmonics

The angular part of the internal wave function of a two-particle system is described by the spherical harmonics $Y_{\ell_1 m_1}(\hat{\eta}_1)$. Adding another particle, described by the function $Y_{\ell_2 m_2}(\hat{\eta}_2)$, one can form a three particle internal state $\Phi_{L_2 M_2;\ell_1\ell_2}\left(\Omega_{(2)}\right)$ with $\Omega_{(2)} \equiv \{\hat{\eta}_1, \hat{\eta}_2\}$, which is eigenstate of the operators $\hat{\ell}^2_1$, $\hat{\ell}^2_2$, $\hat{L}^2_2$ and $\hat{L}^z_2$. It is obtained by coupling the angular momenta of the states $Y_{\ell_1 m_1}(\hat{\eta}_1)$ and $Y_{\ell_2 m_2}(\hat{\eta}_2)$ in the conventional way

$$\Phi_{L_2 M_2;\ell_1\ell_2}\left(\Omega_{(2)}\right) = \sum_{m_1,m_2} \langle \ell_1\ell_2 L_2 | m_1 m_2 M_2\rangle\, Y_{\ell_1 m_1}(\hat{\eta}_1)\, Y_{\ell_2 m_2}(\hat{\eta}_2)\,, \qquad \text{(B.12)}$$

where only the Jacobi angular coordinates $\hat{\eta}_1$ and $\hat{\eta}_2$ are involved.

The eigenfunctions of the hyperspherical angular momentum $\hat{K}^2_2$, expressed in Eq. (B.8), are functions of the hyperangular coordinate φ_2 and depend on the values of the quantum numbers K_2, ℓ_2 and $K_1 \equiv \ell_1$, in the following way

$$\psi_{K_2;\ell_2\ell_1}(\varphi_2) = \mathcal{N}_2(K_2;\ell_2\ell_1)(\sin\varphi_2)^{\ell_2}(\cos\varphi_2)^{\ell_1} P_{n_2}^{\left(\ell_2+\frac{1}{2},\ell_1+\frac{1}{2}\right)}(\cos 2\varphi_2)\,, \qquad \text{(B.13)}$$

where $P_{n_2}^{\left(\ell_2+\frac{1}{2},\ell_1+\frac{1}{2}\right)}$ is a Jacobi polynomial[2] [Wea75], n_2 is a non-negative integer number and $K_2 = 2n_2 + \ell_1 + \ell_2$. The normalization constant is

$$\mathcal{N}_2\left(K_2;\ell_2\ell_1\right) = \left[\frac{\left(2K_2+4\right)n_2!\Gamma\left(n_2+\ell_2+\ell_1+2\right)}{\Gamma\left(n_2+\ell_2+\frac{3}{2}\right)\Gamma\left(n_2+\ell_1+\frac{3}{2}\right)}\right]^{\frac{1}{2}}.$$

The eigenvalues of $\hat{K}_2^2$, corresponding to the eigenfunctions in Eq. (B.13), are $K_2\left(K_2+4\right)$, where $K_2 \geq \ell_1+\ell_2 \geq L_2 \geq 0$. The parity of the functions in Eq. (B.13) is $(-)^{\ell_1+\ell_2}$.

The hyperspherical harmonics for a three-particle system which are eigenfunctions both of $\hat{K}_2^2$ and $\hat{L}_2^2$, are obtained by the product of the (B.13) with the functions in (B.12),

$$\mathcal{Y}_{[K_2]}\left(\Omega_{(2)},\varphi_{(2)}\right) = \psi_{K_2;\ell_2\ell_1}\left(\varphi_2\right)\Phi_{L_2M_2;\ell_1\ell_2}\left(\Omega_{(2)}\right). \tag{B.14}$$

With the notation $[K_2]$ we denote the set of good quantum numbers K_2, L_2, M_2, ℓ_1 and ℓ_2, that label completely the states that depend on the five angular internal coordinates, $\hat{\eta}_1 \equiv (\theta_1,\phi_1)$, $\hat{\eta}_2 \equiv (\theta_2,\phi_2)$ (in $\Omega_{(2)}$) and φ_2.

In order to appreciate the recursion procedure one needs to consider a four-body system. Starting from the above three-particle wave funtions, one can construct the hyperspherical harmonics for a four-particle system by coupling these functions to the spherical harmonics $Y_{\ell_3m_3}\left(\hat{\eta}_3\right)$. This is obtained in three steps. First of all, one couples the angular momenta L_2 and ℓ_3 to L_3 obtaining

$$\Phi_{L_3M_3;[K_2]\ell_3}\left(\Omega_{(3)},\varphi_2\right) = \sum_{M_2,m_3}\left\langle L_2\ell_3L_3|M_2m_3M_3\right\rangle \mathcal{Y}_{[K_2]}\left(\Omega_{(2)},\varphi_2\right)Y_{\ell_3m_3}\left(\hat{\eta}_3\right). \tag{B.15}$$

This function has seven internal coordinates $\hat{\eta}_1 = (\theta_1,\phi_1)$, $\hat{\eta}_2 = (\theta_2,\phi_2)$, φ_2 and $\hat{\eta}_3 = (\theta_3,\phi_3)$. Then, using the transformation in Eq. (B.3), one constructs the eigenfunctions for the hyperspherical angular momentum $\hat{K}_3^2$,

$$\psi_{K_3;\ell_3K_2}\left(\varphi_3\right) = \mathcal{N}_3\left(K_3;\ell_3K_2\right)\left(\sin\varphi_3\right)^{\ell_3}\left(\cos\varphi_3\right)^{K_2}P_{n_3}^{\left(\ell_3+\frac{1}{2},K_2+2\right)}\left(\cos 2\varphi_3\right), \tag{B.16}$$

where, again, $P_{n_3}^{\left(\ell_3+\frac{1}{2},K_2+2\right)}$ is a Jacobi polynomial, and n_3 is a non-negative integer

[2] $P_n^{\alpha,\beta}\left(x\right) = \frac{(-1)^n}{2^n n!(1-x)^\alpha(1-x)^\beta}\frac{d^n}{dx^n}\left[\left(1-x\right)^{\alpha+n}\left(1-x\right)^{\beta+n}\right]$ with $x \in [-1,1]$

number, such that $K_3 = 2n_3 + K_2 + \ell_3$. The normalization constant $\mathcal{N}_3$ is given by

$$\mathcal{N}_3\left(K_3;\ell_3 K_2\right) = \left[\frac{\left(2K_3+7\right) n_3! \Gamma\left(n_3+\ell_3+K_2+\frac{7}{2}\right)}{\Gamma\left(n_3+\ell_3+\frac{3}{2}\right)\Gamma\left(n_3+K_2+3\right)}\right]^{\frac{1}{2}}.$$

The eigenvectors of $\hat{K}_3^2$ corresponding to the eigenfunctions in (B.16) are $K_3\left(K_3+7\right)$, where $K_3 \geq K_2 + \ell_3 \geq 0$. These eigenfunctions have the parity $(-)^{K_2+\ell_3}$. From the product of the functions $\Phi_{L_3 M_3;[K_2]\ell_3}$ in Eq. (B.15), and $\psi_{K_3;\ell_3 K_2}$ in Eq. (B.16) one constructs the hyperspherical harmonics $\mathcal{Y}_{[K_3]}$

$$\mathcal{Y}_{[K_3]}\left(\Omega_{(3)},\varphi_{(3)}\right) = \psi_{K_3;\ell_3 K_2}\left(\varphi_3\right)\Phi_{L_3 M_3;[K_2]\ell_3}\left(\Omega_{(3)},\varphi_2\right),$$

where $[K_3]$ represent the set of good quantum numbers K_3, L_3, M_3, K_2, L_2, ℓ_3, ℓ_2 and ℓ_1.

In order to formulate the general recursive procedure for the construction of the hyperspherical harmonics of an A-body system, with $A-1$ Jacobi coordinates, one assumes that the hyperspherical functions for an $(A-1)$-body system, $\mathcal{Y}_{[K_{A-2}]}$, with $A-2$ Jacobi coordinates, are already available. These functions possess a well defined hyperspherical angular momentum K_{A-2} and an orbital angular momentum L_{A-2} with projection M_{A-2}. They depend on the set of angular coordinate $\Omega_{(A-2)}$ and the hyperspherical coordinates $\varphi_{(A-2)}$. The hyperspherical harmonics for A-body are obtained in three steps.
First of all one couples the functions $\mathcal{Y}_{[K_{A-2}]}$ and $Y_{\ell_{A-1}m_{A-1}}\left(\Omega_{A-1}\right)$ in order to obtain

$$\Phi_{L_{A-1}M_{A-1};[K_{A-2}]\ell_{A-1}}\left(\Omega_{(A-1)},\varphi_{(A-2)}\right) = \tag{B.17}$$
$$\sum_{M_{A-2},m_{A-1}} \langle L_{A-2}\ell_{A-1}L_{A-1}|M_{A-2}m_{A-1}M_{A-1}\rangle \mathcal{Y}_{[K_{A-2}]}\left(\Omega_{(A-2)},\varphi_{(A-2)}\right) Y_{\ell_{A-1}m_{A-1}}(\hat{\eta}_{A-1}).$$

Then, using the transformation (B.4), one constructs the orthonormalized eigenfunctions of the hyperspherical angular momentum $\hat{K}_{A-1}^2$ by

$$\psi_{K_{A-1};\ell_{A-1}K_{A-2}}\left(\varphi_{A-1}\right) = \tag{B.18}$$
$$\mathcal{N}_{A-1}(K_{A-1};\ell_{A-1}K_{A-2})(\sin\varphi_{A-1})^{\ell_{A-1}}(\cos\varphi_{A-1})^{K_{A-2}} P_{n_{A-1}}^{\left(\ell_{A-1}+\frac{1}{2},K_{A-2}+\frac{3A-8}{2}\right)}(\cos 2\varphi_{A-1}),$$

where n_{A-1} is a non-negative integer number, such that

$$K_{A-1} = 2n_{A-1} + K_{A-2} + \ell_{A-1}, \tag{B.19}$$

and the normalization coefficient $\mathcal{N}_{A-1}$ is

$$\mathcal{N}_{A-1}\left(K_{A-1};\ell_{A-1}K_{A-2}\right) = \left[\frac{\left(2K_{A-1}+3A-5\right)n_{A-1}!\Gamma\left(n_{A-1}+K_{A-2}+\ell_{A-1}+\frac{3A-5}{2}\right)}{\Gamma\left(n_{A-1}+\ell_{A-1}+\frac{3}{2}\right)\Gamma\left(n_{A-1}+K_{A-2}+\frac{3A-6}{2}\right)}\right]^{\frac{1}{2}}. \quad \text{(B.20)}$$

The eigenvalues of the operator $\hat{K}^2_{A-1}$ corresponding to the eigenfunctions in (B.18) are

$$K_{A-1}\left(K_{A-1}+3A-5\right),$$

where $K_{A-1} \geq K_{A-2}+\ell_{A-1} \geq 0$. The functions in (B.18) have the parity $(-)^{K_{A-2}+\ell_{A-1}}$.

Finally, the hyperspherical harmonics for $A-1$ Jacobi coordinates, $\mathcal{Y}_{[K_{A-1}]}$, with angular momentum L_{A-1}, are built by the product of the functions $\Phi_{L_{A-1}M_{A-1};[K_{A-2}]\ell_{A-1}}$, in Eq. (B.17) and the $\psi_{K_{A-1};\ell_{A-1}K_{A-2}}$ in Eq. (B.18), as

$$\mathcal{Y}_{[K_{A-1}]}\left(\Omega_{(A-1)},\varphi_{(A-1)}\right) = \psi_{K_{A-1};\ell_{A-1}K_{A-2}}\left(\varphi_{(A-1)}\right)\Phi_{L_{A-1}M_{A-1};[K_{A-2}]\ell_{A-1}}\left(\Omega_{(A-1)},\varphi_{(A-2)}\right). \quad \text{(B.21)}$$

Here $[K_{A-1}]$ represent the set of quantum numbers K_{A-1}, L_{A-1}, M_{A-1}, $[K_{A-2}]$ and ℓ_{A-1}. The hyperspherical harmonics $\mathcal{Y}_{[K_{A-1}]}$ for an A-body system, defined in Eq. (B.21), form a complete orthonormal set of eigenfunctions on the hypersphere that satisfy the relation

$$\left\langle \mathcal{Y}_{[K_N]} \mid \mathcal{Y}_{[K_{N'}]} \right\rangle = \delta_{[K_N],[K_{N'}]},$$

with

$$\delta_{[K_N],[K_{N'}]} = \delta_{K_N,K_{N'}}\ \delta_{L_N,L_{N'}}\ \delta_{M_N,M_{N'}}\ \delta_{[K_{N-1}],[K_{N'-1}]}.$$

Appendix C

Multipole Expansions and Matrix Elements

In this Appendix we present the multipole expansion of the charge operator $\tilde{\rho}_{(1)}(\mathbf{q})$ and of the current operator $\mathbf{J}(\mathbf{q})$, to which we have referred in Chapter 6. The discussion on the current operator is separated into three sections: spin current $\mathbf{J}^s_{(1)}(\mathbf{q})$, convection current $\mathbf{J}^c_{(1)}(\mathbf{q})$ and finally MEC $\mathbf{J}_{(2)}(\mathbf{q})$ consistent with the MTI-III potential. In case of convection current and MEC we present also the explicit derivation of the Siegert part of the electric multipole.

As the structure of each multipole operator is derived we discuss briefly how we calculate the corresponding matrix element.

C.1 The Charge Operator

In Chapter 3 the multipole decomposition of the charge operator has been shown. Here we recall that the charge operator can be written by means of the Coulomb multipoles as

$$\tilde{\rho}_{(1)}(\mathbf{q}) = 4\pi \sum_{J\mu} i^J Y^*_{J\mu}(\hat{q}) C_{J\mu}(q). \tag{C.1}$$

In case of the electron scattering the longitudinal response function is determined via the charge operator, choosing the direction of the photon momentum to be along the $\hat{z}$ axis, i.e. $\mathbf{q} = q\hat{z}$. This means that the spherical harmonics can be reduced to

$$Y^*_{J\mu}(\hat{q}) = \frac{\hat{J}}{\sqrt{4\pi}} \delta_{\mu 0},$$

such that the expression in (C.1) becomes

$$\tilde{\rho}_{(1)}(q) = \sqrt{4\pi} \sum_J i^J \hat{J} C_{J0}(q), \tag{C.2}$$

where

$$C_{J0}(q) = \int d^3x \rho_{(1)}(\mathbf{x}) j_J(qx) Y_0^J(\hat{x}). \tag{C.3}$$

We use the expression of the charge operator in the coordinate space as in Eq. (3.34) (without the electric charge e), separating the isoscalar and the isovector part in

$$\rho_{(1)}^{s/v}(\mathbf{x}) = \sum_k \delta(\mathbf{x} - \mathbf{r'}_k) O^{\mathcal{T}\mathcal{T}_z}(t_k), \tag{C.4}$$

where the isospin operator $O^{\mathcal{T}\mathcal{T}_z}(t_k)$ is $\frac{1}{2}$, i.e. $\mathcal{T} = 0$ and $\mathcal{T}_z = 0$, for the isoscalar (s) part and $\frac{\tau_k^3}{2}$, i.e. $\mathcal{T} = 1$ and $\mathcal{T}_z = 0$, for the isovector (v) part. Using the antisymmetrization of the wave function we can write

$$\rho_{(1)}^{s/v}(\mathbf{x}) \equiv A\ \delta(\mathbf{x} - \mathbf{r'}_A) O^{\mathcal{T}\mathcal{T}_z}(t_A), \tag{C.5}$$

where the operator now acts only on the last coordinate. Consequently the isoscalar and isovector Coulomb multipoles become then

$$C_{J0}^{s/v}(q) = A j_J(q r'_A) Y_0^J(\hat{r}'_A) O^{\mathcal{T}\mathcal{T}_z}(t_A), \tag{C.6}$$

after the integration of the δ-function. The multipole expansion of the charge operator can also be written as

$$\rho_{(1)}^{s/v}(q) = \sum_J \tilde{C}_J^{s/v}(q), \tag{C.7}$$

where the new multipoles $\tilde{C}_J^{s/v}(q)$ contain all factors as $\tilde{C}_J^{s/v}(q) = \sqrt{4\pi} i^J \hat{J} C_{J0}(q)$, with the expression of $C_{J0}(q)$ as in Eq. (C.6).

In the calculation of the matrix elements of the Coulomb multipoles as in (4.15), one has (up to factors) a radial matrix element as in Eq. (4.18) where the radial function to consider is essentially the Bessel $j_J(qr'_A)$ with $r'_A = \sqrt{\frac{A-1}{A}} \rho \sin\varphi$ and an

angular reduced matrix element as in Eq. (4.16) which turns out to be simply[Edm74]

$$\langle(\ell\ s)j\|\,Y^J(\hat{r}'_A)\,\|(\ell'\ s)j'\rangle = (-1)^{s+j'+J}\hat{j}\hat{j}'\left\{\begin{array}{ccc}\ell & j & s\\ j' & \ell' & J\end{array}\right\}\frac{\hat{\ell}\hat{\ell}'\hat{J}}{\sqrt{4\pi}}\left(\begin{array}{ccc}\ell & J & \ell'\\ 0 & 0 & 0\end{array}\right). \tag{C.8}$$

The isospin matrix elements of $O^{\mathcal{T}T_z}(t_A)$ are trivial.

C.2 The Spin Current Operator

In order to calculate the multipole expansion of the spin current we will make use of the formalism that has been introduced in Chapter 3.

First of all we will evaluate the quantity in Eq. (3.14) in case of the spin current $\mathbf{J}^s_{(1)}$, i.e.

$$J^\mu_{Jl}(q) = \frac{1}{4\pi}\int d\hat{q}'\mathbf{J}^s_{(1)}(\mathbf{q}')\cdot\mathbf{Y}^\mu_{Jl1}(\hat{q}'). \tag{C.9}$$

The electric and magnetic mutlipoles are defined in terms of this quantity. Concerning the spin current operator, we will firstly separate it in isoscalar and isovector components, neglecting the form factor contributions. We will therefore use the expression given in (6.16) for the isoscalar and isovector parts, where we already made use of the antisymmetrization of the wave function in the matrix element. In the derivation of the multipole decomposition we will, for simplicity, consider only the structure of the operator in the spin-space configuration, i.e. $(\boldsymbol{\sigma}_A\times\mathbf{q})e^{i\mathbf{q}\mathbf{r}'_A}$. This is namely the same for both isoscalar and isovector components, if one neglects the factor $\frac{Ai}{2m}$ and the isospin operators $\frac{1}{2}$ and $\frac{\tau^3_A}{2}$ for the isoscalar and isovector part, respectively. They will be added at the very end of the calculation.

The quantity to calculate is then

$$J^\mu_{Jl}(q) = \frac{1}{4\pi}\int d\hat{q}'(\boldsymbol{\sigma}_A\times\mathbf{q}')e^{i\mathbf{q}'\mathbf{r}'_A}\cdot\mathbf{Y}^\mu_{Jl1}(\hat{q}'), \tag{C.10}$$

where one can use the fact that the vector product in Eq. (C.10) is related to the tensor product of rank 1 in the following way

$$(\boldsymbol{\sigma}_A\times\mathbf{q}') = \frac{\sqrt{2}}{i}[\boldsymbol{\sigma}^1_A\times\mathbf{q}'^1]^1, \tag{C.11}$$

where the superscript denotes the rank of the operator. Using the definition of the

vector spherical harmonics given in the (3.11) one obtains for the scalar product

$$[\boldsymbol{\sigma}_A^1 \times \mathbf{q}'^1]^1 \cdot \mathbf{Y}^\mu_{Jl1}(\hat{q}') = \sqrt{\frac{4\pi}{3}} q \, [Y^l(\hat{q}') \times [\boldsymbol{\sigma}_A^1 \times Y^1(\hat{q}')]^1]^J_\mu, \tag{C.12}$$

where $|\mathbf{q}| = |\mathbf{q}|' = q$ has been used. If one then recouples the two tensor products in the last expression such that the two spherical harmonics, which are functions of $\hat{q}'$, are coupled to a third spherical harmonics one gets

$$[\boldsymbol{\sigma}_A^1 \times \mathbf{q}'^1]^1 \cdot \mathbf{Y}^\mu_{Jl1}(\hat{q}') = (-1)^l q \sqrt{3}\, \hat{l} \sum_h \hat{h} \left\{ \begin{array}{ccc} 1 & 1 & 1 \\ l & J & h \end{array} \right\} \left(\begin{array}{ccc} 1 & l & h \\ 0 & 0 & 0 \end{array} \right) [\boldsymbol{\sigma}_A^1 \times Y^h(\hat{q}')]^J_\mu. \tag{C.13}$$

We can now expand the plane wave appearing in Eq. (C.10) as

$$e^{i\mathbf{q}'\mathbf{r}'_A} = 4\pi \sum_\ell (-i)^\ell \hat{\ell} j_\ell(qr'_A)[Y^\ell(\hat{r}'_A) \times Y^\ell(\hat{q}')]^0, \tag{C.14}$$

where the $j_\ell(qr'_A)$ are Bessel functions. Using now the expressions in Eq. (C.13) and (C.14) one gets for the $J^\mu_{Jl}(q)$ that

$$\begin{aligned} J^\mu_{Jl}(q) &= \frac{\sqrt{6}}{i} q \sum_\ell (-i)^\ell \hat{\ell} j_\ell(qr'_A)(-1)^l \hat{l} \sum_h \hat{h} \left\{ \begin{array}{ccc} 1 & 1 & 1 \\ l & J & h \end{array} \right\} \left(\begin{array}{ccc} 1 & l & h \\ 0 & 0 & 0 \end{array} \right) \\ &\int d\hat{q}' [[Y^\ell(\hat{r}'_A) \times Y^\ell(\hat{q}')]^0 \times [\boldsymbol{\sigma}_A^1 \times Y^h(\hat{q}')]^J]^J_\mu. \end{aligned} \tag{C.15}$$

If one now recouples the three tensor products appearing in the last formula such that the two spherical harmonics, which are functions of $\hat{q}'$, are coupled again to a third one, one gets, after some steps, the final expression for $J^\mu_{Jl}(q)$ as

$$\begin{aligned} J^\mu_{Jl}(q) &= \frac{\sqrt{6}}{i} q \sum_\ell (-i)^\ell (-1)^{l+1+J} \hat{\ell}\hat{l}\, j_\ell(qr'_A) \left\{ \begin{array}{ccc} 1 & 1 & 1 \\ l & J & \ell \end{array} \right\} \left(\begin{array}{ccc} 1 & l & \ell \\ 0 & 0 & 0 \end{array} \right) \\ &[Y^\ell(\hat{r}'_A) \times \boldsymbol{\sigma}_A^1]^J_\mu. \end{aligned} \tag{C.16}$$

Now, we would like to calculate the electric $T^{el}_{J\mu}(q)$ and magnetic $T^{mag}_{J\mu}(q)$ multipoles, which are related to the $J^\mu_{Jl}(q)$ as shown in (3.22) and (3.24), respectively.

For the electric multipoles one firstly needs to consider $J^\mu_{JJ-1}(q)$ for which one can explicitly write the sum in ℓ, since the three-j symbol leads to $\ell = J, J-2$.

Consequently one obtains

$$J^{\mu}_{JJ-1}(q) = \frac{\sqrt{6}}{i} q(-i)^J \hat{J}\widehat{J-1}\; j_J(qr'_A) \left\{ \begin{array}{ccc} 1 & 1 & 1 \\ J-1 & J & J \end{array} \right\} \left(\begin{array}{ccc} 1 & J-1 & J \\ 0 & 0 & 0 \end{array} \right) [Y^J(\hat{r}'_A) \times \boldsymbol{\sigma}^1_A]^J_{\mu}, \tag{C.17}$$

where one readily sees that only the case $\ell = J$ contributes, since the case $\ell = J-2$ is zero due to the coupling in the tensor product. Analogously for $J^{\mu}_{JJ+1}(q)$ one obtains

$$J^{\mu}_{JJ+1}(q) = \frac{\sqrt{6}}{i} q(-i)^J \hat{J}\widehat{J+1}\; j_J(qr'_A) \left\{ \begin{array}{ccc} 1 & 1 & 1 \\ J+1 & J & J \end{array} \right\} \left(\begin{array}{ccc} 1 & J+1 & J \\ 0 & 0 & 0 \end{array} \right) [Y^J(\hat{r}'_A) \times \boldsymbol{\sigma}^1_A]^J_{\mu}. \tag{C.18}$$

Using the last two expression one can write, after some steps, the electric multipole as (see (3.22))

$$T^{el}_{J\mu}(q) = -A \frac{\sqrt{2}q}{2m} (i)^J j_J(qr'_A) \langle J1J|011\rangle [Y^J(\hat{r}'_A) \times \boldsymbol{\sigma}^1_A]^J_{\mu} O^{\mathcal{T}T_z}_{s/v}(t_A), \tag{C.19}$$

where we have reduced the three-j and six-j symbols to a Clebsch-Gordan coefficient and we have added the factors and the isospin operators we had omitted before for simplicity. In the last expression $O^{\mathcal{T}T_z}_{s/v}(t_A)$ is equal to $\frac{1}{2}$ and $\frac{\tau^3_A}{2}$ for the isoscalar and isovector part, respectively.

For the magnetic multipoles one needs to consider only $J^{\mu}_{JJ}(q)$ (see (3.24)), for which one can explicitly write the sum in ℓ, where both cases $\ell = J-1$ and $\ell = J+1$ contribute to give finally

$$T^{mag}_{J\mu}(q) = -A \frac{\sqrt{2}q}{2m} \left\{ (i)^{J-1} \frac{\widehat{J-1}}{\hat{J}} \langle J-11J|011\rangle\, j_{J-1}(qr'_A) [Y^{J-1}(\hat{r}'_A) \times \boldsymbol{\sigma}^1_A]^J_{\mu} + (i)^{J+1} \frac{\widehat{J+1}}{\hat{J}} \langle J+11J|011\rangle\, j_{J+1}(qr'_A) [Y^{J+1}(\hat{r}'_A) \times \boldsymbol{\sigma}^1_A]^J_{\mu} \right\} O^{\mathcal{T}T_z}_{s/v}(t_A). \tag{C.20}$$

In the last expression all factors of the current and the isospin operators have been considered. One sees from (C.20) that the structure of the magnetic multipoles is very similar to the electric ones, with the main difference that there are two Bessel functions and two spherical harmonics which contributes to $T^{mag}_{J\mu}(q)$ and only one to $T^{el}_{J\mu}(q)$. The parities of $T^{el}_{J\mu}(q)$ and $T^{mag}_{J\mu}(q)$ are clearly $(-1)^J$ and $(-1)^{J+1}$, respectively.

Choosing now the direction of the photon momentum to be along the $\hat{z}$ axis

one can use the formula given in (3.26) to obtain the expression of the multipole decomposition for the J_+ component of the spin current

$$J^s_{(1)+}(q) = -\sqrt{2\pi}\sum_J \hat{J}\left(T^{el}_{J1}(q) + T^{mag}_{J1}(q)\right). \tag{C.21}$$

Via the expression for $T^{el}_{J\mu}(q)$ and $T^{mag}_{J\mu}(q)$ in (C.19) and (C.20), we can rewrite the multipole decomposition for the isoscalar (s) and isovector (v) spin current as

$$J^{s(s/v)}_{(1)+}(q) = \sum_J \left(E^{s/v}_J(q) + M^{s/v}_J(q)\right), \tag{C.22}$$

where $E^{s/v}_J(q)$ is the electric multipole and $M^{s/v}_J$ the magnetic with projection $\mu = 1$. Their final expressions are

$$E^{s/v}_J(q) = A\sqrt{4\pi}\frac{q}{2m}(i)^J j_J(qr'_A)\,\langle J1J|011\rangle\,[Y^J(\hat{r}'_A)\times\boldsymbol{\sigma}^1_A]^J_1 O^{\mathcal{T}T_z}_{s/v}(t_A) \tag{C.23}$$

and

$$\begin{aligned} M^{s/v}_J(q) \;=\; & A\sqrt{4\pi}\frac{q}{2m}\Big\{(i)^{J-1}\widehat{J\text{–}1}\,\langle J\text{–}11J|011\rangle\, j_{J-1}(qr'_A)\,[Y^{J-1}(\hat{r}'_A)\times\boldsymbol{\sigma}^1_A]^J_1 + \\ & (i)^{J+1}\widehat{J\text{+}1}\,\langle J\text{+}11J|011\rangle\, j_{J+1}(qr'_A)[Y^{J+1}(\hat{r}'_A)\times\boldsymbol{\sigma}^1_A]^J_1\Big\}O^{\mathcal{T}T_z}_{s/v}(t_A), \end{aligned} \tag{C.24}$$

respectively, where, the difference between the isoscalar and isovector multipoles is only in the isospin operator $O^{\mathcal{T}T_z}_{s/v}(t_A)$.

In the calculation of the matrix elements of the electric and magnetic multipoles of the one-body spin current operator as in (4.15) one finds a radial matrix element, as in Eq. (4.18), where the radial function to consider is practically the Bessel $j_L(qr'_A)$, up to some factors, with $r'_A = \sqrt{\frac{A-1}{A}}\rho\sin\varphi$ and with $L = J-1, J, J+1$ depending whether it is an electric or a magnetic multipole. Finally, the angular reduced matrix element, as in Eq. (4.16), can be easily calculated and it turns out to be simply [Edm74]

$$\begin{aligned} &\langle(\ell\ s)j\|\left[Y^L(\hat{r}'_A)\times\boldsymbol{\sigma}^1_A\right]^J\|(\ell'\ s)j'\rangle = \\ &\hat{j}\hat{j}'\hat{J}\begin{Bmatrix} \ell & \ell' & L \\ s & s & 1 \\ j & j' & J \end{Bmatrix}\left\langle\ell\left\|Y^L(\hat{r}'_A)\right\|\ell'\right\rangle\left\langle s\left\|\boldsymbol{\sigma}^1_A\right\|s\right\rangle = \end{aligned} \tag{C.25}$$

$$= \hat{j}\hat{j}'\hat{J} \begin{Bmatrix} \ell & \ell' & L \\ s & s & 1 \\ j & j' & J \end{Bmatrix} (-1)^{\ell} \frac{\hat{\ell}\,\hat{L}\,\hat{\ell}'}{\sqrt{4\pi}} \begin{pmatrix} \ell & L & \ell' \\ 0 & 0 & 0 \end{pmatrix} \sqrt{6}, \tag{C.26}$$

where $L = J-1, J, J+1$ depending whether it is an electric or a magnetic multipole. The isospin matrix elements are trivial and they are exactly the same as for the isoscalar and isovector charge operators.

C.3 The Convection Current Operator

We would like to decompose in multipoles the transverse convection current to include its effect on the transverse response. For this purpose, as done for the spin current, we want to evaluate the quantity in Eq. (3.14) in case of the convection current $\mathbf{J}^{c}_{(1)}$. In Chapter 6 we have shown that the part of convection current which includes a transverse term, i.e. $\mathbf{J}^{c,b}_{(1)}$ of (6.19), can be separated into isoscalar and isovector parts which have the expression as in (6.26) as a function of the last internal coordinate $\mathbf{r}'_A$. Thus we clearly deal with isoscalar and isovector multipoles. In order to perform the multipole expansion we will consider only the main structure of the operators in (6.26), i.e. $e^{i\mathbf{q}\mathbf{r}'_A}\boldsymbol{\nabla}'_A$ with $\boldsymbol{\nabla}'_A \equiv \frac{d}{d\mathbf{r}'_A}$, where we neglect the factor $-i\frac{A-1}{m}$ and the isospin operators $O^{\mathcal{T}T_z}_{s/v}(t_A)$.

The quantity to calculate is then

$$J^{\mu}_{Jl}(q) = \frac{1}{4\pi} \int d\hat{q}' e^{i\mathbf{q}'\mathbf{r}'_A} \boldsymbol{\nabla}'_A \cdot \mathbf{Y}^{\mu}_{Jl1}(\hat{q}'), \tag{C.27}$$

where $\boldsymbol{\nabla}'_A \cdot \mathbf{Y}^{\mu}_{Jl1}(\hat{q}') = [Y^{l}(\hat{q}') \times \boldsymbol{\nabla}'^{1}_{A}]^{J}_{\mu}$ and the plane wave $e^{i\mathbf{q}'\mathbf{r}'_A}$ can be expanded as in (C.14). This means that we have to evaluate

$$J^{\mu}_{Jl}(q) = \sum_{\ell} (-i)^{\ell}\hat{\ell} j_{\ell}(qr'_A) \int d\hat{q}' [[Y^{l}(\hat{q}') \times \boldsymbol{\nabla}'^{1}_{A}]^{J} \times [Y^{\ell}(\hat{r}'_A) \times Y^{\ell}(\hat{q}')]^{0}]^{J}_{\mu}. \tag{C.28}$$

Recoupling the tensor products appearing in the last formula such that the two spherical harmonics, which are functions of $\hat{q}'$, are coupled to a third one as function of $\hat{q}'$, and then performing the angular integration one gets the final expression for $J^{\mu}_{Jl}(q)$ as

$$J^{\mu}_{Jl}(q) = i^{l} j_{l}(qr'_A)[Y^{l}(\hat{r}'_A) \times \boldsymbol{\nabla}'^{1}_{A}]^{J}_{\mu}. \tag{C.29}$$

Now, we can write the electric $T^{el}_{J\mu}(q)$ and magnetic $T^{mag}_{J\mu}(q)$ multipoles using the

(3.22) and (3.24) as a function of the $J^{\mu}_{Jl}(q)$. The electric multipoles become

$$T^{el}_{J\mu}(q) = -\sqrt{2}\sum_{l=J-1}^{J+1} i^l j_l(qr'_A)\frac{\hat{l}}{\hat{J}}\langle l1J|011\rangle[Y^l(\hat{r}'_A)\times\boldsymbol{\nabla}'^1_A]^J_\mu, \tag{C.30}$$

where we have the contributions of two Bessel functions, and the magnetic multipoles are

$$T^{mag}_{J\mu}(q) = -\sqrt{2}i^J j_J(qr'_A)\langle J1J|011\rangle[Y^J(\hat{r}'_A)\times\boldsymbol{\nabla}'^1_A]^J_\mu. \tag{C.31}$$

The multipole decomposition of the J_+ for the transverse convection current using the formula in (3.26) becomes

$$J^{c,b(s/v)}_{(1)+}(q) = \sum_J \big(E^{s/v}_J(q) + M^{s/v}_J(q)\big), \tag{C.32}$$

with

$$\begin{aligned} E^{s/v}_J(q) &= -i\frac{A-1}{m}\sqrt{4\pi}\Big\{\sum_{l=J-1}^{J+1} i^l j_l(qr'_A)\hat{l}\langle l1J|011\rangle[Y^l(\hat{r}'_A)\times\boldsymbol{\nabla}'^1_A]^J_1\Big\}O^{\mathcal{T}T_z}_{s/v}(t_A) \\ M^{s/v}_J(q) &= -i\frac{A-1}{m}\sqrt{4\pi}i^J j_J(qr'_A)\hat{J}\langle J1J|011\rangle[Y^J(\hat{r}'_A)\times\boldsymbol{\nabla}'^1_A]^J_1 O^{\mathcal{T}T_z}_{s/v}(t_A), \end{aligned} \tag{C.33}$$

where we have finally added all the coefficients and the isospin operators. Clearly, electric and magnetic multipoles have different parities, which are $(-1)^J$ and $(-1)^{J+1}$, respectively.

In the calculation of the matrix elements of these multipoles as in (4.15) we have to take care of the reduced matrix element, as in Eq. (4.16), which is now $\Big\langle(\ell\ s)j\Big\|\big[Y^l(\hat{r}'_A)\times\boldsymbol{\nabla}'^1_A\big]^J\Big\|(\ell'\ s')j'\Big\rangle$ with $l = J-1, J, J+1$ depending whether it is an electric or magnetic multipole, and where both the spherical harmonics and the gradient act on the angular part of wave function. After some steps [Edm74] it becomes

$$\begin{aligned} &\Big\langle(\ell\ s)j\Big\|\big[Y^l(\hat{r}'_A)\times\boldsymbol{\nabla}'^1\big]^J\Big\|(\ell'\ s)j'\Big\rangle = (-1)^{s+j'+\ell'+\ell}\hat{j}\hat{j}'\begin{Bmatrix}\ell & j & s\\ j' & \ell' & J\end{Bmatrix}\hat{J}\times \\ &\sum_{\ell''}\begin{Bmatrix} l & 1 & J\\ \ell' & \ell & \ell''\end{Bmatrix}\frac{\hat{\ell}\hat{\ell}''\hat{l}}{\sqrt{4\pi}}\begin{pmatrix}\ell & l & \ell''\\ 0 & 0 & 0\end{pmatrix}\big\langle\ell''\big\|\boldsymbol{\nabla}'^1_A\big\|\ell'\big\rangle. \end{aligned} \tag{C.34}$$

Using the gradient formula the reduced matrix element of the gradient can be written

as

$$\left\langle \ell'' \left\| \boldsymbol{\nabla}'^{1}_{A} \right\| \ell' \right\rangle = \sqrt{\ell'+1}\left(\frac{d}{dr'_A} - \frac{\ell'}{r'_A}\right)\delta_{\ell'',\ell'+1} - \sqrt{\ell'}\left(\frac{d}{dr'_A} + \frac{\ell'+1}{r'_A}\right)\delta_{\ell'',\ell'-1}, \quad \text{(C.35)}$$

where, thanks to the Kronecker δ one can explicitly write the sum in (C.34). Clearly, in the last expression r'_A is the modulus $|\mathbf{r}'_A|$, which is as usual related to the last Jacobi coordinate and thus to the hyperspherical coordinates $\rho \equiv \rho_{A-1}$ and $\varphi \equiv \varphi_{A-1}$ as

$$r'_A = \sqrt{\frac{A-1}{A}}\rho \sin\varphi. \quad \text{(C.36)}$$

Therefore the derivative becomes

$$\frac{d}{dr_A} = \sqrt{\frac{A}{A-1}}\left(\sin\varphi \frac{d}{d\rho} + \frac{\cos\varphi}{\rho}\frac{d}{d\varphi}\right). \quad \text{(C.37)}$$

as a function of the hyperspherical coordinates. Finally, the reduced matrix element in (C.34) becomes

$$\begin{aligned}&\left\langle (\ell\ s)j \left\| \left[Y^{l}(\hat{r}'_A) \times \boldsymbol{\nabla}'^{1}_{A}\right]^{J} \right\| (\ell'\ s)j' \right\rangle = \\ &CA\sqrt{\frac{A}{A-1}}\sin\varphi\frac{d}{d\rho} + CA\sqrt{\frac{A}{A-1}}\frac{\cos\varphi}{\rho}\frac{d}{d\varphi} - CB\frac{1}{\sqrt{\frac{A-1}{A}}\rho\sin\varphi}\end{aligned} \quad \text{(C.38)}$$

where the constants A, B and C are

$$A = \widehat{\ell'+1}\sqrt{\ell+1}\begin{Bmatrix} l & 1 & J \\ \ell' & \ell & \ell'+1 \end{Bmatrix}\begin{pmatrix} \ell & l & \ell'+1 \\ 0 & 0 & 0 \end{pmatrix} \quad \text{(C.39)}$$

$$- \widehat{\ell'-1}\sqrt{\ell'}\begin{Bmatrix} l & 1 & J \\ \ell' & \ell & \ell'-1 \end{Bmatrix}\begin{pmatrix} \ell & l & \ell'-1 \\ 0 & 0 & 0 \end{pmatrix}, \quad \text{(C.40)}$$

$$\begin{aligned}B = {} & \widehat{\ell'+1}\sqrt{\ell+1}\ell'\begin{Bmatrix} l & 1 & J \\ \ell' & \ell & \ell'+1 \end{Bmatrix}\begin{pmatrix} \ell & l & \ell'+1 \\ 0 & 0 & 0 \end{pmatrix} + \\ & \widehat{\ell'-1}\sqrt{\ell'}(\ell'+1)\begin{Bmatrix} l & 1 & J \\ \ell' & \ell & \ell'-1 \end{Bmatrix}\begin{pmatrix} \ell & l & \ell'-1 \\ 0 & 0 & 0 \end{pmatrix}\end{aligned} \quad \text{(C.41)}$$

and

$$C = (-1)^{s+j'+\ell'+\ell}\hat{j}\hat{j}'\begin{Bmatrix} \ell & j & s \\ j' & \ell' & J \end{Bmatrix}\hat{J}\frac{\hat{\ell}\hat{l}}{\sqrt{4\pi}}, \quad \text{(C.42)}$$

respectively.

Therefore, in the radial matrix element, as in Eq. (4.18), the radial functions to consider are now not only the Bessel function, but we have to take care also of the derivatives $\frac{d}{d\varphi}$ and $\frac{d}{d\rho}$. Since the basis functions we use in the matrix elements (4.18) and (4.21) are practically polynomials, i.e. Jacobi polynomials as functions of φ and Laguerre polynomials as functions of ρ (see Chapter 4), we can evaluate the derivatives analytically, using the properties of the mentioned polynomials. This means, that finally, the integrations in φ and ρ can be done using again two numerical quadratures.

C.3.1 Siegert Part of the Electric Multipole

In order to evaluate the contribution of the convection current to the Siegert part of the electric multipole we have to consider the following quantity (see Eq. (3.27))

$$T'^{el}_{J\mu}(q) = -\frac{1}{4\pi}\sqrt{\frac{J+1}{J}}\int d\hat{q}'\hat{\mathbf{q}}'\cdot\mathbf{J}^c_{(1)}(\mathbf{q}')Y^J_\mu(\hat{q}'), \tag{C.43}$$

with $\hat{\mathbf{q}}' = \frac{\mathbf{q}'}{|\mathbf{q}'|}$ and $|\mathbf{q}| = |\mathbf{q}'| = q$ as usual. For this purpose we have to take into account both parts of the convection current in Eq. (6.19), since they both contain a longitudinal term which contributes to the scalar product present in the above integration. In the derivation of the Siegert part of the electric multipole we will consider for simplicity only the main structure of the operators in coordinate space, i.e.

$$\begin{aligned}\mathbf{J}^{c,a}_{(1)}(\mathbf{q}') &= \frac{Aq}{2m}\hat{z}e^{i\mathbf{q}'\cdot\mathbf{r}'_A},\\ \mathbf{J}^{c,b}_{(1)}(\mathbf{q}') &= -\frac{i(A-1)}{m}e^{i\mathbf{q}'\cdot\mathbf{r}'_A}\boldsymbol{\nabla}'_A,\end{aligned} \tag{C.44}$$

where we neglect the form factors and the isospin operator for simplicity, and we directly use the antisymmetrization of the wave function. The contribution of the purely longitudinal convection current in (C.44) to the integration in (C.43) is clearly proportional to a Coulomb multipole, since only the plane wave has to be expanded. Namely, the contribution to the Siegert operator form the part (a) of the current is given by

$$T'^{el(a)}_{J\mu}(q) = -\frac{1}{4\pi}\sqrt{\frac{J+1}{J}}\frac{Aq}{2m}\int d\hat{q}'e^{i\mathbf{q}'\cdot\mathbf{r}'_A}Y^J_\mu(\hat{q}'). \tag{C.45}$$

Expanding the plane wave one gets

$$T'^{el(a)}_{J\mu}(q) = -\sqrt{\frac{J+1}{J}}\frac{Aq}{2m}\sum_{\ell,m} i^\ell j_\ell(qr'_A)Y^\ell_m(\hat{r}'_A)\int d\hat{q}' Y^\ell_m(\hat{q}')Y^J_\mu(\hat{q}'), \tag{C.46}$$

which becomes, using the orthogonality of the spherical harmonics,

$$T'^{el(a)}_{J\mu}(q) = -\sqrt{\frac{J+1}{J}}\frac{Aq}{2m} i^J j_J(qr'_A)Y^J_\mu(\hat{r}'_A). \tag{C.47}$$

The last expression is proportional to the Coulomb multipole $C_{J\mu}$ as

$$T'^{el(a)}_{J\mu}(q) = -\sqrt{\frac{J+1}{J}}\frac{q}{2m} i^J C_{J\mu}(q). \tag{C.48}$$

The parity of the last operator is clearly $(-1)^J$ and the calculation of the corresponding matrix elements proceeds as for the Coulomb multipoles.

In the following we will calculate the contribution of the second part of the convection current, (b), to the Siegert operator. The quantity to study is then

$$T'^{el(b)}_{J\mu}(q) = \frac{1}{4\pi}\sqrt{\frac{J+1}{J}}\frac{i(A-1)}{m}\int d\hat{q}'\ \hat{\mathbf{q}}'\cdot\boldsymbol{\nabla}'_A\ e^{i\mathbf{q}'\cdot\mathbf{r}'_A}Y^J_\mu(\hat{q}'). \tag{C.49}$$

First of all we can use the fact that the scalar product appearing in the last expression is

$$\hat{\mathbf{q}}'\cdot\boldsymbol{\nabla}'_A = -\sqrt{3}[\hat{\mathbf{q}}'^1\times\boldsymbol{\nabla}'^1_A]^0,$$

and then, expanding the plane wave as in (C.14), one gets

$$\begin{aligned} T'^{el(b)}_{J\mu}(q) &= -\sqrt{\frac{J+1}{J}}\frac{i\sqrt{3}(A-1)}{m}\sum_\ell(-i)^\ell\hat{\ell}j_\ell(qr'_A) \\ &\int d\hat{q}'\ [[\hat{\mathbf{q}}'^1\times\boldsymbol{\nabla}'^1_A]^0\times[[Y^\ell(\hat{r}'_A)\times Y^\ell(\hat{q}')]^0\times Y^J(\hat{q}')]^J]^J_\mu. \end{aligned} \tag{C.50}$$

Recoupling then the tensor products such that the two spherical harmonics, which are functions of $\hat{q}'$, are coupled to a third one, and using the fact that $\hat{\mathbf{q}}'^1 = \sqrt{\frac{4\pi}{3}}Y^1(\hat{q}')$ one gets

$$T'^{el(b)}_{J\mu}(q) = -\sqrt{\frac{J+1}{J}}\frac{i(A-1)}{m}\sum_\ell(-i)^\ell\hat{\ell}j_\ell(qr'_A)\sum_h\hat{h}(-1)^h\begin{pmatrix}\ell & J & h\\ 0 & 0 & 0\end{pmatrix}$$

$$\cdot \int d\hat{q}' \; [[Y^1(\hat{q}') \times \boldsymbol{\nabla}'_A]^0 \times [Y^\ell(\hat{r}'_A) \times Y^h(\hat{q}')]^J]^J_\mu. \tag{C.51}$$

At this point one can proceed, as done for the spin current, recoupling the three tensor products in the last expression such that again the two spherical harmonics, which are functions of $\hat{q}'$, are coupled to a third one; then one can perform the angular integration in $d\hat{q}'$. After some steps, calculating explicitly the values of the nine-j and six-j symbols deriving from the coupling, one gets the final result which reads

$$T'^{el(b)}_{J\mu}(q) = -\sqrt{\frac{J+1}{J}}\frac{(A-1)}{m}(-1)^{J+1}\sum_\ell (i)^{\ell+1}\hat{\ell} j_\ell(qr'_A) \begin{pmatrix} \ell & J & 1 \\ 0 & 0 & 0 \end{pmatrix} [Y^\ell(\hat{r}'_A) \times \boldsymbol{\nabla}'_A]^J_\mu.$$

Clearly, in the last expression the sum over ℓ can be written explicitly, since due to the presence of the three-j symbol only the terms with $\ell = J-1$ and $\ell = J+1$ contribute. Therefore, we can finally write

$$T'^{el(b)}_{J\mu}(q) = -\sqrt{\frac{J+1}{J}}\frac{(A-1)}{m}(-1)^{J+1}(i)^J \Bigg[\widehat{J\text{–}1} j_{J-1}(qr'_A) \begin{pmatrix} J\text{–}1 & J & 1 \\ 0 & 0 & 0 \end{pmatrix}$$
$$[Y^{J-1}(\hat{r}'_A) \times \boldsymbol{\nabla}'_A]^J_\mu - \widehat{J\text{+}1} j_{J+1}(qr'_A) \begin{pmatrix} J\text{+}1 & J & 1 \\ 0 & 0 & 0 \end{pmatrix} [Y^{J+1}(\hat{r}'_A) \times \boldsymbol{\nabla}'_A]^J_\mu \Bigg], \tag{C.52}$$

where one clearly sees that the Siegert part of the electric multipole derived from the second part of the convection current $\mathbf{J}^{c,b}_{(1)}$ contains two contributions with two different Bessel functions, j_{J-1} and j_{J+1}, and two spherical harmonics with multipolarity $J-1$ and $J+1$. The parity is clearly $(-1)^J$ for both parts. The matrix element of this operator is calculated in the usual way. The reduced matrix element of the tensor products $[Y^{J+1/J-1}(\hat{r}'_A) \times \boldsymbol{\nabla}'_A]^J_\mu$ are defined as in (C.38).

C.4 MEC Operator

We are now interested in performing a multipole expansion of the MEC we have derived in case of the MTI-III potential. For this purpose we have to consider the quantity in Eq. (3.14) with the current in (6.39), which represents a consistent two-body current for the MTI-III potential with the approximation discussed in Chapter 6. We will perform the multipole expansion using for simplicity only the structure

of such an operator, i.e.

$$\mathbf{J}^a_{(2)}(\mathbf{q}) = \boldsymbol{\nabla}'_{A,A-1} I_m(\mathbf{q}, \mathbf{r}'_{A,A-1}), \tag{C.53}$$

with $\mathbf{r}'_{A,A-1} = \mathbf{r}'_A - \mathbf{r}'_{A-1}$ in the center of mass frame, and $\boldsymbol{\nabla}'_{A,A-1} \equiv \frac{d}{d\mathbf{r}'_{A,A-1}}$. We consider only the operator acting on the last two particles, assuming to have already used the antisymmetrization of the wave function in the matrix element of the two-body operator, yielding also the factor $\frac{A(A-1)}{2}$, which we now omit.

The quantity to calculate is then

$$J^\mu_{Jl}(q) = \frac{1}{4\pi} \int d\hat{q}' \boldsymbol{\nabla}'_{A,A-1} I_m(\mathbf{q}', \mathbf{r}'_{A,A-1}) \cdot \mathbf{Y}^\mu_{Jl1}(\hat{q}'), \tag{C.54}$$

where we can use the fact that $\boldsymbol{\nabla}'_{A,A-1} \cdot \mathbf{Y}^\mu_{Jl1}(\hat{q}') = [Y^l(\hat{q}') \times \boldsymbol{\nabla}'^{\,1}_{A,A-1}]^J_\mu$ and where we can expand the function $I_m(\mathbf{q}, \mathbf{r}'_{A,A-1})$ as shown in [Fab76, Lei80]

$$I_m(\mathbf{q}, \mathbf{r}_{A,A-1}) = (4\pi)^2 \sum_{\ell=\text{even}} (-i)^\ell \hat{\ell} \Phi^0_{\ell,\ell}(q, r_{A,A-1}) \left[Y^\ell(\hat{q}) \times Y^\ell(\hat{r}_{A,A-1})\right]^0. \tag{C.55}$$

The functions $\Phi^\nu_{\sigma,l}(q, r_{A,A-1})$, with $r_{A,A-1} = |\mathbf{r}_{A,A-1}|$, are generally defined in terms of the Bessel functions as

$$\Phi^\nu_{\sigma,\ell}(q, r_{A,A-1}) = \frac{1}{q^2} \int_0^\infty \frac{dpp^\nu}{z} j_\sigma(pr_{A,A-1}) Q_\ell(z), \tag{C.56}$$

with

$$Q_\ell(z) = \frac{1}{2} \int_{-1}^1 dx \frac{P_\ell(z)}{z - x}, \tag{C.57}$$

where $P_\ell(z)$ is a Legendre polynomial with

$$z = \frac{1}{pq}(p^2 + \frac{1}{4}q^2 + m^2).$$

Using the last relations we get

$$J^\mu_{Jl}(q) = 4\pi \sum_{\ell=\text{even}} (-i)^\ell \hat{\ell} \int d\hat{q}' [[Y^l(\hat{q}') \times \boldsymbol{\nabla}'^{\,1}_{A,A-1}]^J \times [Y^\ell(\hat{q}') \times Y^\ell(\hat{r}_{A,A-1})]^0]^J_\mu \Phi^0_{\ell,\ell}(q, r_{A,A-1}), \tag{C.58}$$

where as usual one has to recouple the tensor products such that the two spherical harmonics, which are functions of $\hat{q}'$, are coupled to a third one. Performing the

angular integration, after some steps one gets

$$J^{\mu}_{Jl}(q) = 4\pi(-i)^l(-1)^{1+J}[\boldsymbol{\nabla}'^{\,1}_{A,A-1} \times Y^l(\hat{r}_{A,A-1})]^J_{\mu}\ \Phi^0_{l,l}(q, r_{A,A-1}), \tag{C.59}$$

with l even. Using the generalized gradient formula [Edm74, Var88] one can show that

$$[\boldsymbol{\nabla}'^{\,1}_{A,A-1} \times Y^l(\hat{r}_{A,A-1})]^J_{\mu}\Phi^0_{l,l}(q, r_{A,A-1}) = i^{J-l-1}(-1)^l\hat{l}\begin{pmatrix} 1 & l & J \\ 0 & 0 & 0 \end{pmatrix} Y^J_{\mu}(\hat{r}_{A,A-1})\Phi^1_{J,l}(q, r_{A,A-1}), \tag{C.60}$$

with $\Phi^1_{J,l}(q, r_{A,A-1})$ as in (C.56), such that the quantity $J^{\mu}_{Jl}(q)$ becomes finally

$$J^{\mu}_{Jl}(q) = 4\pi(i)^{J-1}\hat{l}\begin{pmatrix} 1 & l & J \\ 0 & 0 & 0 \end{pmatrix} Y^J_{\mu}(\hat{r}_{A,A-1})\ \Phi^1_{J,l}(q, r_{A,A-1}), \tag{C.61}$$

with l even. From the expression in (C.61) one can easily see, that in case of $J = l$ the operator is identically zero, which means that no magnetic multipoles exist for such a meson-exchange current, since $T^{mag}_{J\mu}(q) = J^{\mu}_{JJ}(q) = 0$. The electric multipoles can be calculated inserting the above expression with $l = J - 1$ and $l = J + 1$ in Eq. (3.22).

One can easily understand that the calculation of the matrix element of these two-body multipole operators proceeds in an analogous way as in (4.15), where in the radial matrix element we have to consider the functions $\Phi^1_{J,l}(q, r_{A,A-1})$. Concerning their calculation we have made use of an integral representation in terms of the Hankel functions with complex argument, see [Lei80, Wea75].

The expression in (C.61) has to be used in case one wants to write explicitly the electric multipoles of the MEC to study its effect on the transverse response function. In the following we will proceed with the calculation of the Siegert part of the electric multipole deriving from the MEC (see Eq. (3.27)). This will be used in the Siegert check.

C.4.1 Siegert Part of the Electric Multipole

In order to evaluate the contribution of the MEC to the Siegert part of the electric multipole we have to consider the following quantity (see Eq· (3.27))

$$T'^{el}_{J\mu}(q) = -\frac{1}{4\pi}\sqrt{\frac{J+1}{J}}\int d\hat{q}'\hat{\mathbf{q}}' \cdot \mathbf{J}^a_{(2)}(\mathbf{q}')Y^J_{\mu}(\hat{q}'), \tag{C.62}$$

in analogy to what we have done in case of the convection current. Therefore, we have to calculate

$$T'^{el}_{J\mu}(q) = -\frac{1}{4\pi}\sqrt{\frac{J+1}{J}}\int d\hat{q}'\hat{\mathbf{q}}'\cdot\boldsymbol{\nabla}'_{A,A-1}I_m(\mathbf{q}',\mathbf{r}'_{A,A-1})Y^J_\mu(\hat{q}'), \tag{C.63}$$

where the scalar product can be written as

$$\hat{\mathbf{q}}'\cdot\boldsymbol{\nabla}'_{A,A-1} = -\sqrt{3}[\hat{\mathbf{q}}'^1\times\boldsymbol{\nabla}'^1_{A,A-1}]^0 = -\sqrt{4\pi}[Y^1(\hat{q}')\times\boldsymbol{\nabla}'^1_{A,A-1}]^0.$$

Using the expansion in (C.55) we get

$$\begin{aligned} T'^{el}_{J\mu}(q) &= (4\pi)^{\frac{3}{2}}\sqrt{\frac{J+1}{J}}\sum_{\ell=\text{even}}(-i)^\ell\hat{\ell}\;\Phi^0_{\ell,\ell}(q,r_{A,A-1})\times \\ &\int d\hat{q}'[[Y^1(\hat{q}')\times\boldsymbol{\nabla}'^1_{A,A-1}]^0\times[[Y^\ell(\hat{q}')\times Y^\ell(\hat{r}_{A,A-1})]^0\times Y^J(\hat{q}')]^J_\mu. \end{aligned} \tag{C.64}$$

Recoupling two times the tensor products in the last expression such that the spherical harmonics as function of $\hat{q}'$ are coupled to a third one, and performing the angular integration, one gets after some steps

$$T'^{el}_{J\mu}(q) = -4\pi\sum_{\ell=\text{even}}(-i)^\ell\hat{\ell}\begin{pmatrix}\ell & J & 1\\ 0 & 0 & 0\end{pmatrix}[\boldsymbol{\nabla}'^{\,1}_{A,A-1}\times Y^\ell(\hat{r}_{A,A-1})]^J_\mu\;\Phi^0_{\ell,\ell}(q,r_{A,A-1}). \tag{C.65}$$

Finally, making use of the relation (C.60), we can write the Siegert part of the MEC as

$$T'^{el}_{J\mu}(q) = 4\pi i^{J+1}\sum_{\ell=\text{even}}\hat{\ell}^2\begin{pmatrix}\ell & J & 1\\ 0 & 0 & 0\end{pmatrix}^2 Y^J_\mu(\hat{r}_{A,A-1})\;\Phi^1_{J,\ell}(q,r_{A,A-1}), \tag{C.66}$$

where clearly only the cases with $\ell = J-1$ and $\ell = J+1$ will contribute. Namely, in order to calculate the matrix element of this operator we have to take

$$R(r_{A,A-1}) = \widehat{J\text{–}1}^2\begin{pmatrix}J\text{–}1 & J & 1\\ 0 & 0 & 0\end{pmatrix}^2\Phi^1_{J,J-1}(q,r_{A,A-1}) + \widehat{J\text{+}1}^2\begin{pmatrix}J\text{+}1 & J & 1\\ 0 & 0 & 0\end{pmatrix}^2\Phi^1_{J,J+1}(q,r_{A,A-1}) \tag{C.67}$$

as radial function and the spherical harmonics $Y^J_\mu(\hat{r}_{A,A-1})$ will appear in the calculation of the reduced matrix elements.

List of Figures

List of Tables

Bibliography

[Ahr75] J. Ahrens et al., Nucl. Phys. A **251**, 479 (1975).

[Ahk94] A. I. Akhiezer, A. G. Sitenko, V. K. Tartakowsii, *"Nuclear Electrodynamics"*, Springer Verlag, Berin, Heidelberg (1994).

[Are82] H. Arenhövel, *"Exchange currents in nuclei"*, lectures held at the University of Genova (1982).

[Are90] H. Arenhövel, *"Gradi di libertà efficaci nella disintegrazione elettromagnetica del dutone"*, lectures held at the University of Trento (1990).

[Are91] H. Arenhövel and M. Sanzone, Few-Body Syst., Suppl. **3**, 1 (1991).

[Are99] H. Arenhövel, Few-Body Syst. **26**, 43-98 (1999).

[Aum98] T. Aumann *et al.*, Phys.Rev. C **59**, 3 (1998).

[Aum01] T. Aumann, private comunication (2001).

[Bac01] S. Bacca, *"Interazione Efficace nel Calcolo della Sezione d'Urto Inclusiva di Fotodisintegrazione di Nuclei con $A \leq 6$"*, Laurea Thesis, Trento (2001).

[Bac02] S. Bacca, M. A. Marchisio, N. Barnea, W. Leidemann, and G. Orlandini, Phys. Rev. Lett. **89**, 052502 (2002).

[Bac04] S. Bacca, N. Barnea, W. Leidemann, and G. Orlandini, Phys. Rev. C **69**, 057001 (2004).

[Bac04b] S. Bacca, H. Arenövel, N. Barnea, W. Leidemann, and G. Orlandini, Phys. Lett. B **603**, 159-164 (2004).

[Bac05] S. Bacca, N. Barnea, W. Leidemann, G. Orlandini, E. Caurier and P. Navrátil, in preparation.

[Bar97a] N. Barnea, *"Exact Solution of the Schrödinger Equation and Faddeev Equation for Few Body Systems"*, Ph.D. Thesis, Hebrew University, Jerusalem (1997).

[Bar97b] N. Barnea and A. Novoselsky, Ann. Phys (N.Y.) **256**, 192 (1997).

[Bar98] N. Barnea and A. Novoselsky, Phys. Rev. A **57**, 48 (1998).

[Bar99] N. Barnea, W. Leidemann, and G. Orlandini, Nucl. Phys. A **650**, 427-442 (1999).

[Bar01] N. Barnea, W. Leidemann, and G. Orlandini, Phys. Rev. C **61**, 054001 (2000).

[Bar01a] N. Barnea, W. Leidemann, and G. Orlandini, Nucl. Phys. A **693**, 565 (2001).

[Bar01b] N. Barnea, V. D. Efros, W. Leidemann, and G. Orlandini, Phys. Rev. C **63**, 057002 (2001).

[Bar04] N. Barnea, V. D. Efros, W. Leidemann, and G. Orlandini, Few-Body Syst. **35**, 155-167 (2004).

[Ber65] B. L. Berman et al., Phys. Rev. Lett. **15**, 727 (1965).

[Bjo64] J. D. Bjorken and S. D. Drell, *"Relativistic Quantum mechanics"*, McGraw-Hill, New York (1964).

[Car92] J. Carlson, R. Schiavilla, Phys. Rev. Lett. **68**, 3682 (1992).

[Car94] J. Carlson, R. Schiavilla, Phys. Rev. C **49**, R2880 (1994).

[Car02] J. Carlson, J. Jourdan, R. Schiavilla and I. Sick, Phys. Rev. C **65**, 024002 (2002).

[Cio80] C. Ciofi degli Atti, Progr. Part. and Nucl. Phys. **3**, 163-328 (1980).

[Cio91] C. Ciofi degli Atti et al., Phys. Rev. C **44**, R7 (1991).

[DeF84] T. De Forest, Jr., Nucl. Phys. A **414**, 347 (1984).

[Don03] T. W. Donneley, Proceedings of the International School of Physics "Enrico Fermi", Course CLIII, *"From Nuclei and their Constituents to Stars"*, SIT Bologna, 183 (2003).

[Dyt88] S. A. Dytman et al., Phys. Rev. C **38**, 800 (1988).

[Edm74] A. R. Edmonds, *"Angular momentun in quantum mechanics"*, Princeton University Press, Princeton, NJ (1970).

[Efr94] V. D. Efros, W. Leidemann, and G. Orlandini, Phys. Lett. B **338**, 130 (1994).

[Efr97a] V. D. Efros, W. Leidemann, and G. Orlandini, Phys. Rev. Lett. **78**, 432 (1997).

[Efr97b] V. D. Efros, W. Leidemann, and G. Orlandini, Phys. Rev. Lett. **78**, 4015 (1997).

[Efr97c] V. D. Efros, W. Leidemann, and G. Orlandini, Phys. Lett. B **408**, 1 (1997).

[Efr98] V. D. Efros, W. Leidemann, and G. Orlandini, Phys.Rev. C **58** 582-585 (1998).

[Efr99a] V. D. Efros, W. Leidemann and G. Orlandini, Few-Body Systems **26**, 251-269 (1999).

[Efr99b] V. D. Efros, Phys. At. Nucl. 62, 1833 (1999).

[Efr00] V. D. Efros, W. Leidemann, and G. Orlandini, E. L. Tomusiak, Phys. Lett. B **484**, 223 (2000).

[Efr01] V. D. Efros, W. Leidemann, and G. Orlandini, E. L. Tomusiak, Nucl. Phys. **A489**, 421 (2001).

[Efr04] V. D. Efros, W. Leidemann, and G. Orlandini, E. L. Tomusiak, Phys.Rev. C **69** 044001 (2004).

[Eis70] J. M. Eisenberg, W. Greiner, *"Excitation mechanisms of the nucleus"*, North-Holland Publishing Company, Amsterdam (1970).

[Fab76] W. Fabian and H. Arenhövel, Nucl. Phys. **A 258**, 461-479 (1976).

[Fab97] A. Fabrocini, Phys. Rev. C **55**, 338 (1997).

[Fen72] Yu. I. Fenin and V. D. Efros, Yad. Fiz. **15**, 887 (1972); Sov. J. Nucl. Phys. **15**, 497 (1972).

[Fom81] B. A. Fomin, V. D. Efros, Sov J. Nucl. Phys. **34**, 327 (1981).

[Fru84] S. Frullani, J. Mourgey, Advances in Nuclear Physisc **14**, 1 (1984).

[Gal71] S. Galster *et al*, Nucl. Phys. **B 32** , 221 (1971).

[Gaz04] D. Gazit and N. Barnea, Phys. Rev. C **70**, 048801 (2004).

[Glo83] W. Glöckle, *"The quantum mechanical few-body problem"*, Springer-Verlag, Berlin, Heidelberg, New York, Tokio (1983).

[Glo04] W. Gloeckle, J. Golak, R. Skibinski, H. Witala, H. Kamada, A. Nogga, Eur. Phys. J. A21, 335-348 (2004).

[Gol00] J. Golak et al., Phys. Rev. C **62**, 054005 (2000).

[Jou04] J. Jourdan, private comunication (2004).

[Jun79] G. Junghans et al., Z. Physik **A291**, 353 (1979).

[Lag91] J. M. Laget, *"Modern topic in electron scattering"*, ed. B. Frois and I. Sick, World Scientific, Singapore (1991).

[Lap00] A. La Piana, W. Leidemann, Nucl.Phys. **A677**, 42 (2000).

[Lei80] W. Leidemann, *"Untersuchungen zur Elektromagnetischen Struktur des Deuterons: Explizite Auswertung von Summenregeln und der Beitrag Höherer Mesonaustauschströme zu der Elektrodisintegration"*, Diplom-Arbeit, Johannes Gutenberg-Universität, Mainz (1980).

[Lei90] W. Leidemann and G. Orlandini, Nucl.Phys. A **506**, 447 (1990).

[Mar03] M. A. Marchisio, N. Barnea, W. Leidemann, G. Orlandini, Few-Body Syst. **33**, 259 (2003).

[Mal69] R. A. Malfliet and J. A. Tjon, Nucl. Phys. **A127**, 161 (1969).

[Nav96] P. Navrátil and B. R .Barret, Phys. Rev. C **54**, 2986 (1996).

[Nav98] P. Navrátil and B. R. Barret, Phys. Rev. C **57**, 562 (1998).

[Nav99] P. Navrátil and B. R. Barrett, Phys. Rev. C **59**, 1906 (1999).

[Nav00] P. Navrátil, J. Vary and B. R. Barrett, Phys. Rev. C **62**, 054311 (2000).

[Nov88] A. Novoselsky, J. Katriel, R. Gilmore, *J. Math. Phys.* **29**, 1368 (1988).

[Pie02] S. C. Pieper, and R. B. Wiringa, Phys. Rev. Lett. **89**, 182501 (2002).

[Pre92] W. H. Press, S. A. Teukolsky, W. T. Vetterling, B. P. Flannery, *"Numerical Recipes in C"*, Cambridge University Press (1992).

[Qua04] S. Quaglioni, N. Barnea, V. D. Efros, W. Leidemann and G. Orlandini, Phys.Rev. C **69**, 044002 (2004).

[Rei03] C. Reiss, W. Leidemann, G. Orlandini, and E. L. Tomusiak, Eur. Phys. J. A **17**, 589-594 (2003).

[Ros92] S. Rosati, A. Kievsky and M. Viviani, Few Body Syst., Suppl. **6**, 563 (1992).

[Sie37] A. J. F. Siegert, *Phys. Rev.* **52**, 787 (1937).

[Shi75] Y. M. Shin et al., Phys. Lett. B **55**, n.3. (1975).

[Sit72] A. G. Sitenko, V. K. Tartakovskij, *"Lezioni di teoria del nucleo"*, Edizioni Mir, Mosca (1972).

[Suz80] K. Suzuki and S. Y. Lee, Prog. Theor. Phys. **64**, 2091 (1980).

[Suz82] K. Suzuki and S. Y. Lee, *Prog.Theor.Phys.* **68**, 246 (1982).

[Suz83] K. Suzuki and S. Y. Lee, *Prog.Theor.Phys.* **70**, 439 (1983).

[Suz01] Y. Suzuki and K. Varga, *"Stochastic Variational Approach to Quantum Mechanical Few-Body Systems"* Springer-Verlag, Berlin, (1998).

[Tho77] D. R. Thomson, M. LeMere and Y. C. Tang, Nucl. Phys. **A286**, 53 (1977); I. Reichstein and Y. C. Tang, *ibid.* **A158**, 529 (1970).

[Var88] D. A. Varshaolvich, A. N. Moskalev, V. K. Khersonskii, *"Quantum Theory of Angular Momentum"* World Scientific, Singapore, (1988).

[Wea75] R. C. Weast and S. M. Selby, *"Handbook of tables for Matematics"*, CRC Press, Cleveland, Ohio, (1975).

[Wir01] R. B. Wiringa, Steven C. Pieper, J.Carlson, and V.R. Pandharipande, Phys. Rev. C **62**, 014001 (2000).

[Zgh94] A. Zghiche et al., Nucl. Phys. A**572**, 513 (1994).